

REINFORCING DAPPED TIMBER STRINGERS WITH GFRP BARS

BY

KEVIN S. AMY

A Thesis

Submitted to the Faculty of Graduate Studies
In Partial Fulfillment of the Requirements for the Degree of

MASTER OF SCIENCE

Department of Civil Engineering
University of Manitoba
Winnipeg, Manitoba

THE UNIVERSITY OF MANITOBA
FACULTY OF GRADUATE STUDIES

COPYRIGHT PERMISSION

Reinforcing Dapped Timber Stringers with GFRP Bars

BY

Kevin S. Amy

**A Thesis/Practicum submitted to the Faculty of Graduate Studies of The University of
Manitoba in partial fulfillment of the requirement of the degree**

Of

MASTER OF SCIENCE

Kevin S. Amy © 2004

Permission has been granted to the Library of the University of Manitoba to lend or sell copies of this thesis/practicum, to the National Library of Canada to microfilm this thesis and to lend or sell copies of the film, and to University Microfilms Inc. to publish an abstract of this thesis/practicum.

This reproduction or copy of this thesis has been made available by authority of the copyright owner solely for the purpose of private study and research, and may only be reproduced and copied as permitted by copyright laws or with express written authorization from the copyright owner.

TABLE OF CONTENTS

LIST OF TABLES	iii
LIST OF FIGURES	iv
LIST OF SYMBOLS	vi
ACKNOWLEDGEMENTS	viii
ABSTRACT	ix
CHAPTER 1 INTRODUCTION	1
1.1 General	1
1.2 Problem Definition	2
1.3 Objectives and Scope	2
CHAPTER 2 PREVIOUS RESEARCH	4
2.1 General	4
2.2 Fibre-reinforced Polymer Reinforcement	4
2.3 Timber	8
2.4 Timber Strengthening	10
2.5 Timber Strength Models	13
2.5.1 Plain Timber Strength Model	13
2.5.2 Reinforced Timber Strength Model	22
CHAPTER 3 EXPERIMENTAL PROGRAM	25
3.1 General	25
3.2 Objectives of the Experimental Program	25
3.3 Materials	26
3.3.1 Timber Stringers	26
3.3.2 GFRP Bars and Epoxy	28
3.4 Standard Grading Rules for Timber Beams and Stringers	28
3.5 Design and Fabrication of Specimens	31
3.6 Test Beams	33
3.7 Test Setup and Parameters	34
3.8 Instrumentation	35
CHAPTER 4 TEST DATA AND RESULTS	37
4.1 General	37
4.2 Load Deflection Behavior	37
4.2.1 Control Specimens	37
4.2.2 Flexurally Reinforced Specimens	40
4.2.3 Flexural and Shear Reinforced Specimens	43
4.3 Strain Measurements	45
4.3.1 Control Specimens	46
4.3.2 Flexurally Reinforced Specimens	49
4.3.2.1 Cross-Sectional Strain	49
4.3.2.2 GFRP Flexural Bar Strain Profile	54
4.3.3 Flexure and Shear Reinforced Specimens	55
4.3.3.1 Cross-Sectional Strain	55
4.3.3.2 Strain in the Flexural Bar for Group FD	58
4.3.3.3 GFRP Dowel Bar Strain	59

4.4	Failure Modes	60
CHAPTER 5	ANALYSIS OF TEST RESULTS	66
5.1	General	66
5.2	Analysis of the Results for the Current Study	67
5.2.1	Modulus of Elasticity	67
5.2.2	Ultimate Load and Tensile Stress	68
5.2.3	Shear Stress	74
5.2.4	Compressive Stress	78
5.2.5	Reliability Analysis	80
5.3	Analysis of the Results for the Combined Data	86
5.3.1	Modulus of Elasticity for the Combined Data	86
5.3.2	Strength Results of the Combined Data Set	89
5.4	Strength Models	97
5.4.1	Plain and Flexurally Reinforced Strength Models	99
5.4.2	Strength Model using Modified Stress Distributions	104
CHAPTER 6	SUMMARY AND CONCLUSIONS	110
REFERENCES	112
APPENDIX A	115
APPENDIX B	118
APPENDIX C	142

LIST OF TABLES

Table 2.1 – Typical Mechanical Properties of Fibres (ISIS Canada 2001)	5
Table 2.2 – Typical Properties of Thermosetting Resins (ISIS Canada 2001).....	6
Table 2.3 – Mechanical Properties of Commercially Available FRP Reinforcing Bars (ISIS Canada 2001).....	7
Table 3.1 – Grading Rules for all Species No. 1 Structural Beams and Stringers.....	29
Table 3.2 – Allowable Knot Sizes	29
Table 3.3 – Stringer Description.....	34
Table 4.1 –Failure Modes of Tested Beams	64
Table 4.2 – Failure Modes of Individual Stringers	65
Table 5.1 – Test Results for Load, MOE, and Tensile Stress	70
Table 5.2 – Parameters of Weibull Analysis	73
Table 5.3 – Shear Stresses	77
Table 5.4 – Compressive Stresses.....	79
Table 5.5 – Mean and Standard Deviation of the Moment Resistances and Applied Moments	83
Table 5.6 – Safety Factors for a CL-625 Truck Loading.....	83
Table 5.7 – Safety Factors for a CL-700 Truck Loading.....	84
Table 5.8 – Number of Stringer used for Statistical Analysis by Type and Author	90
Table 5.9 – Details of Beams used in Statistical Analysis.....	90
Table 5.10 – Weibull Parameters from Combined Data Set Analysis.....	94
Table 5.11 – Size Effect Factors to Obtain Equivalent Sized Stringers to the Current Study	96
Table 5.12 - Weibull Distribution Parameters for Select Structural Douglas-Fir (Barrett and Lau 1994)	98
Table 5.13 - Sizes of the Tension and Compression Specimens (Barrett and Lau 1994). ..	98
Table 5.14 - Length and Depth Factors for Tensile and Compression Strengths (Barrett and Lau 1994)	98
Table 5.15 - Modulus of Elasticity Results (Barrett and Lau 1994).....	98

LIST OF FIGURES

Figure 2.1– Typical Stress-Strain Relationship for the Fibres, Matrix, and FRP (ISIS Canada 2001)	4
Figure 2.2 – Tension Stress Distribution (Buchanan 1984).....	16
Figure 2.3 – Bi-linear Stress versus Strain Curve (Buchanan 1990).....	18
Figure 2.4 – Stress and Strain Distributions (Buchanan 1984).....	19
Figure 3.1 – Dapped End of Timber Stringer	27
Figure 3.3 – Timber Stringer Reinforcement Details	32
Figure 3.4 – Machining of the Grooves for the Flexural Bars Using Hand Router.....	32
Figure 3.5 – Drilling of Holes for Dowel Bars	33
Figure 3.6 – Test Setup	35
Figure 3.7 – Details of Stringer Instrumentation	36
Figure 4.1 – Load Deflection Curves for Control Specimens 1 through 4	39
Figure 4.2 – Load Deflection Curves for Control Specimens 5 through 8	39
Figure 4.3 – Load Deflection Curves for Flexurally Reinforced Specimens 1 through 5	41
Figure 4.4 - Load Deflection Curves for Flexurally Reinforced Specimens 6 through 10	41
Figure 4.5 – Raw Data Load Deflection Curves for Flexurally Reinforced Specimens 1 through 5	43
Figure 4.6 – Load Deflection Curves for Flexural and Shear Reinforced Specimens 1 through 3	44
Figure 4.7 – Load Deflection Curves for Flexural and Shear Reinforced Specimens 4 through 6	45
Figure 4.8 - Cross-Sectional Strain Profile for C1-4 at 40 kN Load Level	47
Figure 4.9 – Cross-Sectional Strain Profile for C5-8 at 40 kN Load Level.....	47
Figure 4.10 – Cross-Sectional Strain Profile for C8 for Increasing Load	48
Figure 4.11 – Cross-Sectional Strain Profile for F1-5 at 40 kN Load Level	49
Figure 4.12 – Cross-Sectional Strain Profile for F6-10 at 40 kN Load Level and Pi and Strain Gauge Locations.....	50
Figure 4.13 – Pre-existing Crack and Knot Pattern for Stringers F1 and F2.....	51
Figure 4.14a) - Cross-Sectional Strain Profile for F5 for Increasing Load	52
Figure 4.14b) - Cross-Sectional Strain Profile for F5 for Increasing Load	53
Figure 4.15 – GFRP Flexural Bar Strain Profile for F5	54
Figure 4.16 – Cross-Sectional Strain Profile for FD1-3 at 40 kN Load Level	56
Figure 4.17 – Cross-Sectional Strain Profile for FD4-6 at 40 kN Load Level	57
Figure 4.18 – Cross-Sectional Strain Profile for FD3 for Increasing Load	57
Figure 4.19 – GFRP Flexural Bar Strain Profile for FD3	58
Figure 4.20 – GFRP Dowel Bar Strain Profiles for Stringer FD3	59
Figure 4.21 – Dap Failure	61
Figure 4.22 – Shear Failure.....	62
Figure 4.23 – Tension Failure	63
Figure 4.24 – Bearing Failure	63
Figure 5.1 - MOE Results of Current Study	68
Figure 5.2 – Cumulative Normal Distribution for the Ultimate Loads of the Current Study	71

Figure 5.3 - 3 Parameter Weibull Probability Results for the Tensile Stress for the Current Study	73
Figure 5.4 – Shear Stress for the Current Study	75
Figure 5.5 – Compressive Stress Distribution for the Current Study	79
Figure 5.6 – Reliability Analysis Example	81
Figure 5.7 – Stringer Configuration for Typical Bridge	81
Figure 5.8 – Normal Distributions of the Moment Resistances and the CL-625 Load Effects	85
Figure 5.9 - Normal Distributions of the Moment Resistances and the CL-700 Load Effects	85
Figure 5.10 – MOE Results for the Combined Data Set.....	86
Figure 5.11 – Length Effect on MOE (Madsen 1992).....	87
Figure 5.12 - MOE Trend for Timber Beams of Different Lengths	88
Figure 5.13 - Combined Modulus of Rupture Histogram.....	92
Figure 5.14 – Combined 3-parameter Weibull Probability Results for MOR Adjusted to a 38x256 mm size	93
Figure 5.15 – Comparison of CWC No.1 Grade Results and the Combined Data for Control Stringers.....	95
Figure 5.16 – Weibull Distribution for Combined Data Set Showing the CSA Design Value 19.5 MPa	96
Figure 5.17 – Strength Results for the Analysis of the Control Specimens	99
Figure 5.18 - Strength Results for the Analysis of the Flexurally Reinforced Specimens with $\alpha=1.3$	101
Figure 5.19 – Strength Results for the Analysis of the Flexurally Reinforced Specimens with $\alpha=1.1$	102
Figure 5.20 - Strength Values for Flexural and Shear Reinforced Specimens with $\alpha=1.3$	
Figure 5.21- Strength Values for Flexural and Shear Reinforced Specimens with $\alpha=1.6$	103
Figure 5.22 – a) Cross-section b) Axial Tension Stress Distribution of Reinforced Section	104
Figure 5.23 – Strength Results for the Flexurally Reinforced Timbers Stringers using the Modified Stress Distribution Equation	107
Figure 5.24 –Strength Results for the Flexural and Shear Reinforced Timber Stringers using the Modified Stress Distribution Equation.....	108
Figure 5.25 - Strengths of Flexural and Shear Reinforced Timber Stringers using the Modified Stress Distribution Equation and a Factor of 1.5	109

LIST OF SYMBOLS

a	distance between two symmetrical loading points
A'	area from the top of the member to the location of at which the shear stress is to be calculated
A_b	bearing area
A_{frp}	area of FRP reinforcement
b	width of a timber beam
c	ratio of the depth to the neutral axis over the overall depth
C_{tot}	total compressive force
d	depth of a timber stringer
d_b	diameter of the reinforcing bar
d_{CWC}	depth of the timber beam used for testing by the Canadian Wood Council
d'	depth of a single element within the beam
E	modulus of elasticity
E_{frp}	modulus of elasticity of the FRP reinforcement
E_w	modulus of elasticity of a timber beam
f_c	compressive stress
f_{cu}	compressive strength
f_m	bending strength
f_t	tension stress
f_{tu}	axial tensile strength
$F(x)$	cumulative Weibull probability
I	moment of inertia
I_{tr}	transformed moment of inertia
k	shape parameter
k_1	length factor as determined by the Canadian Wood Council
k_2	depth factor as determined by the Canadian Wood Council
k_3	shape parameter (stress-distribution parameter)
L	length of the timber beam in question
L_{CWC}	length of the timber beam used for testing by the Canadian Wood Council
L_e	equivalent length of the timber beam in question
M	moment
$Mean$	arithmetic mean
MOR	modulus of rupture
$MOR_{adjusted}$	modulus of rupture after the effects of depth and load configuration have been accounted for
m_1	scale parameter
n	modular ratio of GFRP bar and timber
P	applied load
P_5	5 th percentile value
Q	shear coefficient $A'y'$
S_b	section modulus of bottom of the timber beam
SD	standard deviation
T_{tot}	total tensile force
V	shear force

x	strength of a timber stringer
x_0	location (minimum strength) parameter
x_1	failure stress of a timber stringer one
x_2	failure stress of a timber stringer two
y	depth co-ordinate
y'	distance from the centroid of A' to the location at which the shear stress is to be calculated
y_b	distance from the tension face to the neutral axis
y_{bfrp}	distance from the tension face to the center of the FRP bars
z	standard normal random variable
α	factor to adjust the strength of a plain timber beam to account for the addition of reinforcement
β	safety factor for bridge components
μ_R	mean of the resistance forces
μ_S	mean of the applied forces
σ_c	compressive stress
σ_R	standard deviation of the resistance forces
σ_S	standard deviation of the applied forces
τ	shear stress

ACKNOWLEDGEMENTS

The author would like to acknowledge the financial support provided by ISIS Canada Network of Centres of Excellence and the Manitoba Department of Transportation and Government Services, Bridges and Structures Branch, and the National Science and Engineering Research Council.

The strengthening of the stringers was completed by Specialty Construction Products, Winnipeg, Manitoba, Canada. The technical staff of the structures laboratory of the Department of Civil Engineering at the University of Manitoba is also gratefully acknowledged for their technical support.

ABSTRACT

The provincial government of Manitoba is responsible for approximately 750 timber bridges, 225 to 250 of which are located on RTAC routes. These bridges have been in service for over 50 years. During this time weathering effects have degraded the timber stringers as well as the allowable truck traffic loads have increased. The combination of these two effects raises some questions as to the current capacity of the timber stringers used in the bridges. Since the cost of replacing the timber bridges with current methods of rehabilitation is too high, approximately \$42,750,000, an economical rehabilitation method is necessary.

The use of glass fibre reinforced polymer (GFRP) bars as reinforcement has been studied as a possible rehabilitation scheme for timber stringers. The approximate cost to rehabilitate the timber bridges with the GFRP bars is approximately 15% of the bridge replacement cost.

Salvaged Douglas fir, timber stringers (100 x 400 x 3400 mm) with dapped ends were tested using flexural reinforcement only and flexural and shear reinforcement. Previous studies in this area did not use dapped timber stringers but rather rectangular sections and thus were not susceptible to dap failures. It was determined that the use of just flexural reinforcement did not obtain the required strength increase of 30%, detailed by Eden (2002). This was a result of dap and shear modes of failure dominating and thus the flexural bars could not inhibit these forms of failure. The use of both flexural and shear reinforcement is required to obtain the desired strength increase. By using both the flexural and shear reinforcement a strength increase of 30 to 66% can be obtained.

A model using the material properties of the flexural reinforcement and the timber stringer was also developed in this thesis and was determined to give very good correlation between the predicted and measured tensile stress results.

CHAPTER 1 INTRODUCTION

1.1 General

Hundreds of timber bridges throughout North America are approaching or have surpassed their service lives. Since the construction of these bridges the allowable truck loads have been increased several times. Thus, the timber bridges must not only be restored to their original capacities but must also have their capacities increased to ensure safe handling of today's truck traffic. With the continued depletion of trees, lumber and timbers are becoming more scarce and costly; it would be impractical to replace current timber bridges with another timber bridge. The current grading standards are not as stringent as they were when the bridges were first constructed. Current select structural grades would have been graded as No.1 at the time of the original construction of the bridges. The costs of building bridges using current designs employing such materials as concrete and steel would be much too costly considering the sheer volume of bridges which are in need of repair or rehabilitation. The provincial government of Manitoba is responsible for approximately 750 timber bridges, 225 to 250 of which are located on the Roads and Transportation Association of Canada (RTAC) routes (Eden 2002). To replace a timer bridge with current bridge construction methods such as multi-plates and corrugated pipes or pre-cast pre-cut concrete, it would cost approximately \$1500 per square meter of road surface (Eden 2002). If the standard road surface area of a bridge is 120 m^2 the estimated cost of the bridge replacement is \$180,000. It would thus be impractical to replace all the bridges on the RTAC routes due to the prohibitive cost of

\$42,750,000. Thus a rehabilitation scheme is required to increase the capacity of the bridges and extend their service lives beyond their current limits.

Previous research in this area has included the strengthening of bridge stringers for flexure by using glass fibre reinforced polymer (GFRP) bars embedded in grooves in the tension zone (Gentile et al. 2002). A shear strengthening scheme using dowel bars perpendicular to the beam axis has also been investigated (Svecova and Eden 2004). These processes have been proven to be effective rehabilitation schemes and very cost competitive with other more traditional methods of rehabilitation or construction (Eden 2002).

1.2 Problem Definition

All previous research for strengthening timber bridge stringers with GFRP bars have been on strictly rectangular cross-sections. It is unknown how a dapped timber stringer reinforced with GFRP bars will perform. Since the majority of the timber stringers used in bridge construction in Manitoba have dapped ends, it is necessary to determine the expected capacity increase when the GFRP bar rehabilitation method is used.

1.3 Objectives and Scope

The main objective of this study is to assess the strength of dapped timber stringers (400 x 100 x 3400 mm) reinforced with GFRP bars in order to provide a 30%

increase in flexural and shear capacity. The test data will be used to formulate a design equation to quantify the flexural strength increases that can be achieved.

Svecova and Eden (2004) state a 30% increase in the flexural and shear capacity is required in order to support the current maximum legal truck loads allowed by Transportation Association of Canada (TAC). The same strength increase was targeted in this experimental program.

The experimental program will test only Douglas fir timber stringers under monotonic, three point loading, and will use GFRP bars only for reinforcement.

CHAPTER 2 PREVIOUS RESEARCH

2.1 General

This chapter will briefly discuss FRP materials and their properties, timber, and timber strengthening systems including the use of FRP materials, and analysis of timber beams.

2.2 Fibre-reinforced Polymer Reinforcement

FRP materials consist of two primary components, the fibres and matrix (or resin). The fibres and the matrix have very different properties and as such the final FRP material can be tailored to best fit the end use requirements. Figure 2.1 displays the stress-strain relationships for the fibres, matrix and the final product of the two, FRP material.

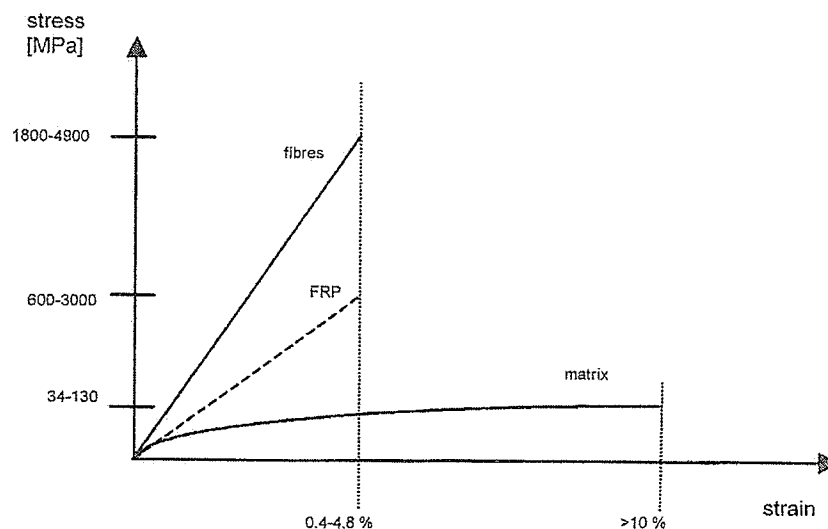


Figure 2.1– Typical Stress-Strain Relationship for the Fibres, Matrix, and FRP (ISIS Canada 2001)

As seen in Figure 2.1 the fibres are of very high tensile strength but brittle and the matrix is of low tensile strength but is capable of reaching very high strain values. The stress-strain relationship of the final product lies between the relationship of the two constituents, and the final stiffness depends on the amount and type of fibre used.

There are many different kinds of fibres available for use, such as, aramid, carbon, and glass. The performance of the fibres is affected by length, cross-sectional shape and chemical composition. Table 2.1 gives some of the typical mechanical properties of individual fibres.

Table 2.1 – Typical Mechanical Properties of Fibres (ISIS Canada 2001)

Fibre Type		Tensile Strength (MPa)	Modulus of Elasticity (GPa)	Elongation (%)	Coefficient of Thermal Expansion ($\times 10^{-6}$)	Poisson's Ratio
Carbon						
Pan	High Strength	3500	200-240	1.3-1.8	(-1.2) to (-0.1)	-0.2
	High Modulus	2500-4000	350-650	0.4-0.8	(α_{fpL}) 7 to 12 (α_{fpT})	
Pitch	Ordinary	780-1000	38-40	2.1-2.5	(-1.6) to (-0.9)	N/A
	High Modulus	3000-3500	400-800	0.4-1.5	(α_{fpL})	
Aramid						
Kevlar 29		3620	82.7	4.4	N/A	0.35
Kevlar 49		2800	130	2.3	-2.0 (α_{fpL}), 59 (α_{fpT})	
Kevlar 129		4210 (est.)	110 (est.)	--	N/A	
Kevlar 149		3450	172-179	1.9	N/A	
Twaron		2800	130	2.3	(-2.0) (α_{fpL}), 59 (α_{fpT})	
Technora		3500	74	4.6	N/A	
Glass						
E-Glass		3500-3600	74-75	4.8	5.0	0.2
S-Glass		4900	87	5.6	2.9	0.22
Alkali Resistant Glass		1800-3500	70-76	2.0-3.0	N/A	N/A

From Table 2.1, glass fibres that will be used in this investigation can obtain a tensile strength of 1800-4900 MPa with a modulus of elasticity (MOE) ranging from 70 to 87 GPa. The glass fibres have small thermal expansion coefficients and thus changes in temperature have little effect on the fibres, but may introduce residual stresses in the matrix.

Another component of FRP is the matrix, or resin. The physical and thermal properties of the matrix significantly affect the final product and must be chosen carefully. The function of the matrix is to coat the fibres, protect the fibres from mechanical abrasion, transfer stresses between the fibres, transfer inter-laminar and in-plane shear in the composite, and laterally support the fibres against buckling when subjected to compressive loads. There are two types of resins, thermosetting and thermoplastic.

Thermosetting polymers are low molecular weight liquids with very low viscosity, and their molecules are joined together by chemical cross-links. They form a rigid three-dimensional structure that once set, cannot be reshaped by applying heat or pressure. However these resins obtain relatively low strain to failure, resulting in low impact strength. Table 2.2 displays typical properties of thermosetting resins.

Table 2.2 – Typical Properties of Thermosetting Resins (ISIS Canada 2001)

Resin	Specific Gravity	Tensile Strength (MPa)	Tensile Modulus (Gpa)	Cure Shrinkage (%)
Epoxy	1.20-1.30	55.00-130.00	2.75-4.10	1.00-5.00
Polyester	1.10-1.40	34.50-103.50	2.10-3.45	5.00-12.00
Vinyl Ester	1.12-1.32	73.00-81.00	3.00-3.35	5.40-10.30

Thermoplastic matrix polymers are made from molecules, which are linear in structural form. They are held in place by weak secondary bonds and as such can be destroyed by heat or pressure. Therefore, thermoplastic resins can be reshaped with the addition of heat or pressure but their mechanical properties degrade with each reshaping event. Most of the FRP bars used in civil engineering applications are made from thermosetting matrices.

FRP reinforcing bars are manufactured from continuous fibres (such as carbon, glass, or aramid) embedded with in a resin (thermosetting or thermoplastic). FRP reinforcing bars can be manufactured in various diameters and with various surface finishes such as spiral, straight, sanded-straight, sanded-braided, and deformed. The mechanical properties of some of the commercially available FRP reinforcing bars are presented in Table 2.3.

Table 2.3 – Mechanical Properties of Commercially Available FRP Reinforcing Bars (ISIS Canada 2001)

Trade Name	Tensile Strength (MPa)	Modulus of Elasticity (Gpa)	Ultimate Tensile Strain
Carbon Fibre			
Leadline	2250	147.0	0.015
ISOROD	1596	111.1	0.023
NEFMAC	1200	100.0	0.012
Glass Fibre			
ISOROD	690	42.0	0.018
C-Bar	770	37.0	0.021
NEFMAC	600	30.0	0.020

2.3 Timber

Timber is a natural material and as such has many growth abnormalities not found in other manufactured building materials. Forest Products Laboratory (1999) has a vast amount of information on wood and timber, and is the source of much of the information gathered about the timber material in this section.

Timber is an orthotropic material, and as such, it has unique and independent mechanical properties in the directions of three mutually perpendicular axes: longitudinal, radial, and tangential. The strength properties of timber are different in all directions such that the compressive strength parallel and perpendicular to the grain are different. Some of the natural characteristics affecting the mechanical properties of timber are specific gravity, knots, slope of the grain, and annual ring orientation.

The specific gravity of timber is approximately 1.5, regardless of timber species, but dry timber of most species floats on water. Thus, the volume of a piece of wood is occupied by cell cavities and pores. The specific gravity is an excellent index of the amount of wood substance contained in the timber, as long as the sample is clear, straight grained, and free from defects.

A knot is the portion of the branch, which becomes integrated with the trunk or bole of the tree. A knot creates a location of discontinuity in the timber and thus affects the mechanical properties. A knot effect depends on the size, location, shape, and soundness of the timber.

The grain creates planes of weakness and as such depending on its orientation could cause premature failure.

Depending on the angle of loading, the orientation of the growth ring could lower the mechanical properties of the timber by 40 to 60%.

Size Effects of Timber Beams

The primary size effects are the load configuration effect and the depth effect. The width does not appear to affect the strength of a timber beam. The size effects were recognized and quantified by Madsen and Buchanan (1986).

The load configuration effect includes the length of the beam and type of loading used during testing. By applying the load configuration effect an equivalent length is determined, which is a reduction in the actual length and represents the highly stressed portion of the beam. This is the portion of the beam carrying most of the load and is affected by how the load is applied. The equivalent length for a four-point bending scheme is given by

$$[2.1] \quad L_e = \frac{1 + \frac{a}{L} k_1}{1 + k_1} L$$

where L_e is the equivalent length, a is the distance between two concentrated loads, L is the simply supported span of the beam and k_1 is the length effect factor and was determined by Barret and Lau (1994) in an extensive testing program for the Canadian Wood Council (CWC).

The equivalent length for a three point bending scheme is given by

$$[2.2] \quad L_e = \frac{1}{1 + k_1} L$$

where all terms are the same as in equation 2.1 with $a = 0$.

The effect of the beam depth on the strength of the timber beam is given by

$$[2.3] \quad \frac{x_1}{x_2} = \left(\frac{d_2}{d_1} \right)^{\frac{1}{k_2}}$$

where x_1 and x_2 are failure stresses of members with depths d_1 and d_2 respectively. k_2 is the depth effect factor and can be determined in the same fashion as k_1 , using data published by the Barrett and Lau (1994)

Using the newly found stressed length L_e , and the depth of the tested beams, the adjusted modulus of rupture (MOR) value can be determined according to

$$[2.4] \quad MOR_{adjusted} = MOR \left(\frac{L_{CWC}}{L_e} \right)^{\frac{1}{k_1}} \left(\frac{d_{CWC}}{d} \right)^{\frac{1}{k_2}}$$

where the MOR is experimentally determined, L_{CWC} and d_{CWC} are the span and characteristic depth of the reference beam as per Barrett and Lau (1994). Further, in Equation 2.4 the values for d and L_e are the depth and equivalent length of the experimental beam. The size effect factors for length and depth in Equation 2.4 are

given by $\left(\frac{L_{CWC}}{L_e} \right)^{\frac{1}{k_1}}$ and $\left(\frac{d_{CWC}}{d} \right)^{\frac{1}{k_2}}$, respectively.

2.4 Timber Strengthening

Lantos (1970) completed an experimental program on glulam beams reinforced with steel bars. A substantial reduction in the coefficient of variation was reported as well as an increase in strength directly proportional to the amount of reinforcement used in the beams. Round steel reinforcement having a diameter greater than 12.7 mm displayed a tendency for early bond failure. The modulus of elasticity (MOE) also increased in direct proportion to the amount of steel reinforcement provided. Glulam

beams with lower elastic modulus experienced a greater increase in strength and stiffness than glulam beams of higher elastic modulus. While significant increases in strength and stiffness can be achieved, problems encountered with using metallic reinforcement to reinforce wood beams are generally related to incompatibilities between the wood and metal (Dagher and Lindyberg 2000). Such incompatibilities are the differences between the hygral-expansion and stiffness of the wood and metallic-reinforcing material. These differences can lead to separation or tension failure at or near the glue-line.

Johns and Lacroix (2000) used carbon fibre reinforced polymer (CFRP) and GFRP sheets to reinforce timber beams. The CFRP was applied on the tension face of the beam in two layers and GFRP sheets were applied in a U-shaped manner in two layers. Specimens used in this study had cross-sectional dimensions of 39 x 89 mm (two-by-four) and a test span of 1500 mm. This testing program found the strength of the timber specimens to be higher than that predicted by simple transformed section analysis. The weakest beams had a 40% gain in strength, but the stiffness and deflection results were as predicted. The U-shaped GFRP reinforcement eliminated weaker failures often present, even in higher strength boards.

Tingely (1996) reports that a 25-30% net economical saving is gained when FiRP™ Panels are used in the manufacturing process of glue laminated wood beams. The added strength allows lower grades of wood to be used as laminations while still maintaining conventional stress grades.

Dagher and Abdel-Magid (1994) reinforced 38 x 89 x 1219 mm Hemlock beams with CFRP sheets and aramid fibre reinforced polymer (AFRP) sheets with the trade name Kevlar. The CFRP reinforced specimens exhibited a 9% increase in the flexural

modulus and 31.5% increase in the average ultimate load. The initial mode of failure was vertical cracking in the compression zone, which propagated down causing horizontal cracking, delamination of the wood near the neutral axis and eventually sudden failure of the CFRP sheet. The AFRP reinforced specimens demonstrated negligible increases in the flexural modulus however noticeably increased the ductility of the beams. An 18% increase in the load capacity of the beams was obtained.

Gentile et al. (2002) tested twenty-two, 100 x 300 x 4300 mm long, creosote treated Douglas Fir timber beams in four-point bending. The beams had reinforcement ratios of 0, 0.27, 0.41, and 0.82 percent. A 20 to 50% increase in flexural strength was obtained and depended primarily on the quality of the timber beams. The higher the quality of the plain timber beams the lower the strength increase. The strengthened beams failed in a ductile manner and the reinforcement reduced the variability of the timber beam strength.

Svecova and Eden (2004) tested timber beams reinforced with GFRP dowel bars as shear reinforcement as well as flexural bars to control the tension failures observed in some of the specimens. The beams used in that study were cut from full size timber bridge stringers (200 x 600 x 10000 mm) to a size of 100 x 300 x 2000 mm. The test span for these specimens was 1.8 m. After cutting the specimens, they had creosote treatment on the top and bottom surfaces only. Through testing, a shear dowel spacing equal to the depth of the section was determined to be the most cost effective and a 33% increase in the MOR was observed. Beams reinforced with both flexural and shear reinforcement experienced 47 to 52% increase in the MOR.

2.5 Timber Strength Models

To date there are two timber strength models of interest, one for determining the strength of plain timber beams (Buchanan 1984) and the other for determining the strength of GFRP reinforced timber beams (Gentile 2000).

2.5.1 Plain Timber Strength Model

Based on the work of Buchanan (1984) the following strength model for plain timber beams was developed.

ASSUMPTIONS

- Plane sections before bending remain plain after bending
- Timber stressed in tension behaves in a linear elastic manner
- Timber stressed in compression behaves in a non-linear fashion as shown in Figure 2.3
- Stress-strain relationships are independent of the rate of loading
- Axial tension and compression strengths decrease as the length of the member increases
- The maximum tension or compression stress attainable at a given cross section is proportional to the area of that section subjected to the given stress
- Failure occurs at the cross section subjected to maximum moment
- The modulus of elasticity is constant along each member
- Torsional or out-of-plane deformations are not considered

The strength model fits tested beams into a previously determined strength distribution. The strength distribution used was determined by Barrett and Lau (1994) after many tests were completed on various species of timber. The mean and 5th percentile MOE values, as determined by Barrett and Lau (1994) for each species, are used to place the beam in question in the normal probability distribution of the MOE. The MOE results for timber beams fit a normal probability distribution very well (Barrett and Lau 1994). Using equation 2.5, the 5th percentile and the mean MOE values determined from Barrett and Lau (1994) can be used to calculate the standard deviation in order to fit the experimental data to a normal distribution.

$$[2.5] \quad P_5 = Mean - 1.645(SD)$$

where: P_5 is the 5th percentile MOE value (from the CWC)

Mean is the mean value of the MOE (from the CWC)

SD is the standard deviation (unknown)

Using the MOE of the beam in question and the standard deviation from Equation 2.5 the standard normal random variable will be calculated using equation 2.6.

$$[2.6] \quad E_w = Mean + z(SD)$$

where: E_w is the MOE of the beam in question

Mean is the mean value of the MOE for a given species (from the CWC)

SD is the standard deviation (determined by using equation 2.5)

z is the standard normal random variable (to be determined using equation 2.6)

With the known standard normal random variable, z , the table of standard normal curve areas (Montgomery et. al. 1998) can be entered to determine the corresponding probability. This probability is then used to place the beam in a Weibull strength

distribution from which the initial ultimate tensile and compressive strengths of the beam are determined (Gentile 2000). Equation 2.7 gives the equation for the three-parameter Weibull distribution.

$$[2.7] \quad F(x) = 1 - e^{\left(-\left(\frac{x-x_0}{m_1}\right)^k\right)}$$

where: $F(x)$ is the cumulative Weibull probability

- x strength (MPa)
- x_0 location (minimum strength) parameter
- m_1 scale parameter
- k shape parameter

To determine the ultimate tensile strength (UTS) and the ultimate compressive strength (UCS) the Weibull parameters determined by Barrett and Lau (1994) for a particular species and grade of timber were used. The strength x , which represents the UTS or UCS, depending on which parameters are chosen can then be back calculated.

Equations 2.1 through 2.4 can be used to make the necessary size adjustments. In equation 2.4 the terms $MOR_{adjusted}$ and MOR are to be substituted with either UTS or UCS , depending on which term is to be calculated. Once all the size effects have been considered equation 2.7 can be used to back calculate the adjusted UTS and UCS .

To calculate the bending strength, f_m , of the timber beam, the stress-distribution effect must now be considered. The bending strength will become a ratio of the ultimate tension stress for pure tension and the tension stress obtained through bending. Figure 2.2 displays the tension stress distributions. According to Buchanan (1984), the two parameter Weibull distribution may be used and gives sufficiently accurate answers and

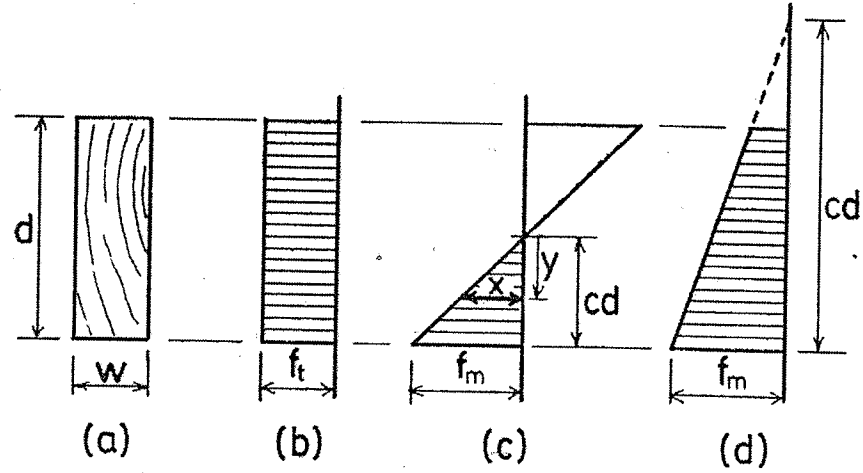


Figure 2.2 – Tension Stress Distribution (Buchanan 1984)

simplifies the calculation process. The two-parameter Weibull distribution takes the form presented in equation 2.8.

$$[2.8] \quad F(x) = 1 - e^{\left(-\frac{1}{d'} \int_d \left(\frac{x}{m} \right)^{k_3} dy \right)}$$

where: x is the failure stress

y is the depth co-ordinate

d' is the depth of a single element within the cross section of the beam

m is the scale parameter

k_3 is the shape parameter

k_3 will be referred to as the stress-distribution parameter. The integration only applies to the portion of the cross section stressed in tension.

For the case where the specimen is stressed in pure tension, as in Figure 2.2(b), equation 2.8 becomes

$$[2.9] \quad F(x) = 1 - e^{\left(-\frac{d}{d_1} \left(\frac{x}{m} \right)^{k_3} \right)}$$

For the case where the stresses vary linearly over the cross section due to bending, as shown in Figure 2.2(c) and (d), the following may be used

$$[2.10] \quad x = \frac{y}{cd} f_m \quad \text{or} \quad x = r f_m \quad \text{where} \quad r = \frac{y}{cd}$$

and

$$[2.11] \quad dy = cd(dr)$$

combining equations 2.8, 2.10, and 2.11, the two-parameter Weibull distribution takes the following form.

$$[2.12] \quad F(r f_m) = 1 - e^{-\left(\frac{cd}{d_1} \int_r \left(\frac{r f_m}{m} \right)^{k_3} dr \right)}$$

For loading conditions shown in Figure 2.2 (c) or (d) the extreme fibre stress at failure, f_m , can be calculated as a ratio of the axial tensile strength, f_{tu} . This strength corresponds to the adjusted *UTS* determined earlier. Thus equating and rearranging equations 2.8 and 2.12 gives

$$[2.13] \quad f_m = \frac{1}{\left(c \int_r r^{k_3} dr \right)^{\frac{1}{k_3}}} f_{tu}$$

For the case where the neutral axis is within the member as shown in Figure 2.2(c) f_m can be calculated if the integral in equation 2.13 is evaluated over a range of r values from 0 to 1 which corresponds to a range of y values of 0 to cd .

$$[2.14] \quad f_m = \left(\frac{k_3 + 1}{c} \right)^{\frac{1}{k_3}} f_{tu}$$

Equation 2.14 represents the tensile bending strength of a timber beam.

To determine the type of failure to be expected, and thus the true value of the parameter c , a strain compatibility analysis must be completed. For this analysis Figure 2.3 and 2.4 may be used. Figure 2.3 is an idealized stress strain relationship proposed by Buchanan (1990). This relationship is used to determine the slope of the descending branch (m) of the stress strain curve. Figure 2.4 is a variation of Figure 2.3 and is used during the strain compatibility analysis process.

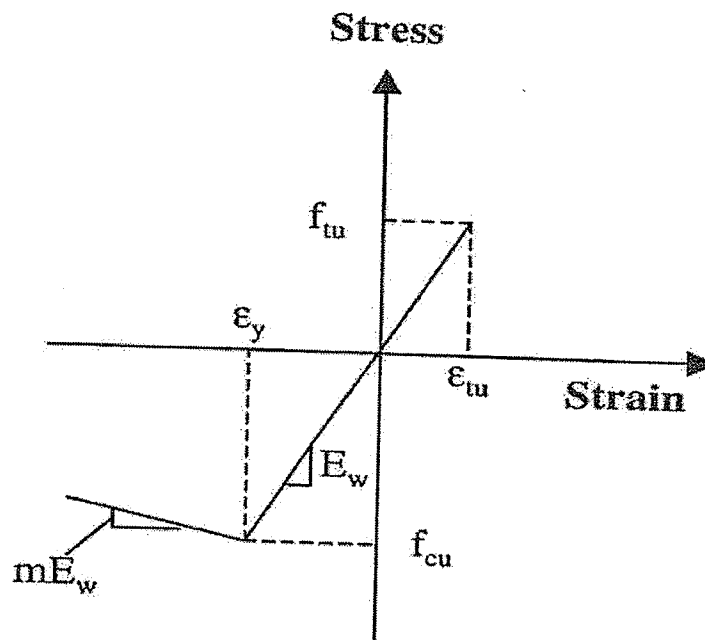


Figure 2.3 – Bi-linear Stress versus Strain Curve (Buchanan 1990)

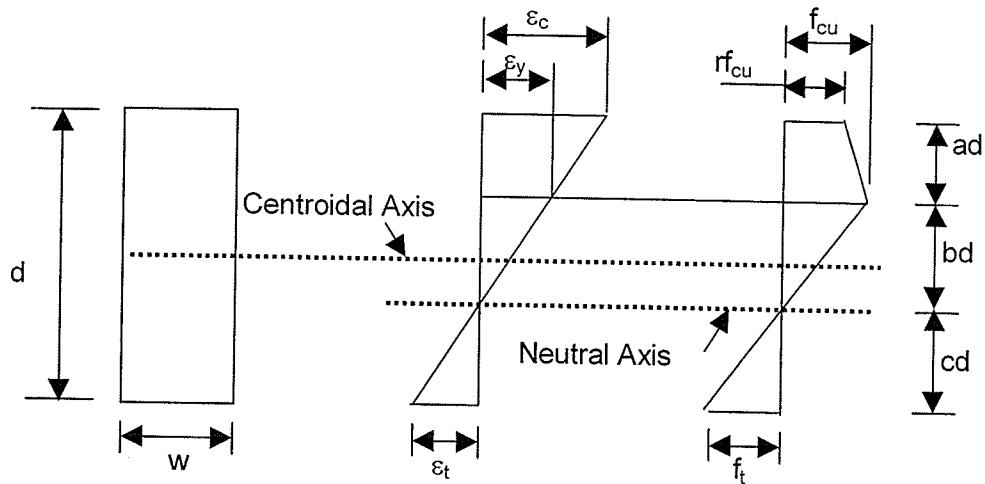


Figure 2.4 – Stress and Strain Distributions (Buchanan 1984)

For plain timber the inputs for the strain compatibility analysis are the width (b), the depth (d), the MOE of the timber (E_w), the ultimate tensile and compressive stresses (f_{tu} and f_{cu}), the slope of the descending branch (m) of the idealized stress-strain relationship seen in Figure 2.3, and the stress distribution parameter (k_3). Follow the steps outlined previously in section 2.5.1 to calculate f_m assuming $c=0.5$. The factor c is determined by taking the ratio of the distance from the tension face to the neutral axis and the overall depth of the beam. For plain timber the neutral axis depth is assumed to be the same as the centroidal axis depth until the compressive strains exceed the yield strain, at which time the stress distribution becomes bi-linear and the neutral axis shifts towards the tension face.

To begin the analysis, a tension strain is assumed and the tension stress (f_t) is calculated by multiplying the MOE of the timber beam by the assumed tension strain. The calculated tension stress is compared with f_m . For values of f_t smaller than f_m , the compressive stress f_c can be calculated. The value of the compressive stress is compared

to f_{cu} , and the curvature of the member is calculated if f_c is less than f_{cu} . If f_c is larger than f_{cu} the value of c must be decreased. The process just described must be repeated with the new value of c . In choosing a new c value a new tension strain is effectively chosen. The objective of this process is to obtain a f_t value which is equal to f_m such that f_c is less than f_{cu} and the total tension force (T_{tot}) is equal to the total compressive force (C_{tot}). Once the objective has been completed the ultimate moment and curvature can be determined.

Figure 2.5 displays a flowchart depicting the process of calculating the strength of a plain timber stringer, used later in this thesis to calculate the strength of plain timber stringers.

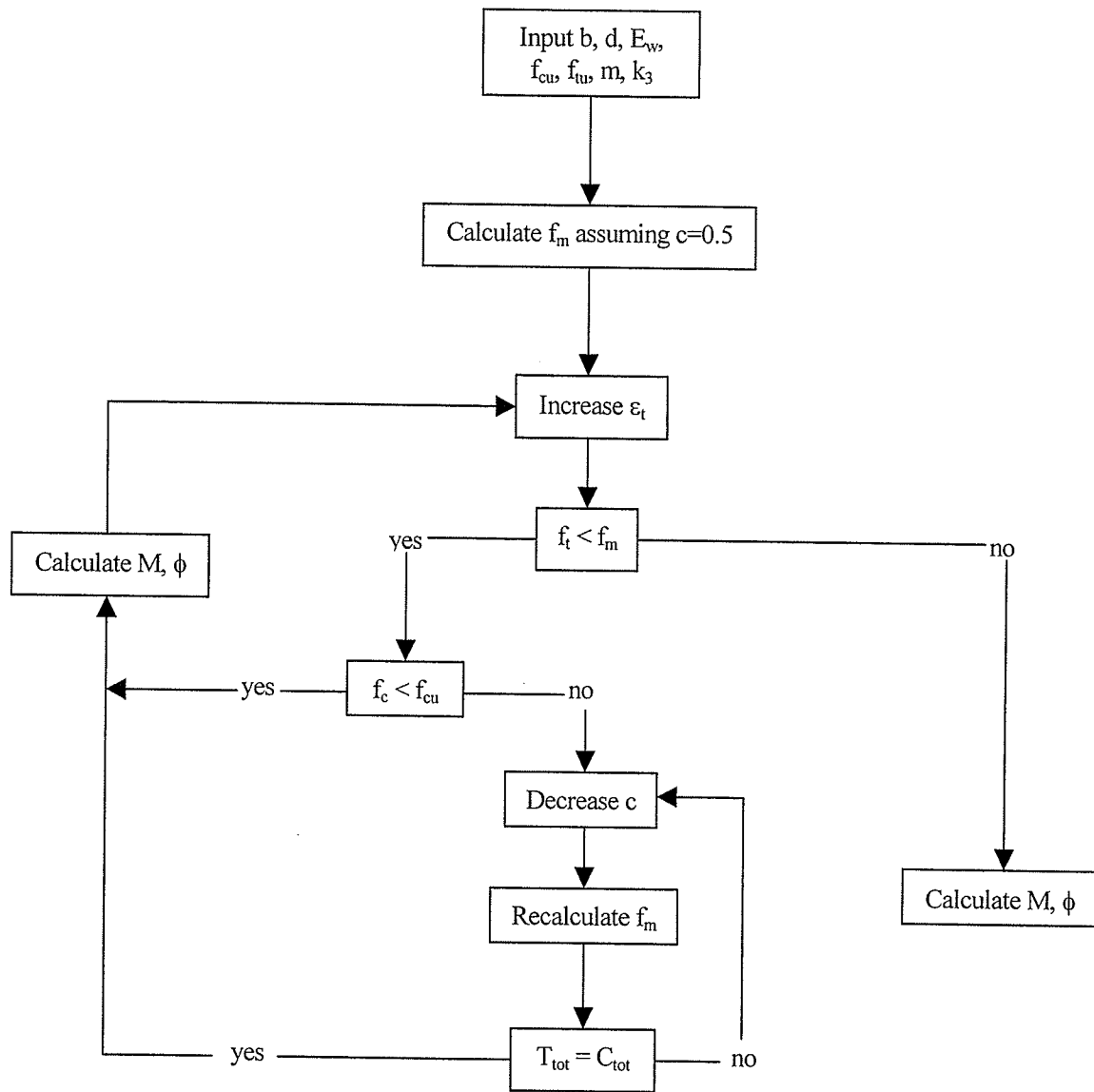


Figure 2.5 – Process of Calculating the Strength of a Plain Timber Beam

2.5.2 Reinforced Timber Strength Model

Gentile (2000) extended the use of the formulas developed by Buchanan (1984) for plain timber beams for GFRP reinforced timber by using a parameter α . The equation developed by Gentile (2000) is as follows

$$[2.15] \quad f_m = \alpha \left(\frac{k_3 + 1}{c} \right)^{\frac{1}{k_3}} f_{tu}$$

After fitting equation 2.14 to the experimental data for the control specimen, Gentile (2000) fit equation 2.15 to the experimental data for the reinforced specimen and arrived at an α factor of 1.3. This implies, with the addition of GFRP flexural reinforcement, an increase in strength of 30% over plain timber beams. The initial depth of the neutral axis is determined by completing a transformed section analysis. The distance from the tension face to the neutral axis can be calculated using equation 2.16.

$$[2.16] \quad y_b = \frac{bd \left(\frac{d}{2} \right) + (n-1)A_{frp}y_{b_{frp}}}{bd + (n-1)A_{frp}}$$

where: b is the width of the beam

d is the depth of the beam

n is the modular ratio, as in equation 2.17

A_{frp} is the area of FRP reinforcement

$y_{b_{frp}}$ is the distance from the tension face to the center of the FRP bars

$$[2.17] \quad n = \frac{E_{frp}}{E_w}$$

where: E_{frp} is the MOE of the FRP bars

E_w is the MOE of the timber beam

Other than the modifications just discussed the process of calculating the bending strength is the same as described in section 2.5.1. Figure 2.6 outlines, in a flowchart, the process for determining the strength of a timber beam reinforced flexurally with FRP bars. Failure of the FRP bar could, in theory, occur but is not considered a possible failure mode due to the high tensile strength of the GFRP compared to the timber. A computer program was developed to complete all the calculations for the plain and reinforced timber strengths. Sample of these calculations is presented in the Appendix A.

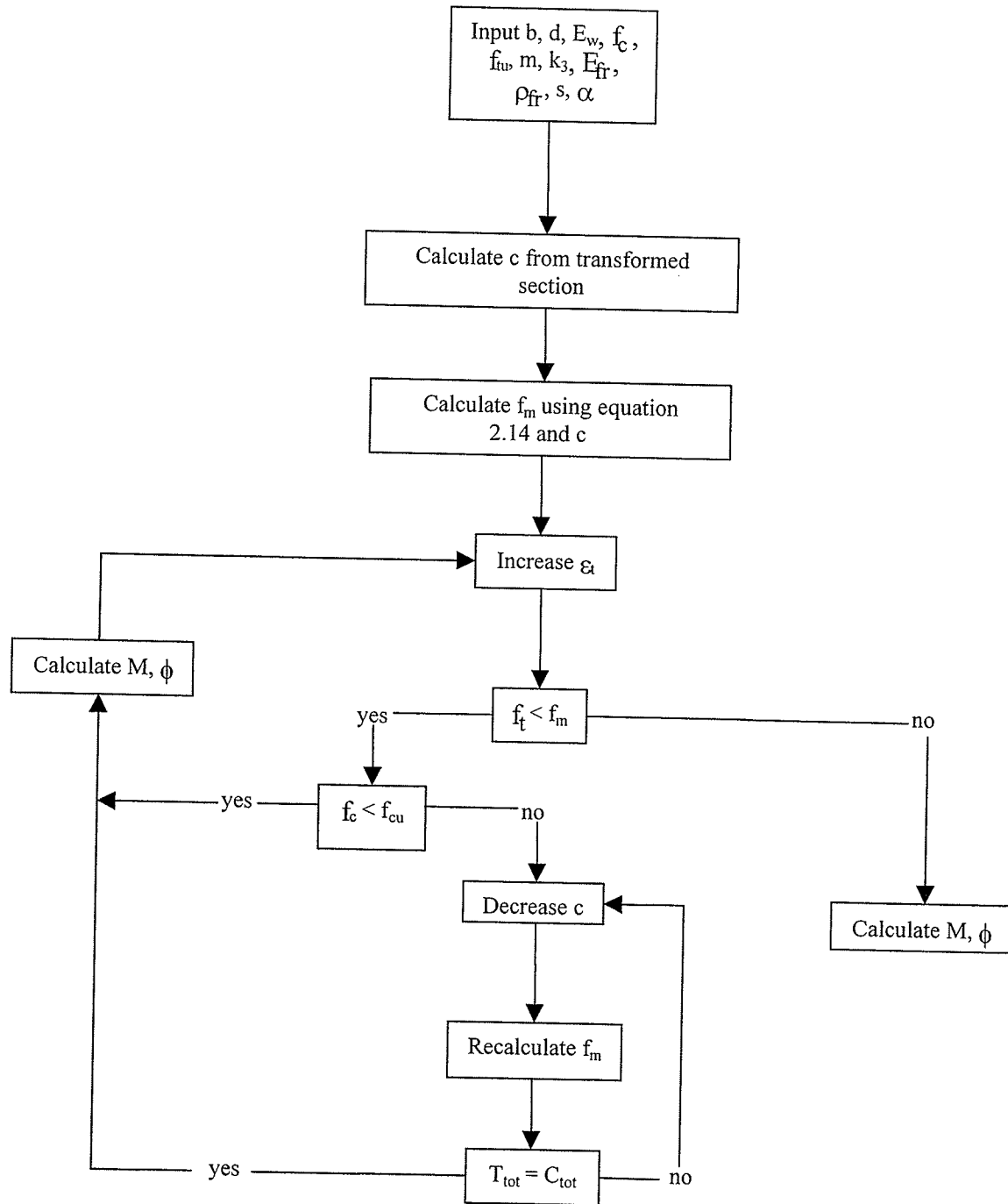


Figure 2.6 – Process of Calculating the Strength of a GFRP Reinforced Timber Beam

CHAPTER 3 EXPERIMENTAL PROGRAM

3.1 General

A total of 26 stringers were tested, 8 control, 12 reinforced for flexure only with GFRP bars, and 6 reinforced for flexure and shear with GFRP bars. Test data was collected using pi-gauges, strain gauges and LVDTs. The stringers were visually graded before testing using the National Lumber Grades Authority (2002) guidelines. The specimens were fabricated using a hand held router and drill and were tested statically under a three point loading scheme by using a servo-hydraulic, stroke controlled testing machine.

This chapter will discuss the material properties of all tested samples, the test set-up and instrumentation. The strengthening process will also be discussed in detail.

3.2 Objectives of the Experimental Program

The experimental program was designed to test the performance of dapped timber stringers reinforced with GFRP bars. Specific importance was placed on increasing the strength of the timber stringers by at least 30%. The dapped ends create stress concentrations and thus may cause premature failure of the beams, and will be addressed during testing if necessary. This is the first time dapped beams have been tested when strengthened with GFRP bars, and the objective of this research is to produce guidelines

for future use of GFRP strengthening for these beams. A strength model for GFRP reinforced timbers stringer was to be developed to be able to predict the strength of a reinforced timber stringer. The model was to use the properties of the GFRP bars and timber stringers to determine the strength increase as opposed to the current model (Gentile 2000), which uses a universal factor to account for strength changes between the reinforced and unreinforced timber stringers.

3.3 Materials

The materials used in this experimental program were timber stringers, GFRP bars, and epoxy.

3.3.1 Timber Stringers

Douglas fir timber bridge stringers, pressure treated with creosote and salvaged from dismantled bridges, were used in this experimental program. The stringers were unaltered in any way before the reinforcement was installed and testing took place. The estimated depth of creosote penetration was 19 mm. The stringers were visually graded according to the recommendations of National Lumber Grades Authority (2002). The grading scheme chosen for the specimens was applicable to beams and stringers (rectangular timbers) 127 mm and thicker, with the depth more than 50.8 mm greater than thickness. Although the stringers used in this study were only 101.6 mm thick, this section best described the stringers. Based on the grading recommendations for holes, skips, splits, wane, and knots the stringers were graded as No. 1, No.2 and reject. Further

information on the grading regulations for timber beams and stringers see section 3.4. None of the stringers retained the original select structural grade, since they have been subjected to many years of environmental and traffic loads.

The timber stringers used in this study have dapped ends, as shown in Figure 3.1. The dap is not considered in the design of the stringers but rather, is used to make the construction process easier.

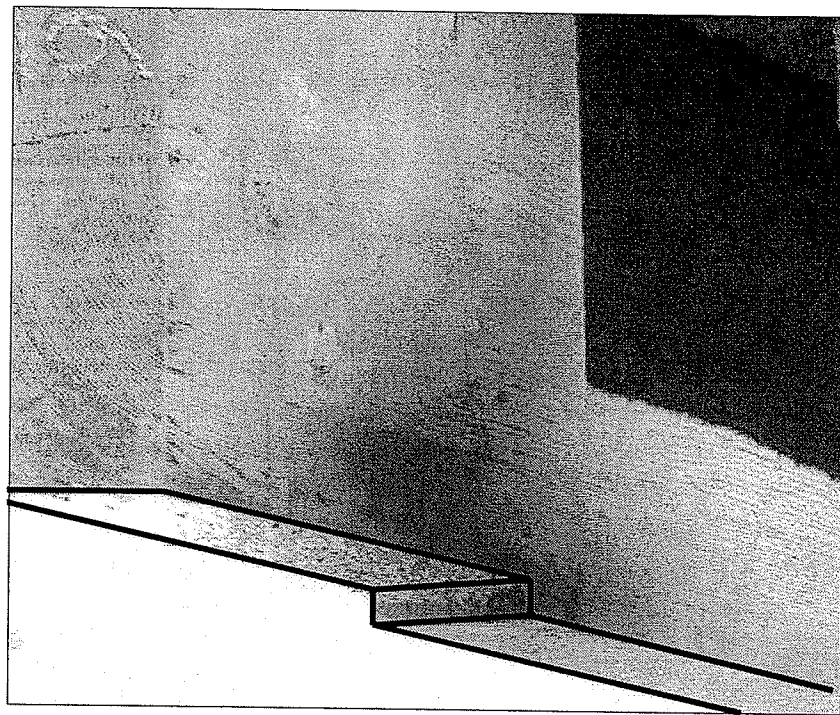


Figure 3.1 – Dapped End of Timber Stringer

The average moisture content for timber stringers was 15%. These readings were taken before testing and after. There was very little change if any over this timber period.

3.3.2 GFRP Bars and Epoxy

Pultruded 12 mm diameter Fulcrum GFRP bars were used as flexural reinforcement for all the beams. The GFRP bars had a strength of 895 MPa, a modulus of elasticity of 47.4 GPa, a glass volume of 56.3%, and a voids ratio of 0.95%. The mechanical properties of the GFRP bars discussed above are as reported by the manufacturer.

The shear reinforcement was pultruded #13 ISOROD GFRP bars. These bars had a strength of 617 MPa and a modulus of elasticity of 42 GPa, as reported by the manufacturer.

The epoxy used to bond the GFRP bars to timber was Tamms, Duralith, high modulus, low temperature epoxy mortar binder.

3.4 Standard Grading Rules for Timber Beams and Stringers

In this section the standard grading rules for timber beams and stringers meeting grade No. 1 is presented to demonstrate the process of visual grading. The following grading characteristics and provisions shown in Table 3.1 and 3.2 are based on the National Lumber Grades Authority (2002). The other grade levels have their own provisions and can be located in the National Lumber Grades Authority (2002). All tested beams were subjected to visual grading before testing. It was determined, from the 26 beams, 38% were No.1, 54% were No. 2 and 8% were reject. The difference between No.1 and No.2 grade is primarily the presence of skips. Figure 3.2 shows some of the split, skip and knot patterns for No.1 and No.2 graded beams.

Beams are characterized as a reject primarily as a result of splits within the cross-section as well as the occurrence of large, unnatural defects such as shown in Figure 3.2.

Table 3.1 – Grading Rules for all Species No. 1 Structural Beams and Stringers

Characteristic Beam or Stringer Imperfections	Limiting Provisions
Checks	-in areas at ends, single or opposite, with a sum total equal to approximately $\frac{1}{4}$ the thickness
Holes	-pin limited -grub and teredo, one for each 1' length -in cedar, holes from any cause $\frac{1}{2}$ the size of the allowable knots
Pitch Streaks	-not limited
Rate of Growth	-pitch or bark, not limited
Shake	-medium, Douglas Fir and Western Larch only
Skips	-occasional $\frac{1}{8}$ " x 2' or equivalent
Slope of Grain	-middle $\frac{1}{3}$ - 1 in 10; balance 1 in 8
Splits	-short or equivalent end checks
Stain	-stained sapwood, heart strain firm
Torn Grain	-heavy
Wane	- $\frac{1}{4}$ of any face or as equivalent $\frac{1}{3}$ of any face for $\frac{1}{4}$ length
Knot	-sound, tight and well spaced, may be present in the sizes presented in Table 3

Table 3.2 – Allowable Knot Sizes

Nom. Face Width	On Narrow Face and Edge of Wide Face in Middle $\frac{1}{3}$ of Length	At Ends and along Centreline of Wide Face
5"	$1\frac{7}{8}$ "	
6"	$2\frac{1}{4}$ "	
8"	$2\frac{1}{2}$ "	3"
10"	$2\frac{3}{4}$ "	$3\frac{3}{4}$ "
12"	$3\frac{1}{4}$ "	$4\frac{1}{2}$ "
14"	$3\frac{1}{2}$ "	5"
16"		$5\frac{1}{4}$ "
18"		$5\frac{1}{2}$ "

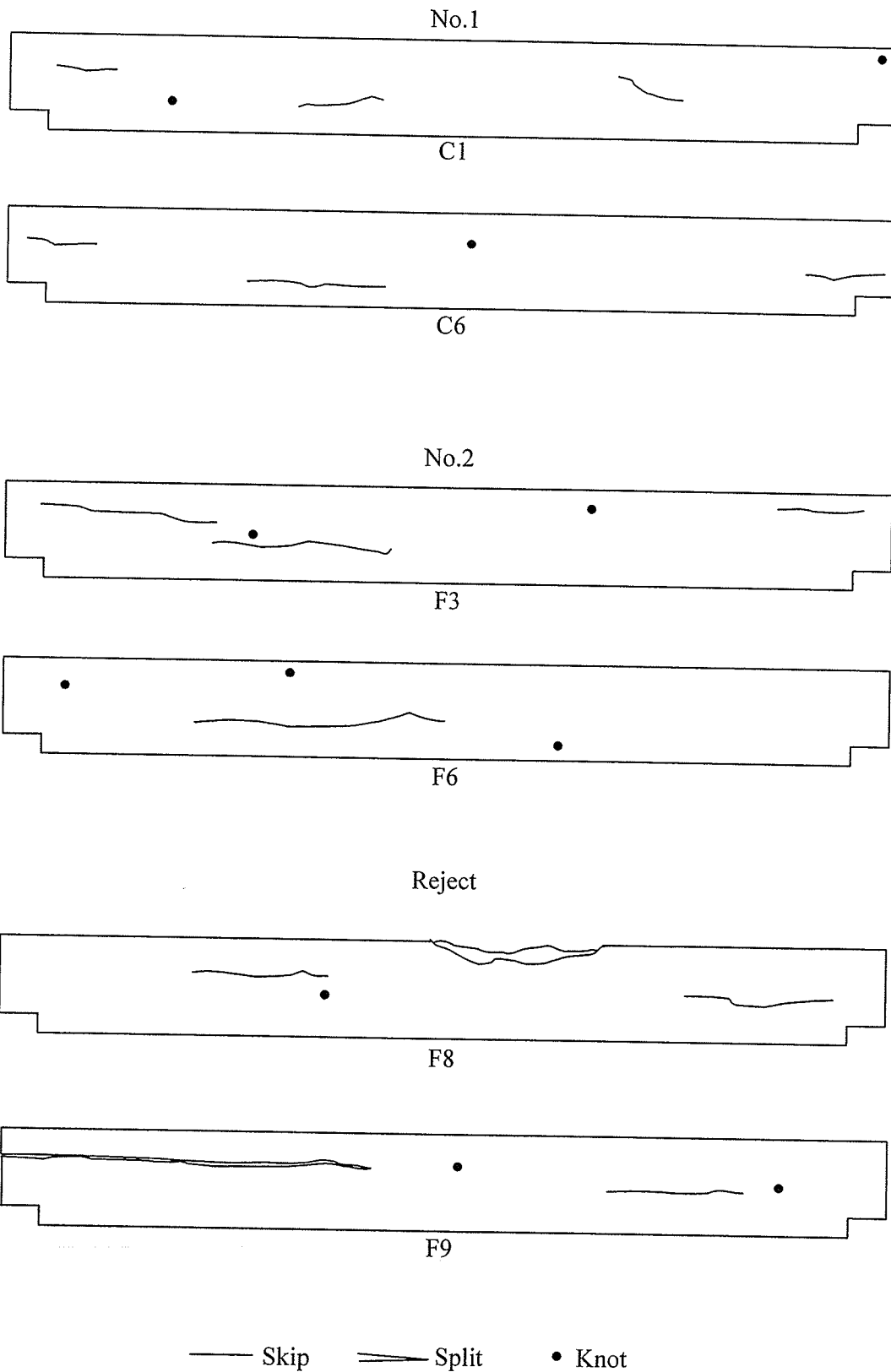


Figure 3.2 – Natural Defects within the Timber Stringers

3.5 Design and Fabrication of Specimens

All 26 timber stringers had nominal cross-section dimensions of 100 x 400 mm and a test length of 3400 mm. The flexural GFRP bars were installed in rounded grooves 19 mm wide and 19 mm deep created by a hand held router. The grooves were first half-filled with epoxy, and then the bar was placed in the groove and the rest of the groove was filled in with epoxy and levelled. The stringers were allowed to cure for at least seven days prior to testing to ensure proper development of the bond between the GFRP, epoxy, and timber system.

The fabrication of specimens with flexural and shear reinforcement were executed by following the steps outlined for flexurally reinforced specimens and by drilling holes through the tension face of the stringer for the dowel bars. The holes were drilled using a 19 mm diameter by 914 mm drill bit inclined at a 30 degree angle to the vertical plane, as shown in Figure 3.3. The holes were partially filled with epoxy and the dowel bars were then threaded into the hole, drawing the epoxy up the length of the hole and bar until the bar reached the end of the hole. The excess epoxy was removed with the use of a trowel and levelled with the bottom of the stringer. The dowel bars placed across the dap were inserted into the drilled holes such that the bottom of the bar was flush with the tension face of the stringer. This was done to ensure enough development length was available to manage the stresses created at the daps. The specimens were allowed to cure for at least seven days before testing. Figure 3.3 shows the details of the timber stringers and bar placements.

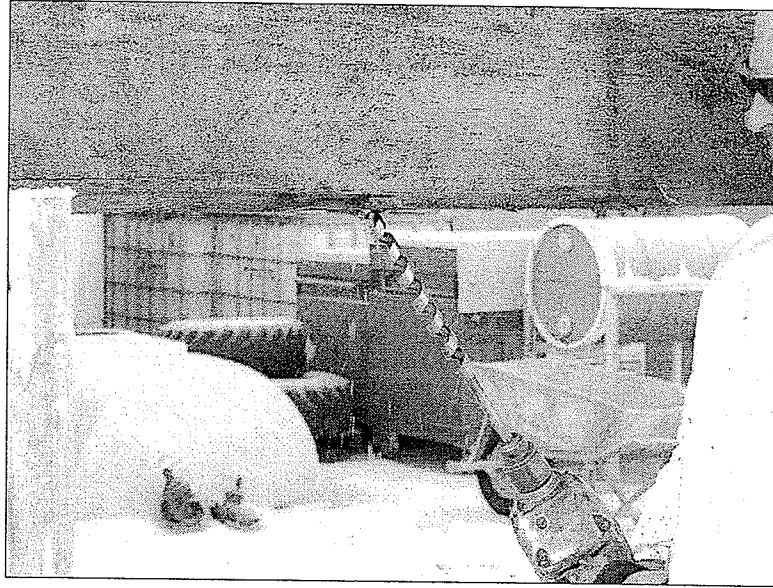


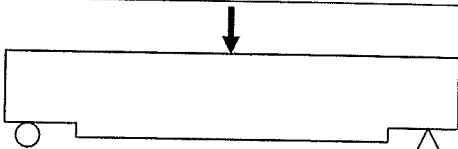
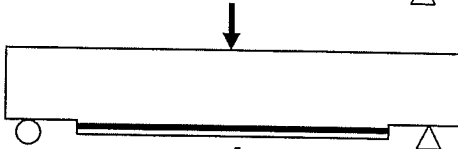
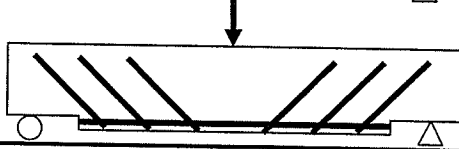
Figure 3.5 – Drilling of Holes for Dowel Bars

3.6 Test Beams

A total of 26 full size (100 x 400 x 3400 mm) salvaged timber bridge stringers were tested until failure in this program. Eight plain timber stringers were tested until failure to establish a control set of data (Group C), twelve stringers were reinforced with GFRP bars in the flexural region only (Group F), and six other stringers were tested with GFRP

bars in the flexural region as well as GFRP dowel bars throughout the depth of the cross-section for shear reinforcement (Group FD), as shown in Table 3.3.

Table 3.3 – Stringer Description

Beam Description	Diagram	# of beams
Control (C)		8
Flexural (F)		12
Flexural and Shear (FD)		6

3.7 Test Setup and Parameters

The tests were completed at the University of Manitoba according to ASTM D198-99 (1999). All stringers were simply supported on rollers and tested under three-point bending with a span of 3.4 m, as shown in Figure 3.6.

A monotonic static load was applied by a servo-hydraulic testing machine with a displacement rate of 4 mm/minute to ensure the stringers failed within six to twenty minutes as per ASTM D198-99 (1999). Bearing plates were used at the point of load application and at the supports to try to avoid any potential damage to the beam due to bearing. The bearing plates were 19 mm thick by 406 mm or 203 mm long rectangular steel plates at the point of load application and at the supports, respectively. Plaster was used at the supports and loading point to ensure an even transfer of load to the beam and then to the supports could be attained.

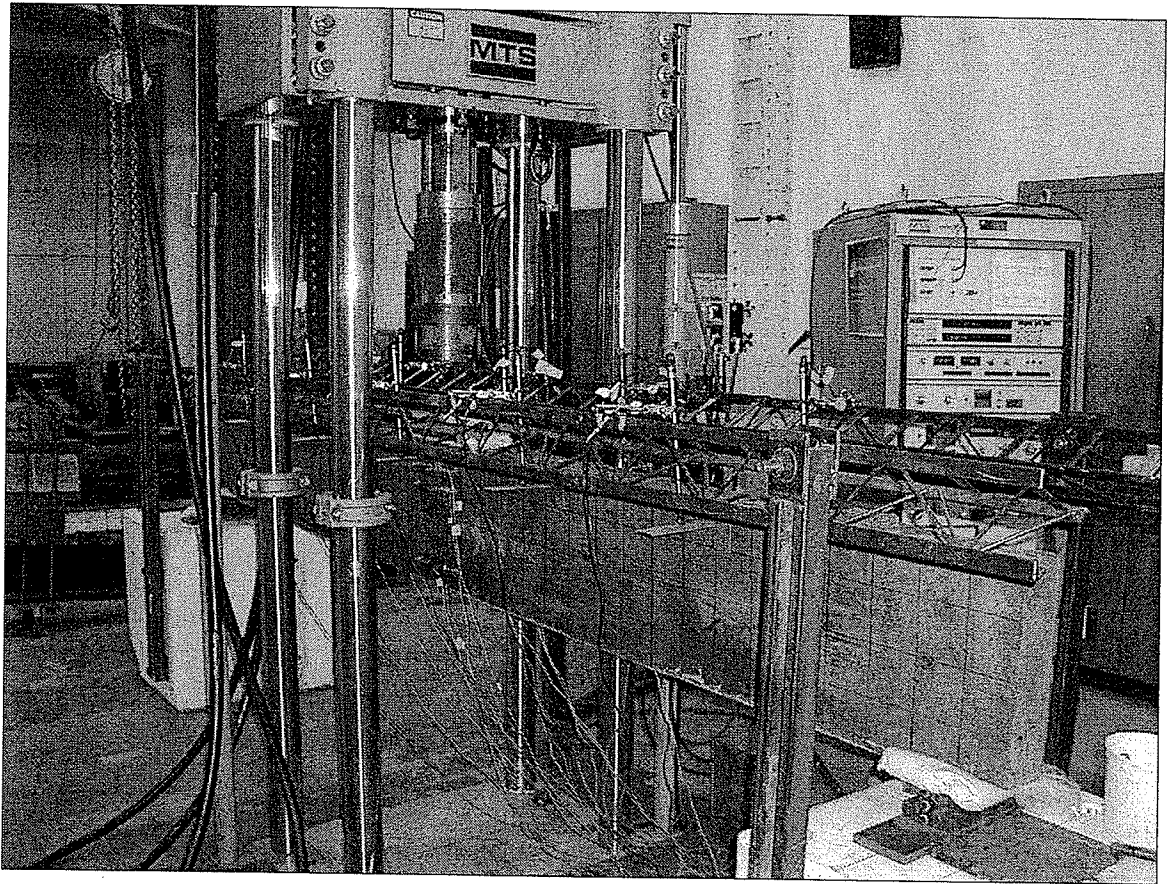


Figure 3.6 – Test Setup

3.8 Instrumentation

The stringers were instrumented with six linear variable deflection transducers (LVDTs) to measure the deflection along the length of the beams. A total of 6 Pi-gauges with a gauge length of 200 mm were used at midspan to measure the strain profile of the timber throughout testing. Figure 3.7 shows the locations of the LVDTs and Pi-gauges. The strains in the GFRP bars (flexural and dowel bars) were recorded using electric resistance strain gauges.

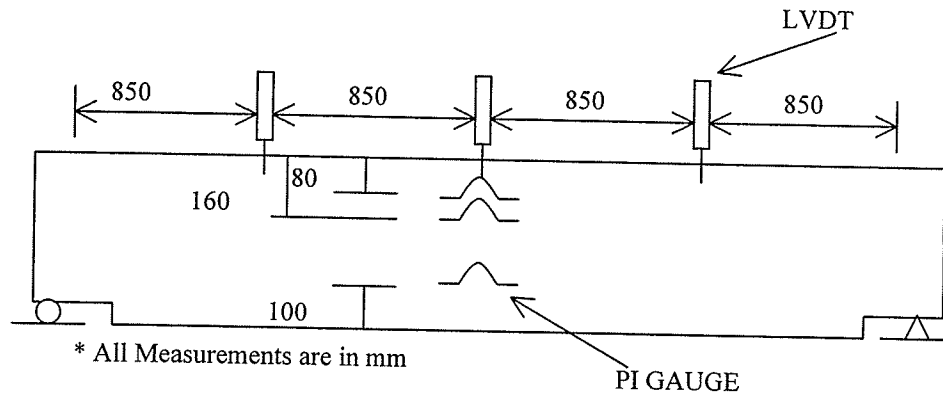


Figure 3.7 – Details of Stringer Instrumentation

The strains in the flexural bars were measured using strain gauges. One of the two flexural bars had three strain gauges placed at either end at a spacing of 50 mm, 100 mm, and 150 mm from the ends, and one strain gauge at the midspan of the bar. The other flexural bar had only one strain gauge at the midspan of the bar. The dowel bars placed across the daps had one strain gauge located at mid-height of the bar with two more equally spaced above and below. The next two dowel bars, closest to the dap, had one strain gauge placed at the midpoint of the bars. The two dowel bars closest to the midspan of the stringer were not gauged. A computerized data acquisition system was used to record all the data from the instrumentation and machines listed above. The data was continuously recorded until the ultimate failure of the stringer.

CHAPTER 4 TEST DATA AND RESULTS

4.1 General

The test results will be presented in terms of the strength, failure modes, strain in the timber and GFRP bars, modulus of elasticity (MOE), tensile, shear, and compressive stresses.

Only experimental data is presented and discussed in this chapter. Further discussions and analysis is presented in Chapter 5.

4.2 Load Deflection Behavior

The load deflection behaviour was recorded using a load cell within the testing machine and two LVDTs placed at the midspan of the stringers. The LVDT data was averaged and then used to plot the load-deflection curves.

4.2.1 Control Specimens

A conscious effort was made to ensure the stringers that were visually graded as being in good condition as the control specimens. This ensured the reinforced specimens were at a disadvantage before the GFRP bars were installed. A total of eight control specimens were tested. Figures 4.1 and 4.2 display the load deflection curves for all eight control stringers. The average ultimate load of the control stringers is 121.3 kN with a standard deviation of 22.6 kN.

In Figure 4.1 a wide range of load-deflection behaviour is observed. Stringer C2 had lower stiffness compared to the rest of the group and failed at a load of 80 kN before reaching a deflection of 30 mm. To demonstrate the large variability in this group of stringers, stringer C1 failed at 160 kN and reached a deflection of nearly 80 mm. Stringers C1 and C3 were able to undergo substantial deflections before failure but the rest of the control stringers were only able to obtain low to moderate deflections (30 to 40 mm) before failing, as seen in Figures 4.1 and 4.2. Other than stringers C1 and C3 the control stringers had fairly linear load-deflection curves right up to failure. Failure was very sudden and catastrophic, meaning little or no deflection at all was attained after the peak load was reached. The sudden drops in the load deflection curves are due to cracking of the timber. The stresses are then redistributed throughout the remaining timber until failure.

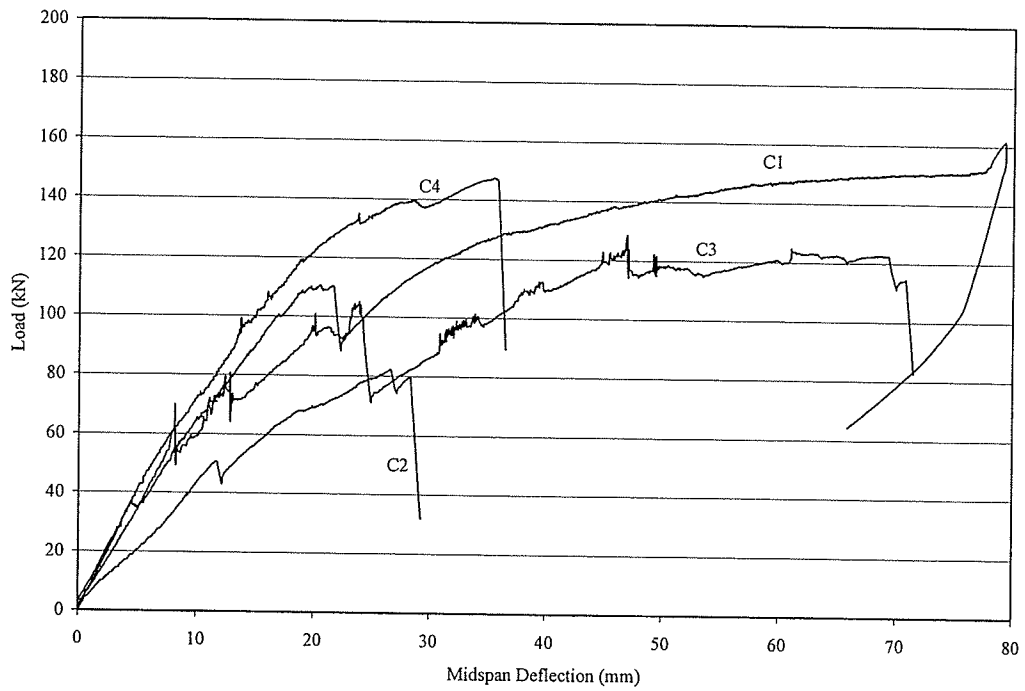


Figure 4.1 – Load Deflection Curves for Control Specimens 1 through 4

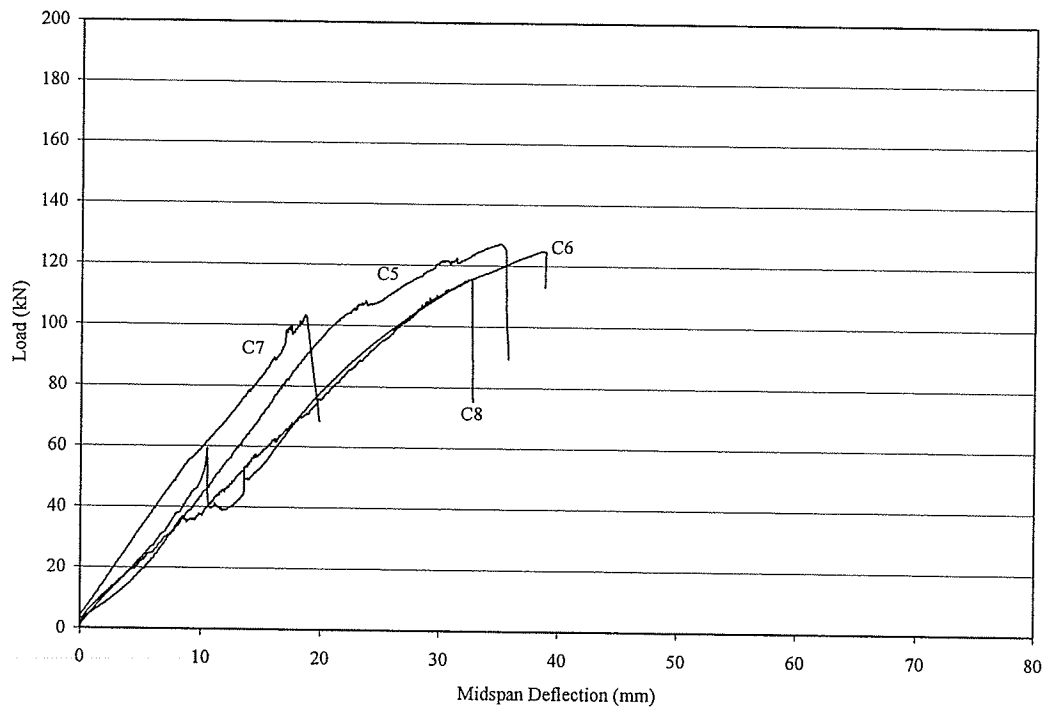


Figure 4.2 – Load Deflection Curves for Control Specimens 5 through 8

4.2.2 Flexurally Reinforced Specimens

The ultimate failure loads of the flexurally reinforced specimens are very similar to those of the control specimens. The average ultimate load of the flexurally reinforced specimens is 125.3 kN with a standard deviation of 25.9. This is due to the similar failure modes of the two groups of stringers and is discussed further in section 4.3. An increase in ductility, on average, can be seen in Figures 4.3 and 4.4 when compared to the control stringers, despite the fact the ultimate loads of the two groups of specimens are very similar. The data files for stringers F11 and F12 were corrupted during the analysis process thus, these stringers load-deflection curves are not shown but the ultimate load data was recorded and used in all strength analyses completed for group F.

The majority of the flexurally reinforced stringers were able to obtain between 40 and 60 mm of deflection whereas the majority of the control stringers were able to obtain deflections of 40 mm or less.

This group of samples exhibited very similar behaviour compared to the control specimens, even though they were reinforced with GFRP bars. The flexural reinforcement was found in an earlier study by Gentile et al. (2002) to increase the strength of the stringers by up to 50% with a smaller increase for stronger timbers. There are two main reasons the strength increases were not obtained when beams in this group (Group F) were compared to the control group (Group C). The beams in the control group were of a higher grade compared to the beams with flexural reinforcement, the other reason is that the flexural reinforcement was not capable of preventing dap failures. None of the previous studies were concentrating on the behaviour of dapped beams.

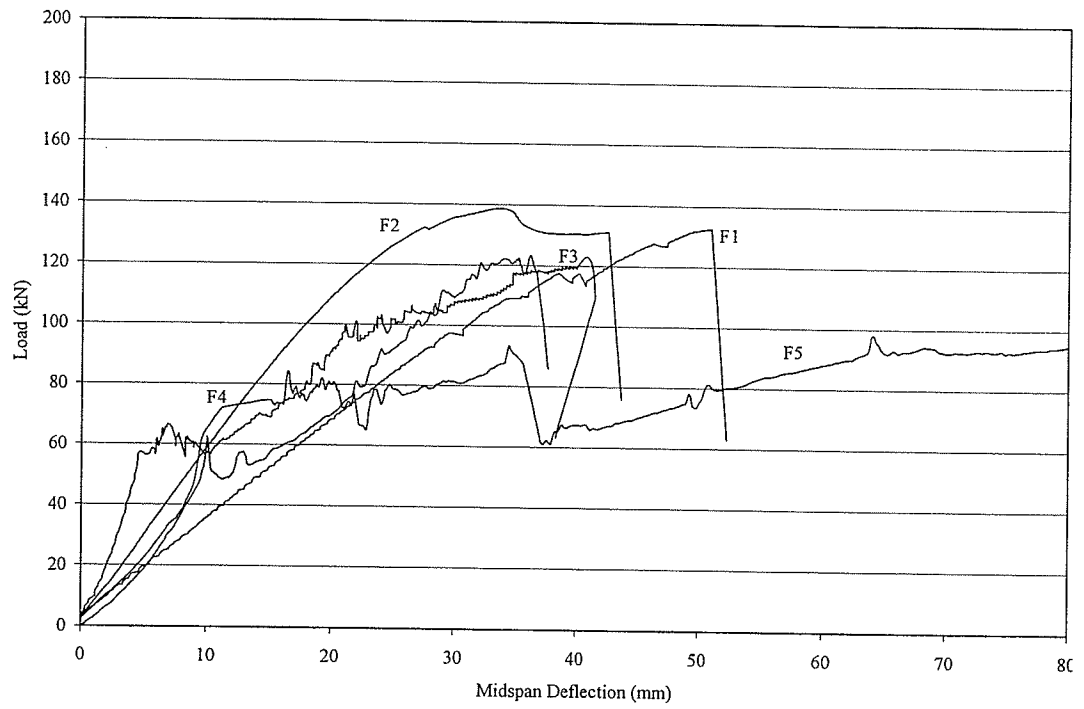


Figure 4.3 – Load Deflection Curves for Flexurally Reinforced Specimens 1 through 5

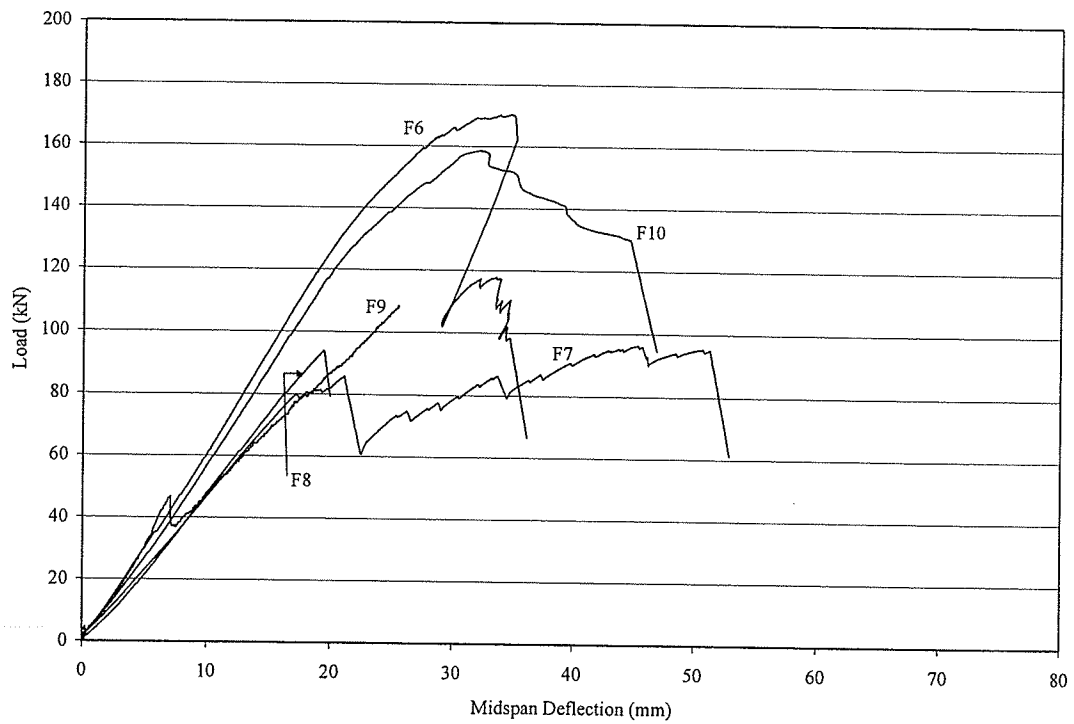


Figure 4.4 - Load Deflection Curves for Flexurally Reinforced Specimens 6 through 10

It should be noted that the data used for the load deflection curves of Figure 4.3 were filtered to obtain the curves shown. The filtering was completed to eliminate the extremely high peaks present for specimens F3 and F4 near the beginning of the tests. The load versus deflection curves obtained through the use of the raw data is shown in Figure 4.5.

As seen in Figure 4.5 the load deflection curves for stringers F4 and F5 have extremely high peaks, which do not occur in any other load deflection curves. The peaks are a result of severe stiffening of the test setup, and are believed to be a result of an obstruction during the testing that was not immediately noted. Once the stringer cracked initially, and was no longer held up by the testing apparatus, the load deflection curve became more realistic. The beams had significantly warped before testing, and because of their slenderness it was decided to have side supports to prevent the beam from tilting during the test. These supports may have held the beam at the start of the test and caused the stiffening of the initial response.

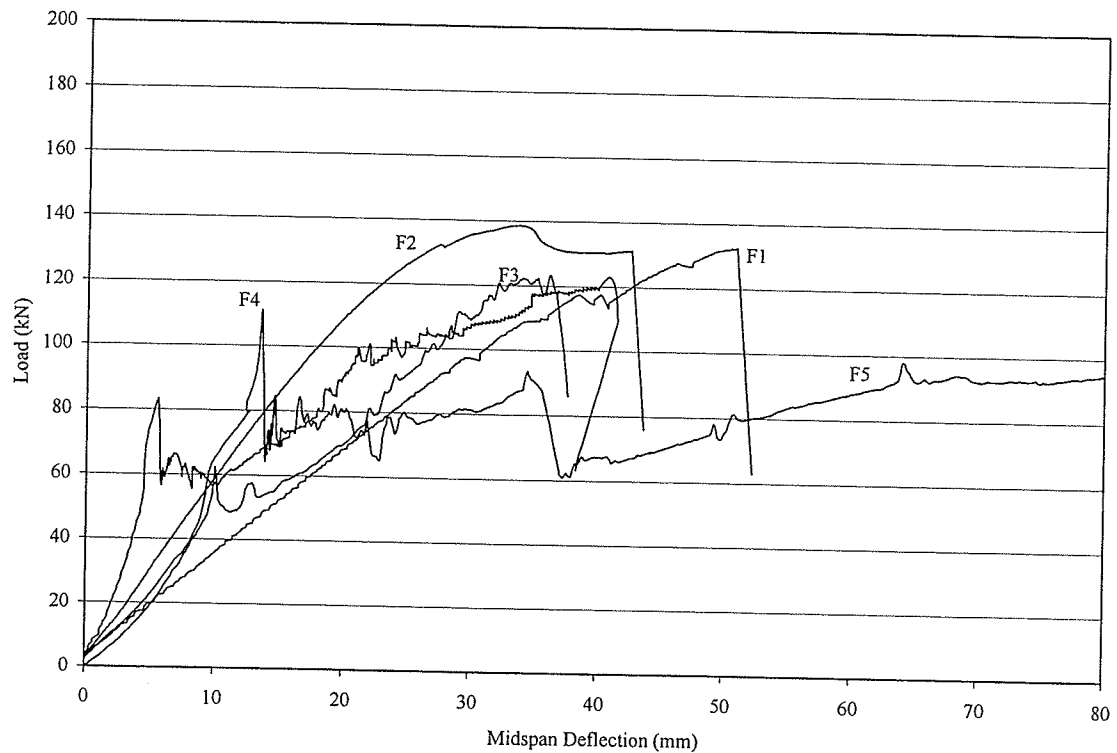


Figure 4.5 – Raw Data Load Deflection Curves for Flexurally Reinforced Specimens 1 through 5

4.2.3 Flexural and Shear Reinforced Specimens

An increase in the average ultimate load and ductility of the specimens reinforced for both flexure and shear can be seen in Figures 4.6 and 4.7, when compared to the control specimens. All specimens reinforced for flexure and shear were able to obtain deflections between 50 and 60 mm except for stringer FD3 which achieved a small deflection before failure.

The average ultimate load of the specimens reinforced for flexure and shear is 149.1 kN with a standard deviation of 25.5 kN. This is an increase of 23% and 19% over the control and flexurally reinforced specimens respectively. The flexure and shear

reinforced stringers were graded as much lower grade stringers compared to the control beams therefore, the estimate of the strength increase is conservative.

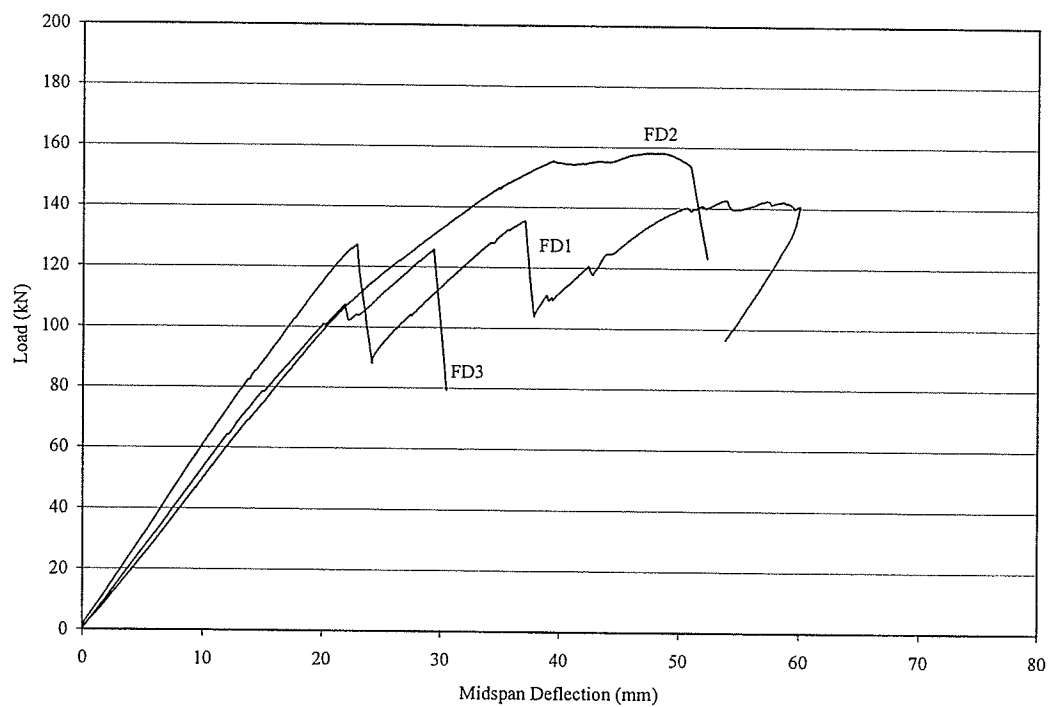


Figure 4.6 – Load Deflection Curves for Flexural and Shear Reinforced Specimens 1 through 3

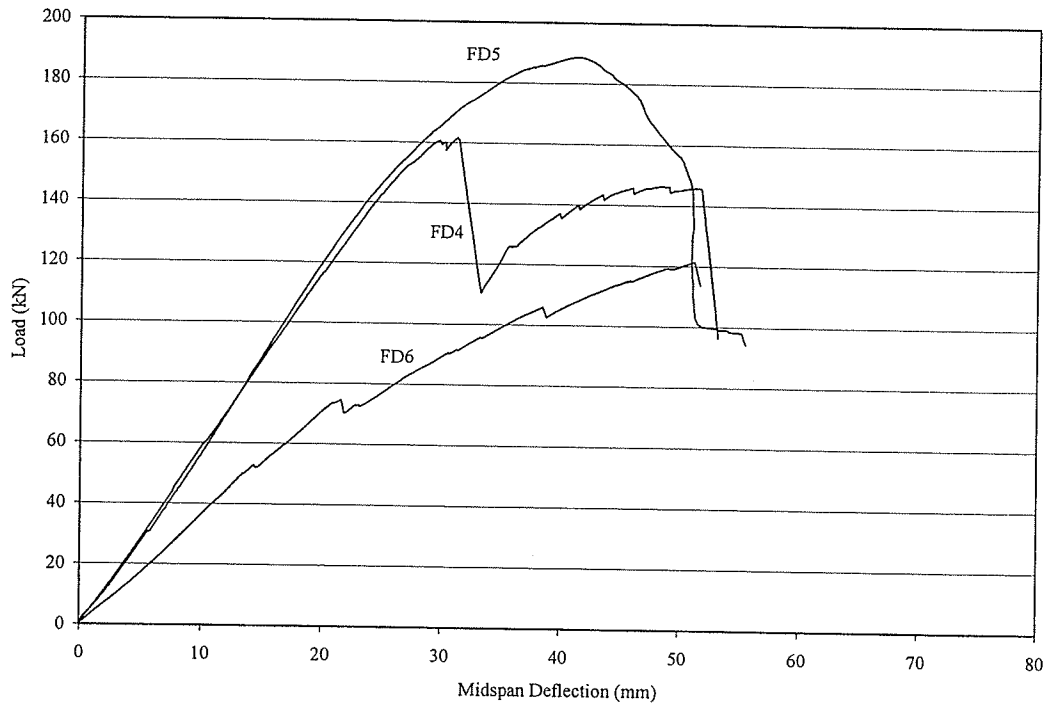


Figure 4.7 – Load Deflection Curves for Flexural and Shear Reinforced Specimens 4 through 6

4.3 Strain Measurements

The strain in the timber and GFRP bars were measured using pi-gauges and strain gauges respectively.

The cross-sectional strain profiles were developed for a load of 40 kN to determine if strain compatibility was satisfied in the reinforced timber. The 40 kN load level was chosen to ensure the stringers were still in the linear region of their load deflection curves thus, their cross-sectional strain profiles should not be affected by the cracking of the timber.

4.3.1 Control Specimens

The cross-sectional strain profiles are presented in Figures 4.8 and 4.9 together with the location of the pi-gauges. Since the pi-gauges were mounted on the surface of the timber stringers, some variability would be expected as some stringers had knots and splits. The majority of the strain profiles did have an obvious linear trend thus, the results confirm, plain sections do remain plain. The presence of knots and splits on the timber stringers would explain the small deviations from the expected linear nature of the strain profiles, but does not explain the large deviations obtained for specimens C2 and C6. Figures 4.1 and 4.2 display the load deflection curves for stringers C2 and C6 show the stringers cracked before reaching the 40 kN load. The cracking is seen as a drop in the load with an increase in the deflection of the stringers load deflection curve. This cracking affects the strain profile such that it would no longer be linear in nature. The 40 kN load was chosen since the majority of the specimens remained linear until this point, as well the load is large enough to close any existing cracks and defects and activate the entire cross-section of the stringer.

Figure 4.10 displays the strain profile for specimen C8 for increasing load. As seen in this figure the strain profile does indeed remain linear until sufficient cracking has occurred causing the profile to become somewhat nonlinear. The neutral axis remains approximately at the midpoint of the cross-section as expected from classical theory.

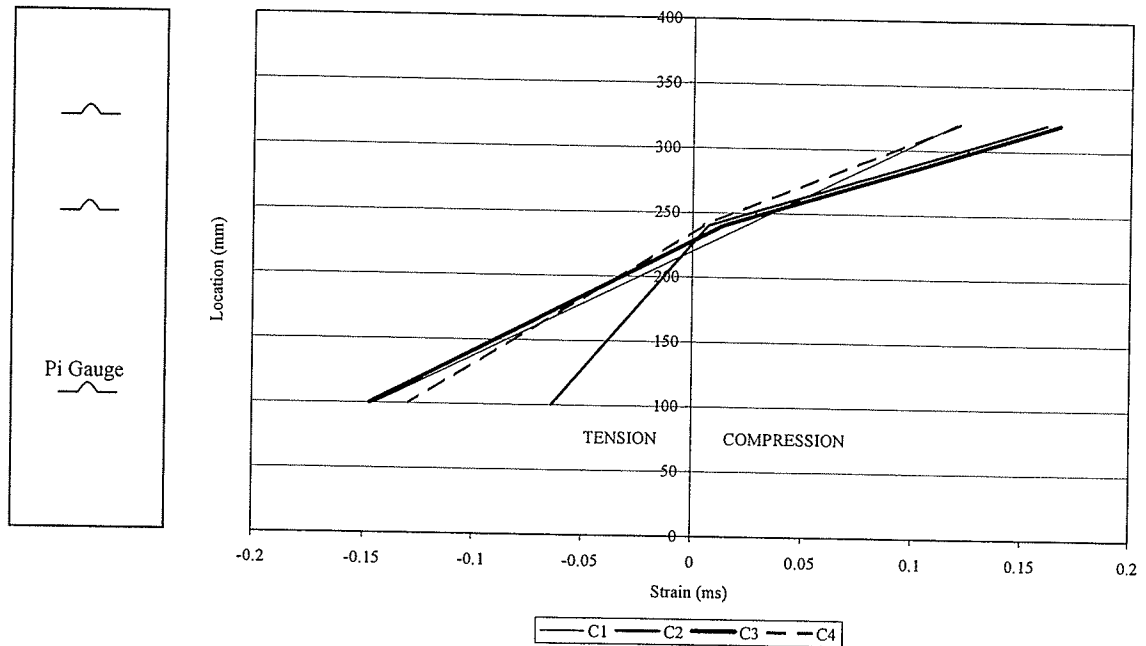


Figure 4.8 - Cross-Sectional Strain Profile for C1-4 at 40 kN Load Level

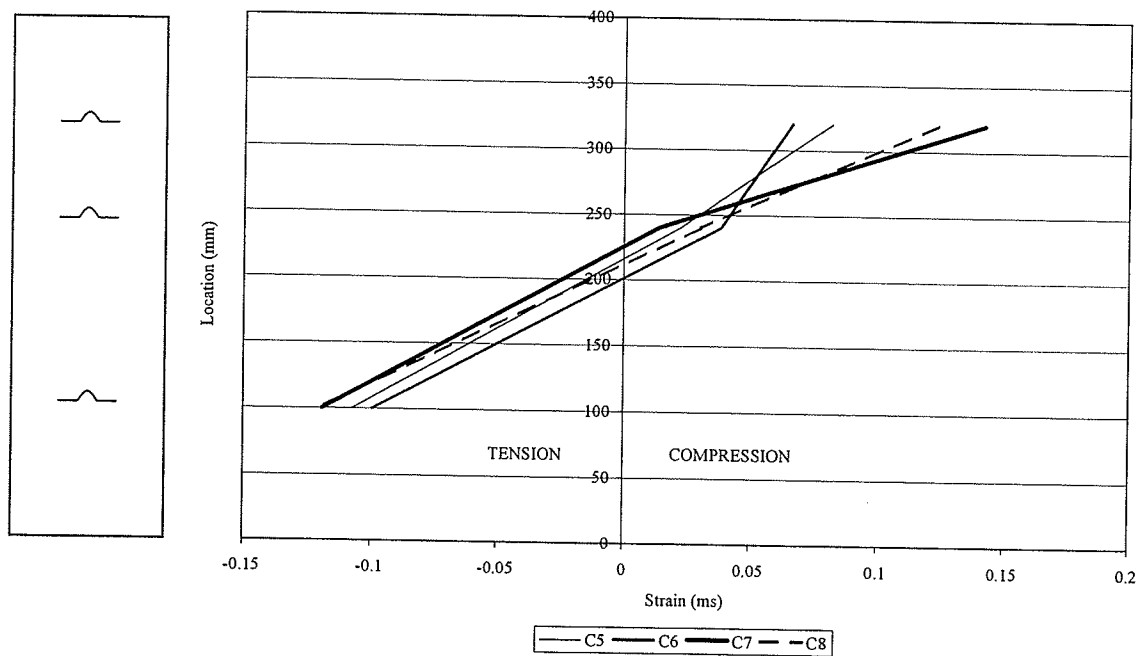


Figure 4.9 - Cross-Sectional Strain Profile for C5-8 at 40 kN Load Level

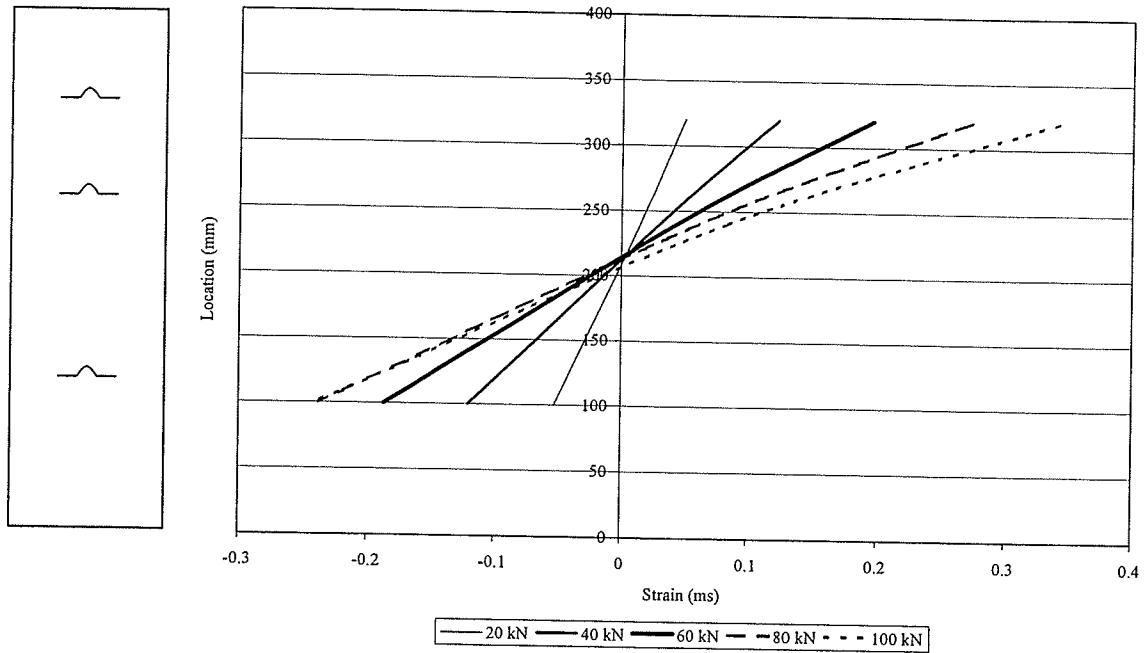


Figure 4.10 – Cross-Sectional Strain Profile for C8 for Increasing Load

4.3.2 Flexurally Reinforced Specimens

The flexurally reinforced specimen had the strains recorded over the cross-section as well as along the GFRP flexural bars.

4.3.2.1 Cross-Sectional Strain

The cross-sectional strain profiles are presented in Figures 4.11 and 4.12.

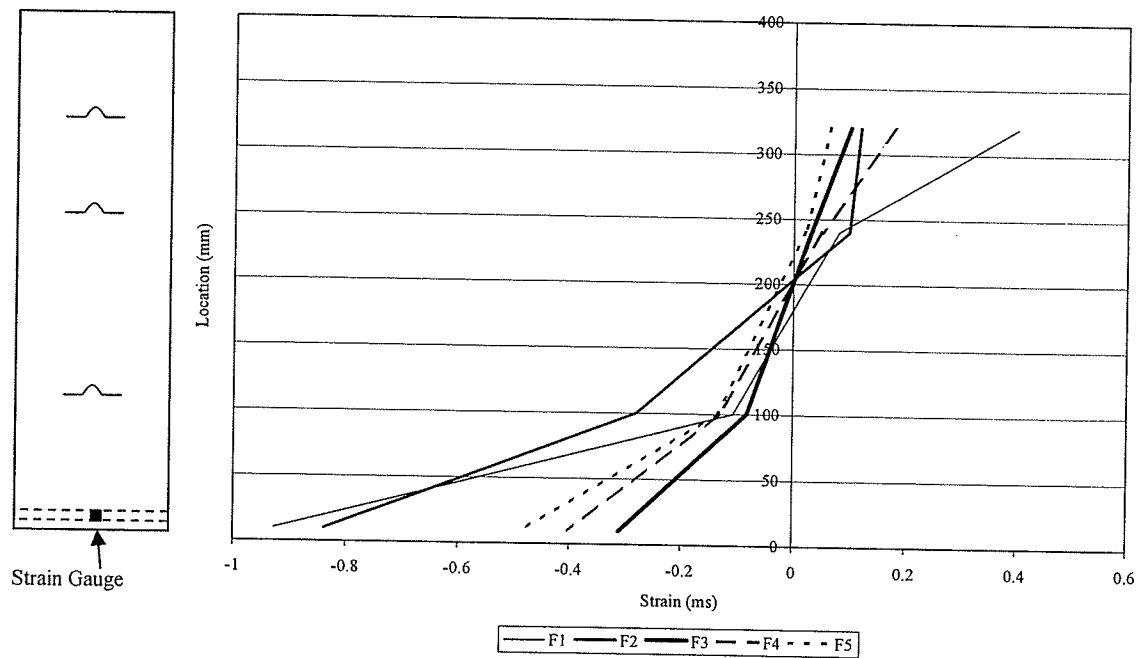


Figure 4.11 – Cross-Sectional Strain Profile for F1-5 at 40 kN Load Level

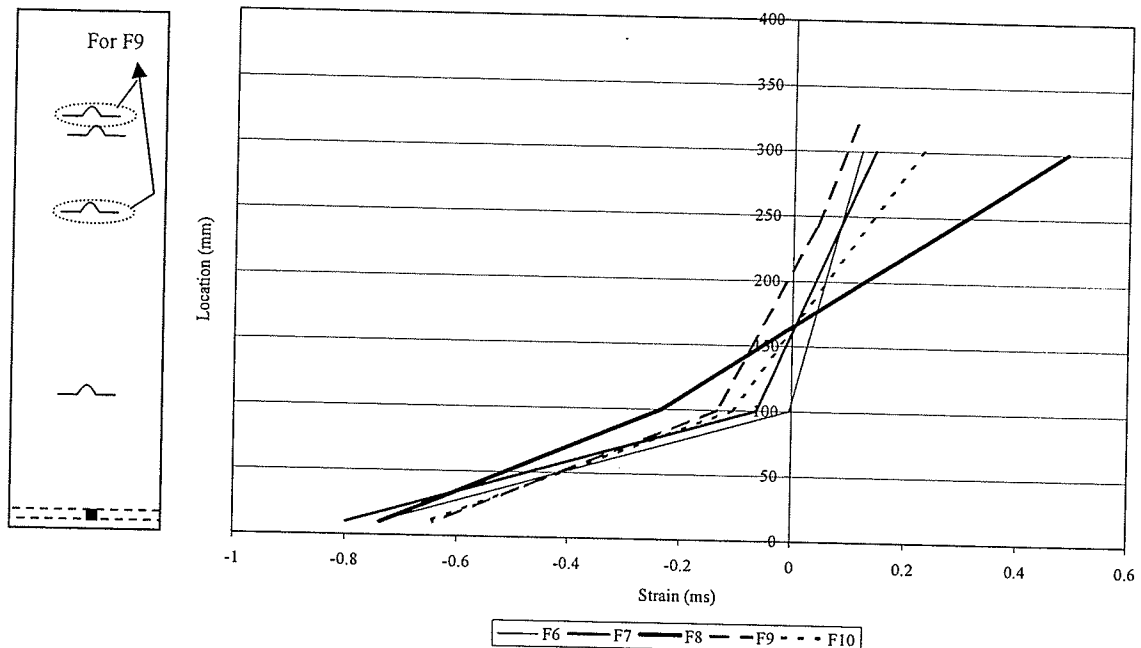


Figure 4.12 – Cross-Sectional Strain Profile for F6-10 at 40 kN Load Level and Pi and Strain Gauge Locations

It should be noted in Figure 4.12 that a change in the pi gauge pattern occurred. This change was a result of a lack of instruments to continue with the use of three pi-gauges on either side of the stringer. Thus, two pi-gauges were used on either side of the stringer to obtain the strain data within the timber.

The majority of the strain profiles, excluding the strain readings from the GFRP bars are linear in nature except for stringers F1 and F2. The load deflection curves of these stringers do not indicate the occurrence of cracking before the 40 kN load level as with the control specimen. Thus, the nonlinear nature of the strain profile, considering just the timber strains, is a result of surface defects in the stringer. Preexisting cracks, knots, and checks have a large effect, if the imperfections are close to the placement of the gauges.

As seen in Figure 4.13 pre-existing knots and cracks could have affected the pi-gauges results since they were located very close to the positioning of the pi gauge closest to the compression face of the stringer

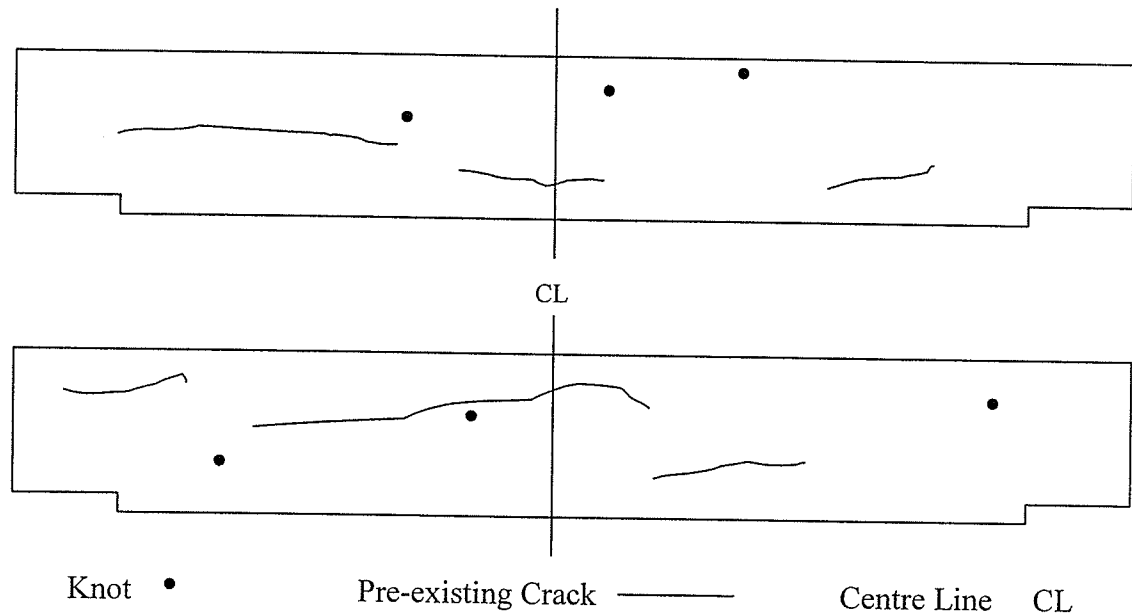


Figure 4.13 – Pre-existing Crack and Knot Pattern for Stringers F1 and F2

Although the majority of the strain profiles for the readings obtained from just the timber are linear in nature, a large discrepancy between the strain in the GFRP bars and the strain in the timber exists. It appears the GFRP bars are bridging the small cracks and imperfection within the timber stringers thus incurring larger strains than the timber area directly around the GFRP bars. This phenomenon has been observed by other researchers (Gentile 2000, Eden 2002) but has not been investigated in detail.

Figure 4.14a) displays the cross-sectional strain profile for stringer F5 for increasing load. The strain profile remains fairly linear with small increases in strain as the load is increased until the 100 kN load level is reached. Stringer F5 began to crack

just after the 80 kN load level as seen in Figure 4.3. Despite the increase in the stiffness of the stringer before the 80 kN load level, the strain profiles were unaffected confirming the suspicion that the setup was causing the increase in stiffness. The cross-sectional strain profile was indeed affected by the severe cracking of the specimen causing the strain profile to become grossly nonlinear.

Figure 4.14a) displays the strain profile for stringer F5 for increasing load until failure. Figure 4.14b) presents the strain profiles for load level 20 kN to 80 kN. The 100 kN and 120 kN load level strains are so much larger than the rest, and therefore the details of the other strain profiles are lost due to the scaling of the curves. Until a large amount of cracking occurs the strain profiles for just the timber are linear in nature. The strains in the GFRP bars are much larger than the strains in the timber right from the 20 kN load level.

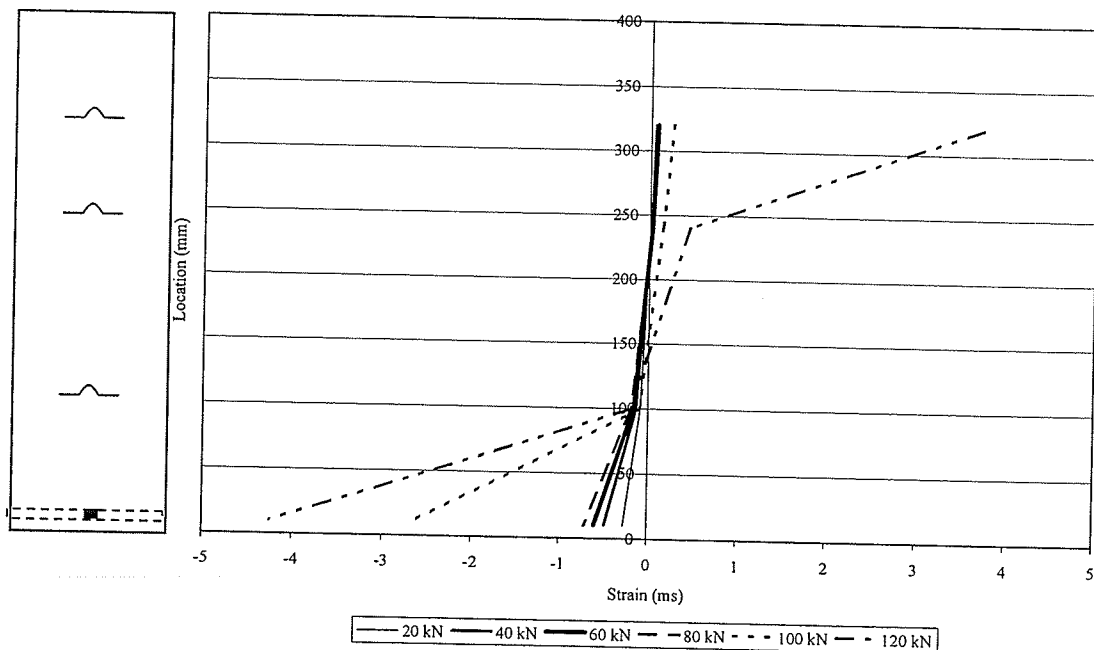


Figure 4.14a) - Cross-Sectional Strain Profile for F5 for Increasing Load

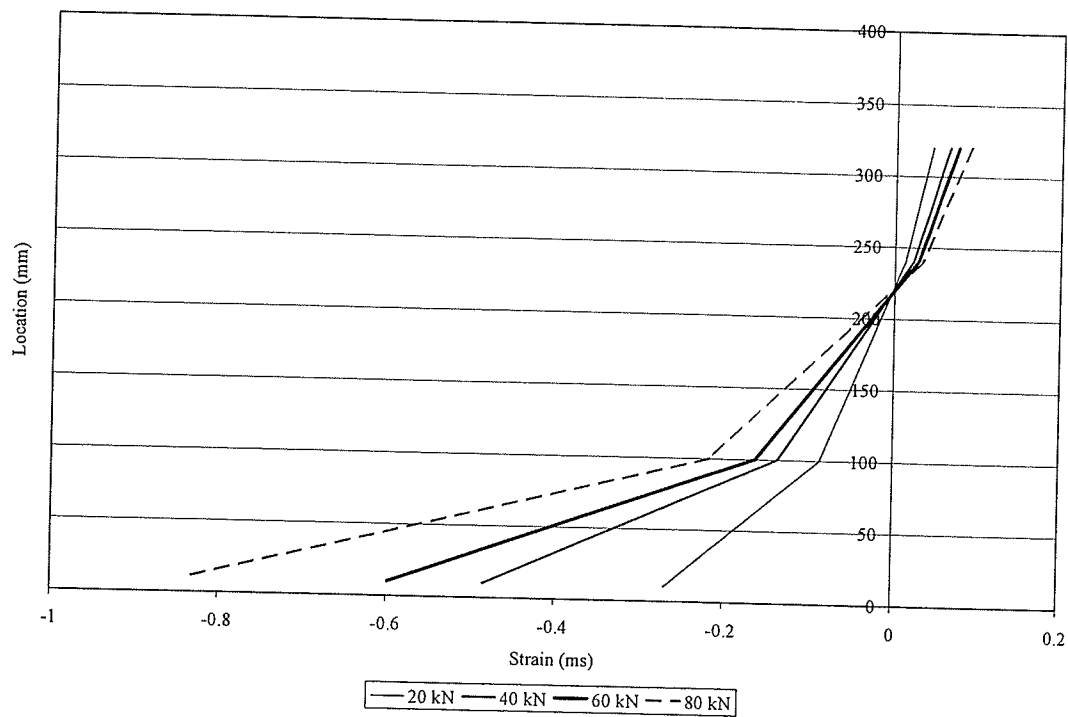


Figure 4.14b) – Cross-Sectional Strain Profile for F5 for Increasing Load

4.3.2.2 GFRP Flexural Bar Strain Profile

The strains were measured at both ends and the midpoint of the flexural bars. The strain profile over the flexural bars for specimen F5 is given in Figure 4.15.

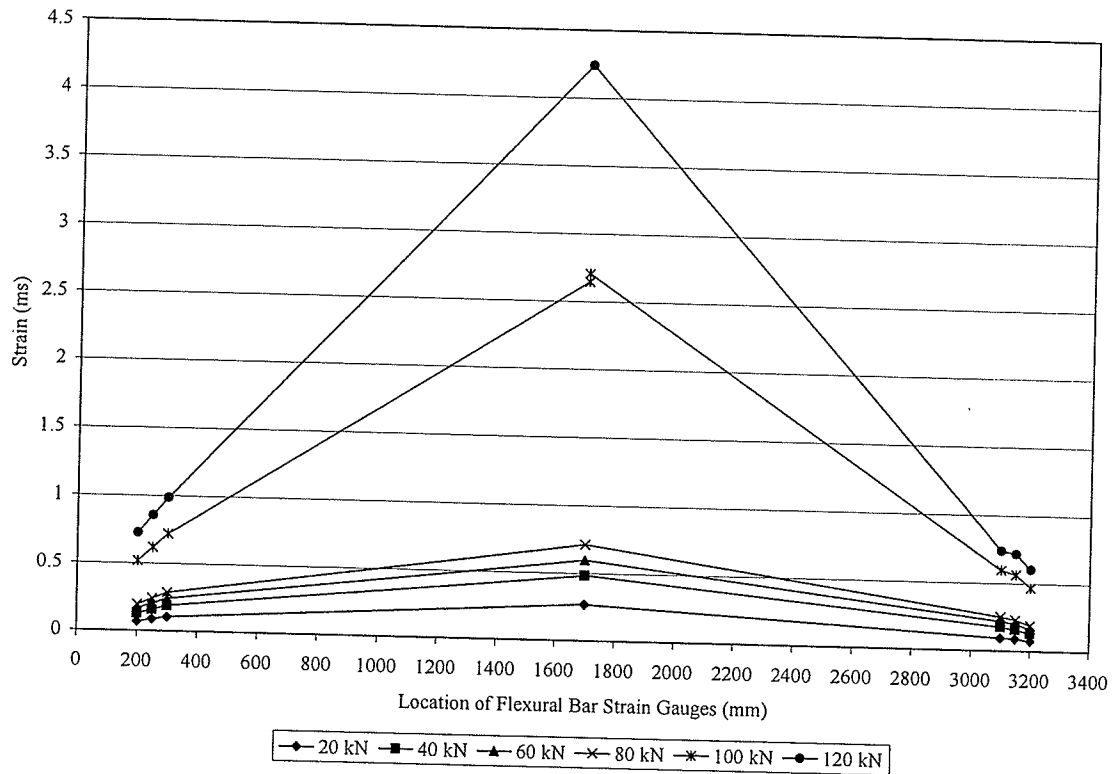


Figure 4.15 – GFRP Flexural Bar Strain Profile for F5

As seen in Figure 4.3 stringer F5 did not crack until just after the 80 kN load level thus, a consistent increase in strain until this level is seen in Figure 4.15. After the 80 kN load level was reached the stringer experienced a large amount of cracking and thus a large increase in the strains in the flexural bars. As seen in Figure 4.15, the strain in the timber and GFRP bars had small increases in strain with an increase in load until the stringer began to crack. After cracking the strain profile has very large increases in the strain values, which correspond to Figure 4.14a) which also depicts very large strain

increases at the same load levels or there may be some discontinuity present between the timber and GFRP bars which has not yet been determined at this time.

4.3.3 Flexure and Shear Reinforced Specimens

The strains for the flexural and shear reinforced specimens were recorded along the depth of the cross-section, the GFRP flexural bar, and the dowel bars.

4.3.3.1 Cross-Sectional Strain

The cross-sectional strain profiles for group FD at 40kN load level are given in Figures 4.16 and 4.17. Much like the cross-sectional strain profiles of group F, the profiles of group FD are linear within the timber with the strains in the GFRP being much larger. The cause of this is unclear but is suspected to be caused by the natural irregularities found within the timber stringers.

The strain profile within the timber is linear, as in the control specimens, but a large discrepancy between the strain in the GFRP bars and the timber exists. Similar to the flexurally reinforced specimens, the strains in the GFRP bars are much larger than the strain in the timber. As for the flexurally reinforced specimens the GFRP bars in the flexural and shear reinforced specimens seem to bridge the small cracks and imperfection within the timber stringer thus incurring larger strains the timber area directly around the GFRP bars.

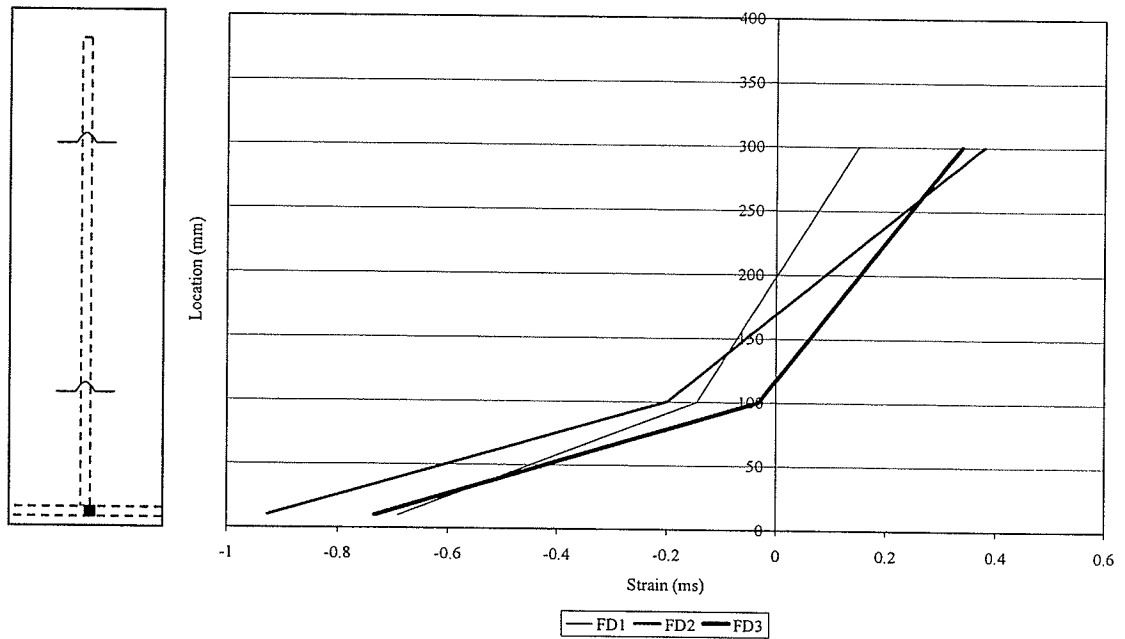


Figure 4.16 – Cross-Sectional Strain Profile for FD1-3 at 40 kN Load Level

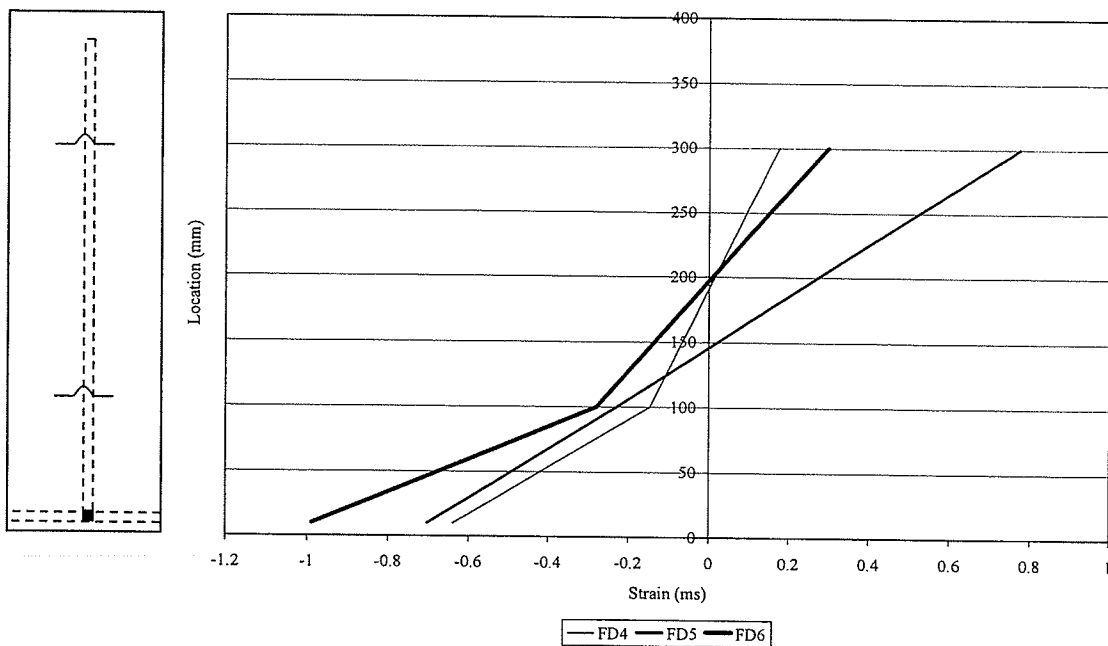


Figure 4.17 – Cross-Sectional Strain Profile for FD4-6 at 40 kN Load Level

Figure 4.18 displays the cross-sectional strain profile for FD3 for increasing load. The strain profile remains very similar with the increase in load and is largely unaffected by any cracking occurring during the test. It was observed during the test that cracking took place primarily near the supports of the stringer (bearing failure), while the strain was measured in the midspan, therefore it was not affected by cracking and shows constant increase in strain with load.

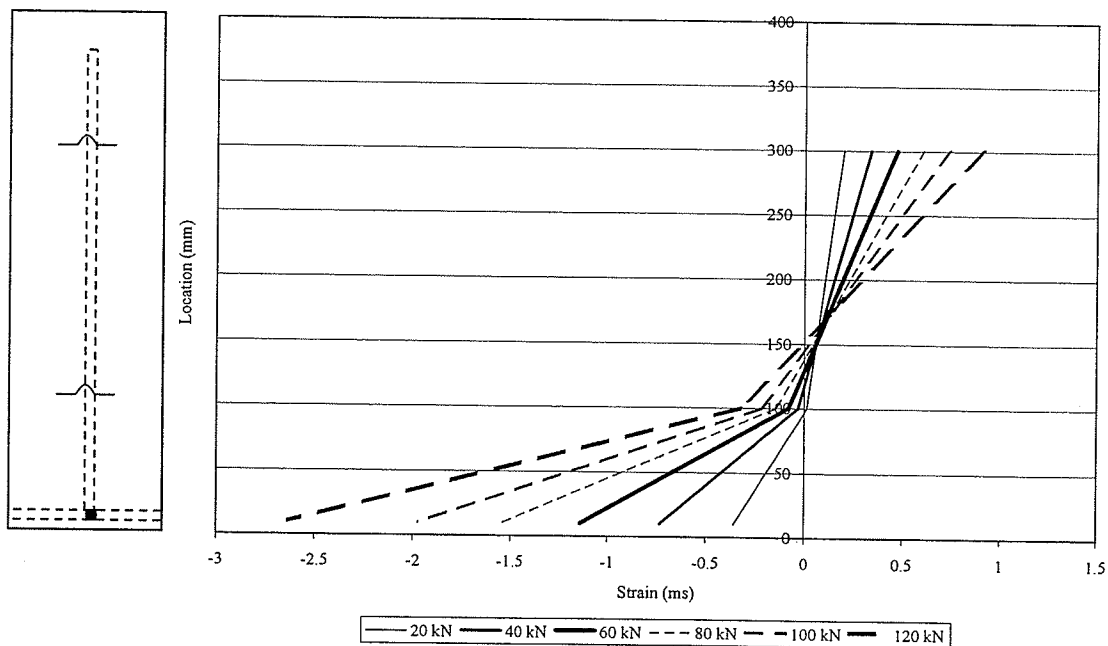


Figure 4.18 – Cross-Sectional Strain Profile for FD3 for Increasing Load

4.3.3.2 Strain in the Flexural Bar for Group FD

As with the flexurally reinforced specimens the specimens reinforced for flexure and shear had the strains in the flexural reinforcement recorded along the length of the bars. Figure 4.19 displays the flexural bar strain profile for stringer FD3. The differences in some of the strain readings at the midspan of the beam are due to the use of two strain gauges, one at the midspan of each flexural bar. Thus as the test proceeded the strain values did begin to vary most likely due to cracking of the timber stringer.

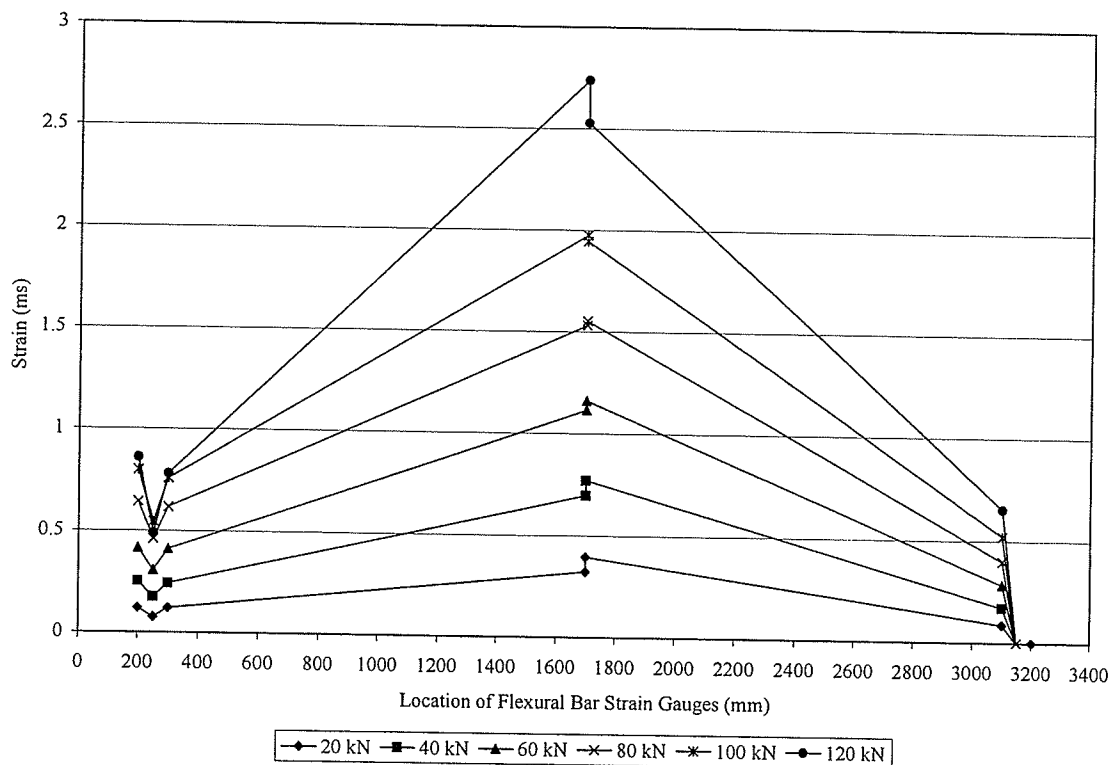


Figure 4.19 – GFRP Flexural Bar Strain Profile for FD3

Although the strain gauges on the right end of the flexural bar did not work during the test, the recorded data still displays the strain profile very well. As seen in Figure 4.19, the strain gauges located between 200 and 350 mm along the flexural bar did not demonstrate a constant increase in strain as the midspan was approached. This is

probably a result of the shifting and cracking of the timber near these locations causing an irregular strain distribution. Larger strains were recorded closest to the dapped end and then increased again as the midspan of the bar was approached, as expected.

4.3.3.3 GFRP Dowel Bar Strain

Figure 4.20 displays the GFRP dowel bar strain profiles for stringer FD3.

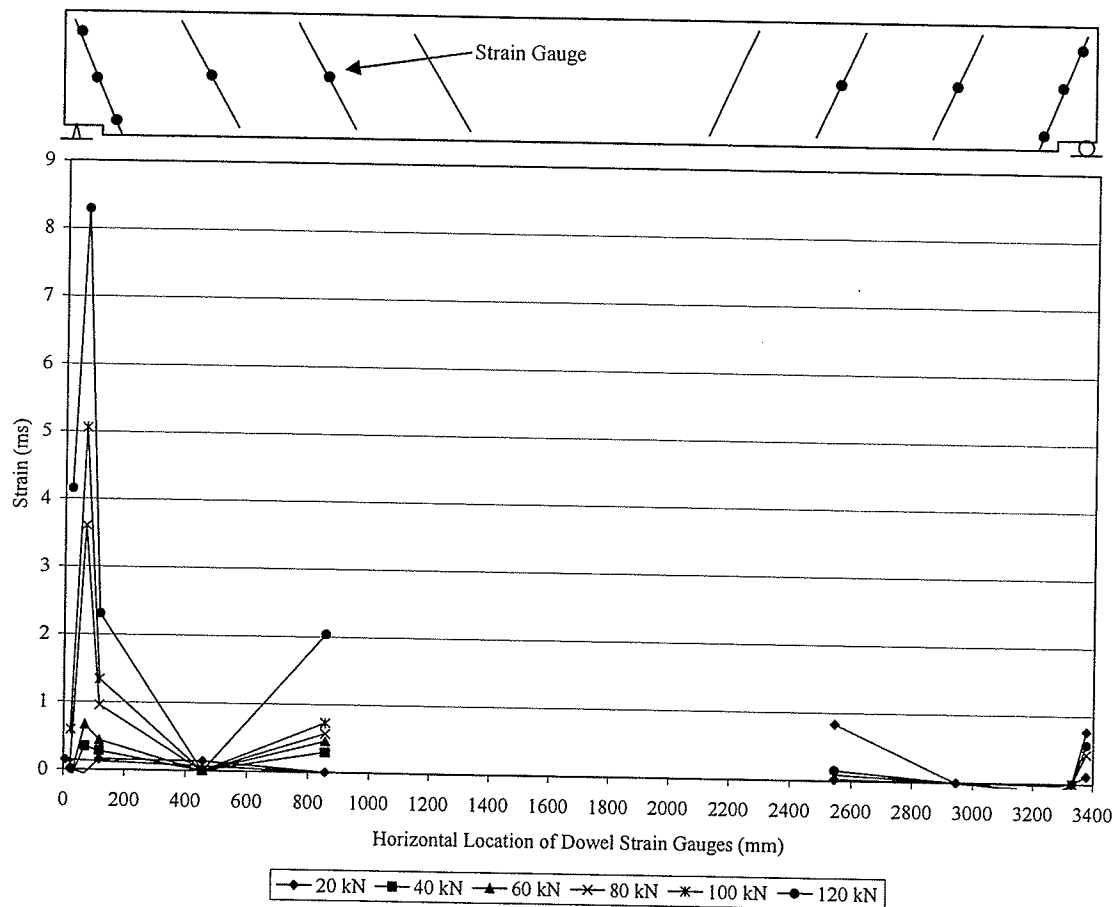


Figure 4.20 – GFRP Dowel Bar Strain Profiles for Stringer FD3

Although some of the gauges did not work during the test the general strain profile can still be observed. If the left most portion of the dowel bar strain profile is ignored for now, a very consistent strain increase is seen as the load increased until the 120kN load

level, which is also true for the flexural bar strain profile seen in Figure 4.19. Very large dowel bar strains were recorded at the dapped end of the stringer. These strains correspond to the flexural bar strains near the dapped end recorded and discussed in the previous section. Figures 4.19 and 4.20 demonstrate the dapped end was causing very large strains in the flexural and dowel bars in this region. As mentioned previously the stringer experienced cracking in between the 60 and 80 kN load levels which correspond to a large increase in the strains in the dowel bar at the dapped end. The rest of the stringer seemed to be relatively unaffected by this cracking since the strain profiles for the dowel and flexural bars along the rest of the length of the stringer remained largely unchanged. A large amount of cracking occurred at approximately the 110 kN load level which is noted in Figure 4.19 as a larger jump in the strains through out the stringer and as strain relief near the dapped end. The cracking at the 110 kN load level is noted in Figure 4.20 as a large jump in most of the strains recorded. The cracking recorded was due to a bearing failure occurring at the left support, which also corresponds to the large strain recorded in the dowel bars. According to the measured strain, the force in the dowel bar was 46 kN or 65% of the strength of the dowel, at that load level.

4.4 Failure Modes

Five distinctive failure modes were observed in the tested beams. These failure modes include, dap, shear, tension, crushing, and bearing.

A typical dap failure originates at the corner of the dap causing the timber to split. The crack then propagates along the grain towards the midspan of the stringer. An observed dap failure is shown in Figure 4.21.

A typical shear failure occurs along the grain of the timber and propagates horizontally along the span of the stringer. Shear failures during testing were observed to originate along pre-existing cracks. During testing the crack widened and propagated along the span of the stringer until ultimate failure occurred. A typical shear failure is displayed in Figure 4.22.

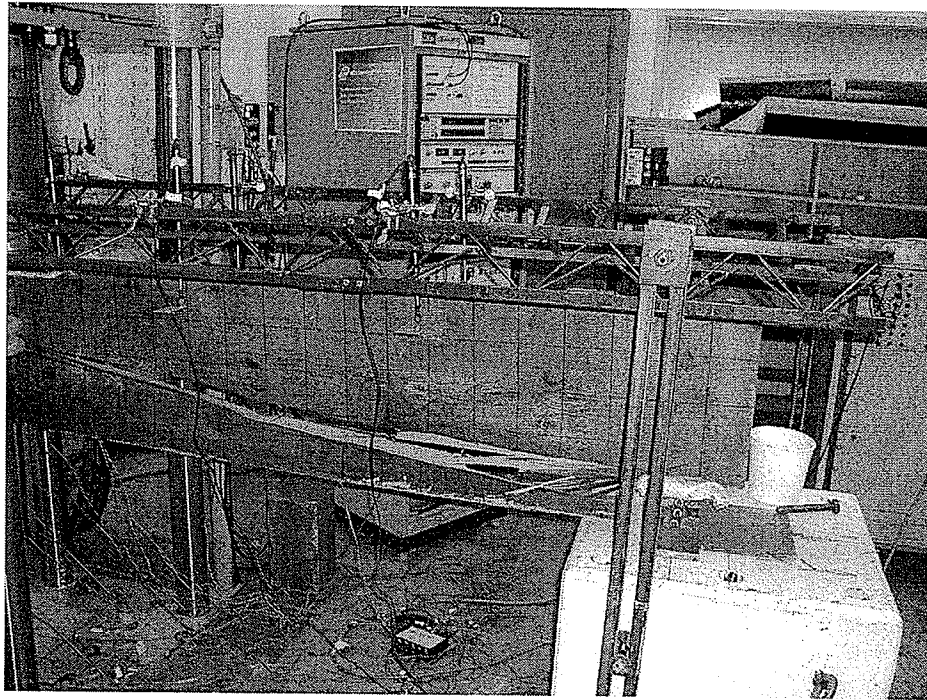


Figure 4.21 – Dap Failure

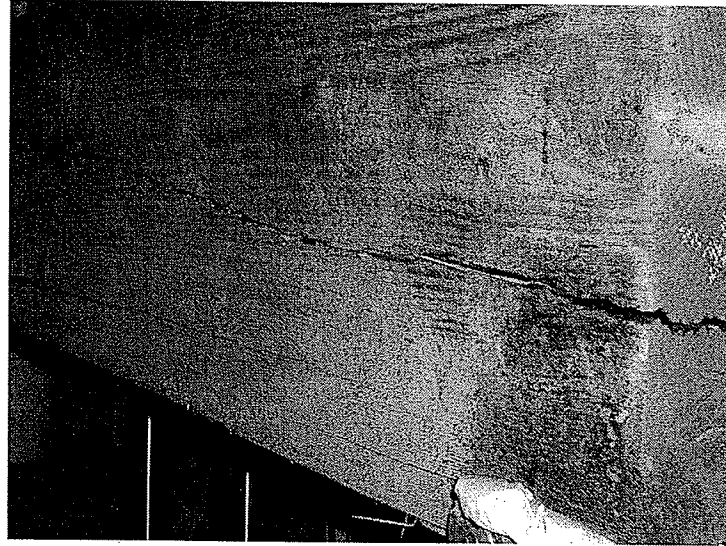


Figure 4.22 – Shear Failure

A typical tension failure originated near the midspan of the stringer, at a pre-existing crack, on the tension face and propagated along the grain toward the middle of the cross-section. The tension failure did not rupture the GFRP bars, nor did it cause a bond failure. The failure was solely in the timber and propagated around the GFRP reinforcement along a plain of weakness within the timber. A typical tension failure is displayed in Figure 4.23.

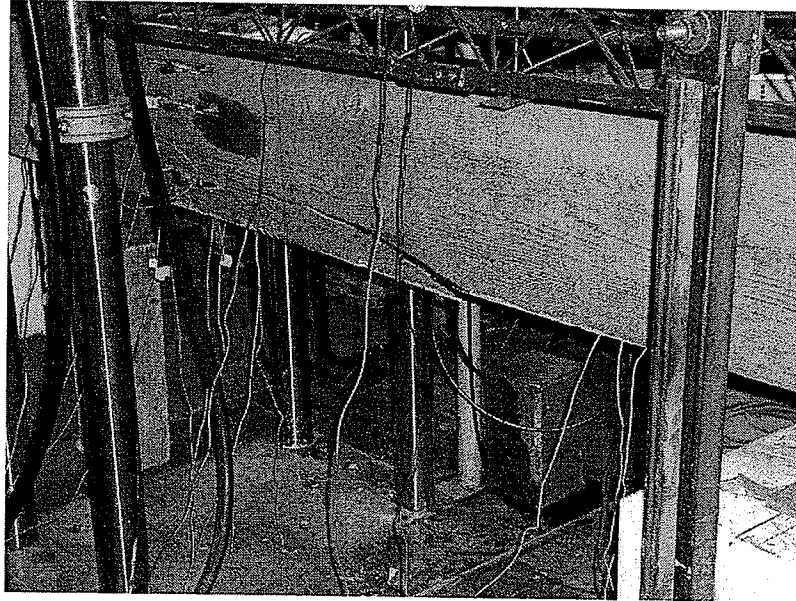


Figure 4.23 – Tension Failure

A typical bearing failure occurs at the supports where the timber crushes causing horizontal cracks to occur. This failure is very localized and did not propagate away from the area of bearing. An example of a bearing failure is shown in Figure 4.24.

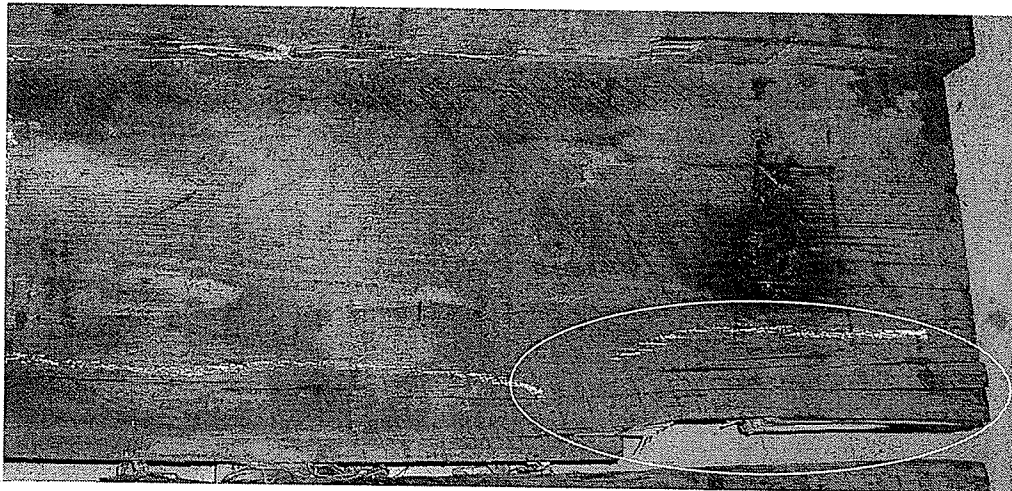


Figure 4.24 – Bearing Failure

A typical crushing failure occurs under the loading point and causes horizontal cracks as well as some vertical cracks originating from the horizontal cracks. This failure is very localized and did not propagate away from the loaded area. A picture of this failure mode is unavailable.

Both the crushing and bearing failure modes are compression failure modes and will result in the highest strength possible.

The failure modes for all specimens are presented in Table 4.1.

Table 4.1 –Failure Modes of Tested Beams

Beam		Failure Modes			
Type	Dap	Shear	Tension	Crushing	Bearing
C	4	3	0	1	0
F	4	5	2	0	1
FD	0	0	0	2	4

Dap and shear failure modes accounted for 87.5% of the ultimate failures of the control stringers. These modes of failure occur at lower load levels than the desired compression mode of failure.

Since the flexural bars were installed in the tension face of the stringers in group F, they could not prevent dap or shear failures. The beams in group F were graded as No. 1 to reject, and all had significant splits and checks, therefore the primary failure modes for the specimens in this group were dap and shear, accounting for 75% of all the failures in group F.

The splits and checks were not able to propagate through the beams of group FD because of the dowel bars. All dap failures were prevented thus, stronger failure modes, such as compression and bearing were developed, causing an increase in the average strength and ductility.

It is clearly shown that by introducing both flexural and shear reinforcement, the shear and dap failures were eliminated.

A summary of the mode of failure for the individual stringers is presented in Table 4.2.

Table 4.2 – Failure Modes of Individual Stringers

Specimen	Failure Mode
C1	Crushing
C2	Dap
C3	Shear
C4	Shear
C5	Dap
C6	Dap
C7	Shear
C8	Dap
F1	Dap
F2	Dap
F3	Shear
F4	Shear
F5	Shear
F6	Bearing
F7	Shear
F8	Tension
F9	Tension
F10	Shear
F11	Dap
F12	Dap
FD1	Compression
FD2	Bearing
FD3	Compression
FD4	Compression
FD5	Compression
FD6	Bearing

CHAPTER 5 ANALYSIS OF TEST RESULTS

5.1 General

The MOE, ultimate load, tensile stress, and MOR results were investigated using a variety of methods such as Weibull distributions, normal distributions, strength models, and size effects.

Weibull analysis and normal distributions of the flexural stresses and the MOE results, respectively, were used to determine the strength and MOE distributions for each of the reinforcement schemes. The strength and MOE distributions indicate the change obtained through the addition of the reinforcement.

The test results of this study were combined with the results of two previous studies completed by Gentile (2000) and Eden (2002). These studies were employed to increase the number of specimens available for analysis, although the timber stringers were not dapped, the results are still applicable and afford the opportunity to create more accurate distributions and thus give more accurate analysis and conclusions.

5.2 Analysis of the Results for the Current Study

5.2.1 Modulus of Elasticity

The MOE results were presented in Figure 5.1 and Table 5.1. The calculation process used to determine the MOE is discussed in conjunction with the tensile stress calculation and are presented in section 5.2.2. The dapped timber stringers of this study, obtained approximately a 44% increase in the 10th percentile MOE values for both the specimens reinforced for flexure and those reinforced for flexure and shear when compared to the control specimens, as seen in Figure 5.1. It had been concluded by Barrett and Lau (1994) and confirmed by this study that the normal distribution fits MOE data well.

Further testing is required to make an absolute conclusion as to the effect of adding GFRP reinforcement on the MOE since the MOE did not increase when the shear reinforcement was added. The MOE was expected to increase with the addition of each type of reinforcement since the MOE of the GFRP bars is greater than the timber. This did not occur, thus further testing of the effects GFRP reinforcing bars on the MOE must be completed.

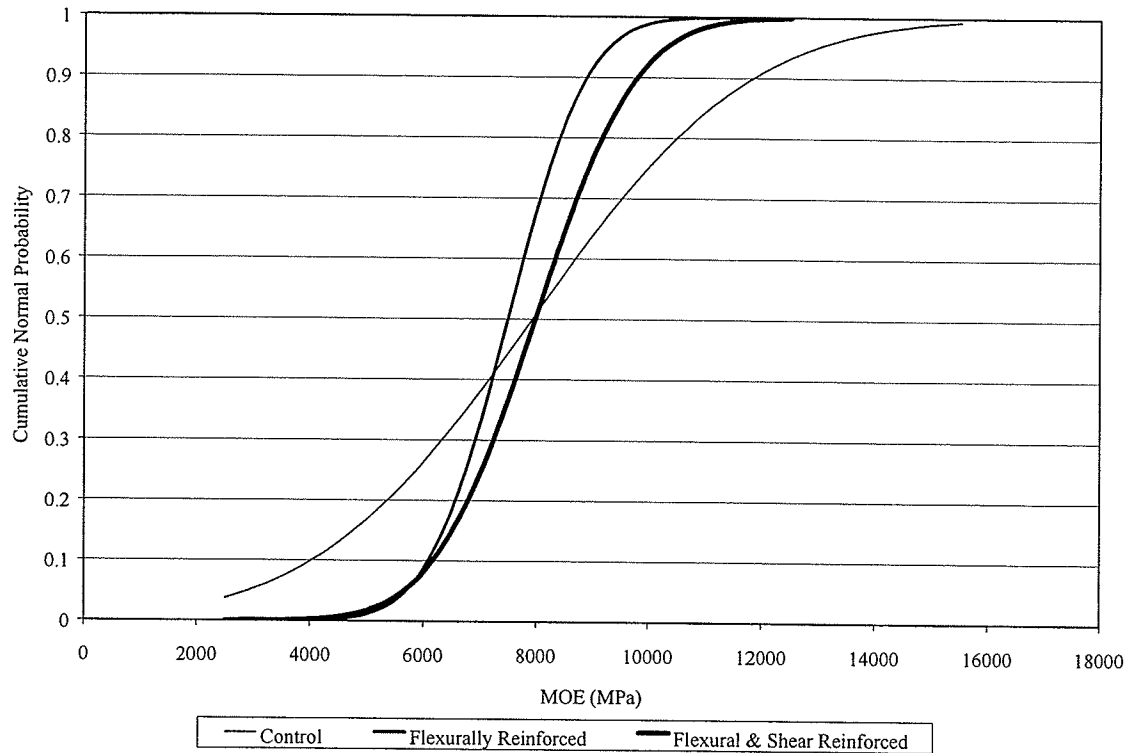


Figure 5.1 - MOE Results of Current Study

5.2.2 Ultimate Load and Tensile Stress

The tensile stress values for the experimental results were calculated using equation 5.1 along with geometric properties.

$$[5.1] \quad f_t = \frac{M}{S_b} = \frac{PL}{4S_b} \text{ for 3 point loading}$$

where: f_t is the tensile stress

M is the moment due to applied load

P is the load recorded during testing

L is the length of the stringer

S_b is the section modulus corresponding to the tension face of the stringer

Once the section modulus is determined f_t of the stringers can be calculated. To determine the section modulus a transformed section analysis using the flexural stiffness (EI) results is employed. The transformed section analysis is completed by taking the stiffness results, estimating the modular ratio, calculating the transformed centroid, and then the transformed moment of inertia (I_{tr}). Once I_{tr} is known the modular ratio (n) is determined by taking the MOE of the GFRP flexural bar times I_{tr} and dividing by EI obtained from the test data. If the originally estimated modular ratio is the same as the one calculated using the section modulus, the MOE can be determined. If it is not, a new estimate of the modular ratio must be made until the estimated and calculated modular ratios are the same. Once they are indeed the same the section modulus and MOE of the stringer can be determined. A sample of the calculation process is presented in Appendix C. MOE is found by dividing EI by I_{tr} , giving the transformed MOE which has been adjusted for the addition of the flexural reinforcement.

The load and the tensile stress results for the current study are presented in Table 5.1.

Table 5.1 – Test Results for Load, MOE, and Tensile Stress

Specimen	Ultimate Load (kN)	MOE (MPa)	Tensile Stress (MPa)
C1	153	10507	48.8
C2	82	5968	25.8
C3	125	7840	39.8
C4	146	6657	46.9
C5	127	12955	40.5
C6	123	7920	39.2
C7	103	3659	32.5
C8	115	7840	36.7
Mean	121.8	7918.3	38.8
Standard Deviation	22.6	2818.8	7.4
Coefficient of Variation (%)	18.6	35.6	19.1
F1	132	7664	40.1
F2	139	12745	43.1
F3	125	19327	38.9
F4	125	14976	39.1
F5	108	9595	33.2
F6	103	10721	31.2
F7	171	9596	52.4
F8	94	7008	28.6
F9	86	7720	26.3
F10	116	7439	35.8
F11	159	9108	48.7
F12	121	9525	37.3
Mean	123.3	10452	37.9
Standard Deviation	24.9	3629.1	7.7
Coefficient of Variation (%)	20.2	34.7	20.3
FD1	136	7821	41.4
FD2	158	7341	48.1
FD3	127	7542	38.5
FD4	162	8656	49.5
FD5	189	9515	58.0
FD6	122	5673	36.6
Mean	149	7758	45.4
Standard Deviation	25.4	1301.2	8.0
Coefficient of Variation (%)	17.1	16.8	17.7

A normal distribution was used to compare the ultimate loads of the various reinforcing schemes to determine the increase of adding each type of reinforcement and is presented in Figure 5.2.

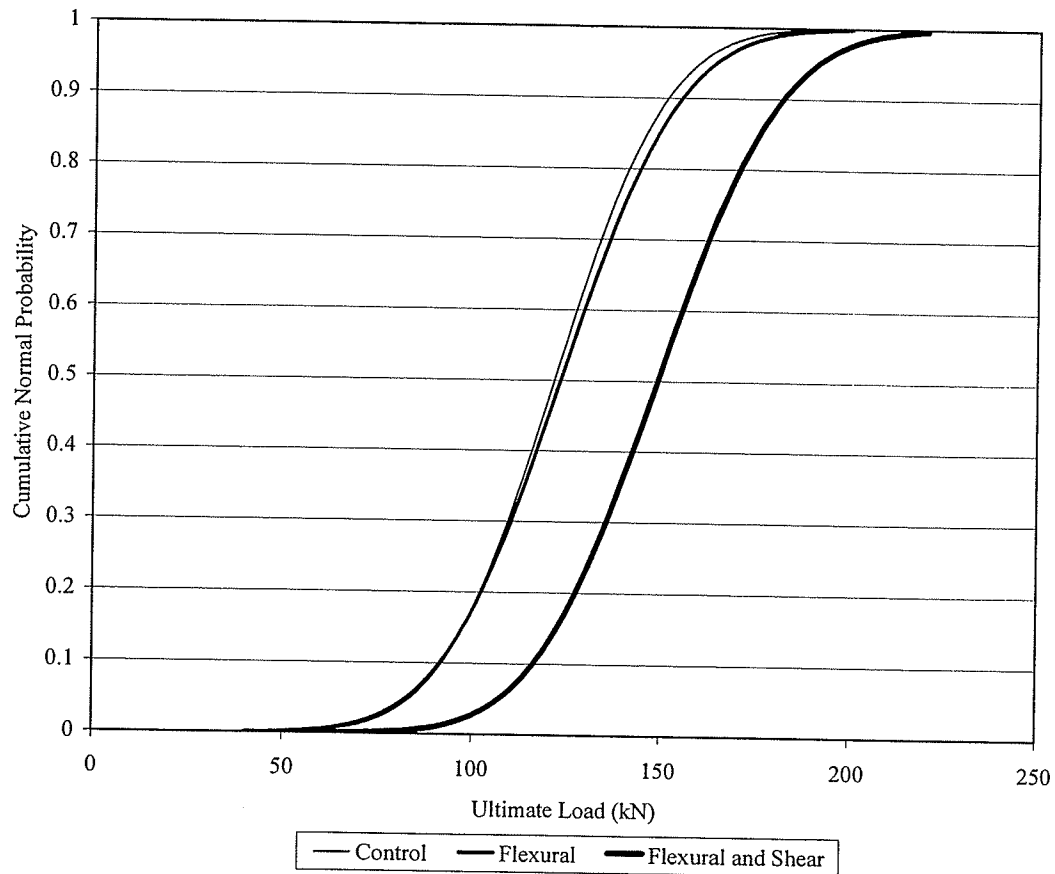


Figure 5.2 – Cumulative Normal Distribution for the Ultimate Loads of the Current Study

The tenth percentile will be discussed in accordance with the findings of Johns and Racine (2001) that given the variability of strength values for wood, it is perilous to draw precise conclusions regarding, for example, fifth percentile of strength if the sample size is not large enough. It may be justified to discuss the tenth percentile values based

on a 3-parameter Weibull distribution fit to the experimental data. Thus, the tenth percentile values are discussed since the number of tests completed was relatively small. As seen in Figure 5.2 there was no increase in the ultimate load of the flexurally reinforced specimens when compared to the control specimens. This was expected since the majority of failure modes were dap and shear for beams in both groups C and F. Using both flexural and shear reinforcement achieved a 30% increase the ultimate load. As stated by Eden (2002) a 30% increase in strength is necessary to ensure the timber bridges can withstand not only loads they were designed for but also the increased traffic load since their construction.

The tensile stresses were determined for the stringers to compare the increase obtained with the addition of each type of reinforcement as well as to compare the design value of 19.5 MPa to the tensile stresses obtained from testing. To this end, a 3-parameter Weibull distribution analysis was completed using the f_t results. A three parameter Weibull distribution was chosen since it represents the tensile stress distribution of timber stringers more accurately. The two parameter Weibull distribution assumes a minimum stress value of 0, which does not accurately represent timber beams since all timber beams have a minimum stress greater than 0. The three parameter Weibull distribution determines the minimum stress based on the data used in the analysis. Figure 5.3 shows little increase in the f_t between the control and flexurally reinforced specimens.

A strength increase of approximately 30% in the tenth percentile tensile stress was obtained for the specimens reinforced for both flexure and shear as compared to the control specimens, as for the comparison of the ultimate loads.

The stringers did not fail in tension and therefore were expected to obtain tensile stresses higher than the 19.5 MPa design stress as they did.

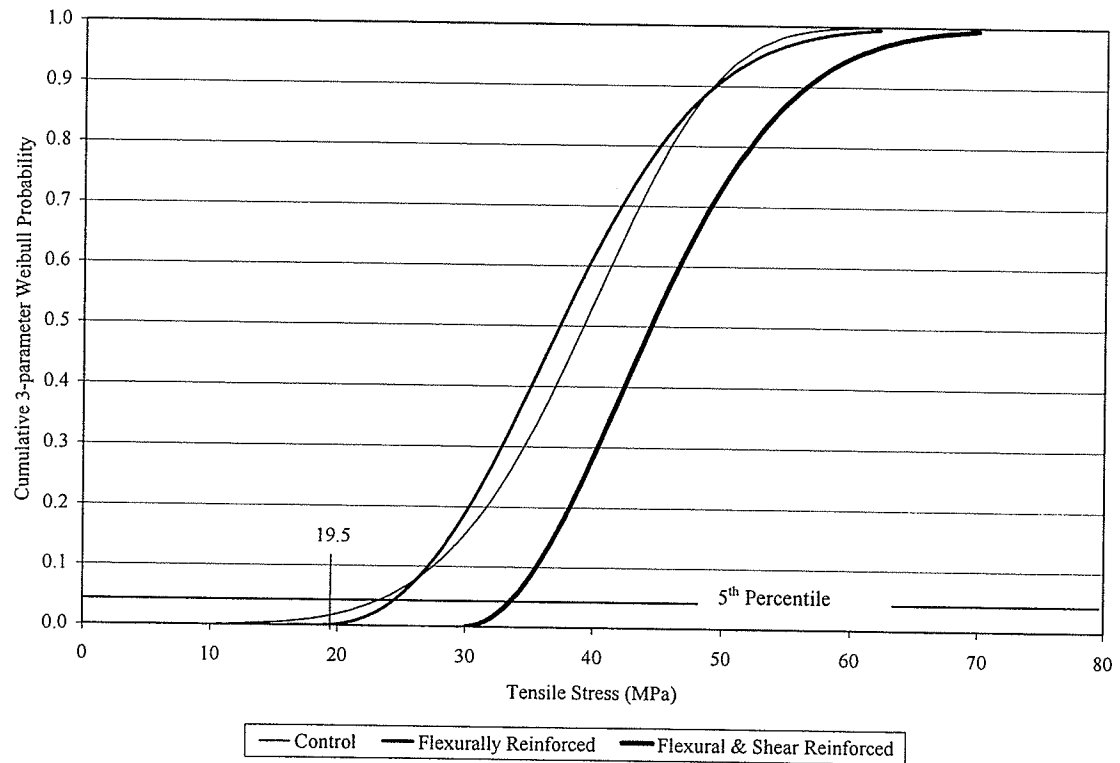


Figure 5.3 - 3 Parameter Weibull Probability Results for the Tensile Stress for the Current Study

The Weibull parameters obtained through the analysis of the tensile stress data from Table 5.1 are presented in Table 5.2

Table 5.2 – Parameters of Weibull Analysis

Specimen	Shape (k)	Scale (m_1)	Location (x_0)
C	3.10	39.70	0.00
F	2.46	22.00	18.25
FD	2.00	29.80	18.00

As seen in Table 5.3 the control data set is best fit by a 2-parameter Weibull distribution. This implies the control data set has a minimum strength value of 0. The 2-parameter Weibull distribution is the basis for the strength models presented in Chapter 2.

5.2.3 Shear Stress

The shear stresses were computed using Equation 5.2.

$$[5.2] \quad \tau = \frac{VA'y'}{Ib}$$

where τ is the shear stress

V is the shear force

A' is the area from the top of the member to the location of at which the shear stress is to be calculated

y' is the distance from the centroid of A' to the location at which the shear stress is to be calculated

I is the moment of inertia

b is the width of the cross-section

$A'y'$ is also commonly known as the shear coefficient Q .

The shear stress values for all specimens are presented in Figure 5.4. Since the control and flexurally reinforced specimens failed in shear, the shear presented in Figure 5.4 is the shear strength for groups C and F only. A design strength of 0.9 MPa is given in CSA (1994) which is larger than the shear strengths of 0.79 and 0.75 MPa obtained by the control and flexurally reinforced specimens respectively. The design strengths given

in the CSA (1994) design code are 5th percentile values thus for direct comparison with the test results the 5th percentile will be discussed.

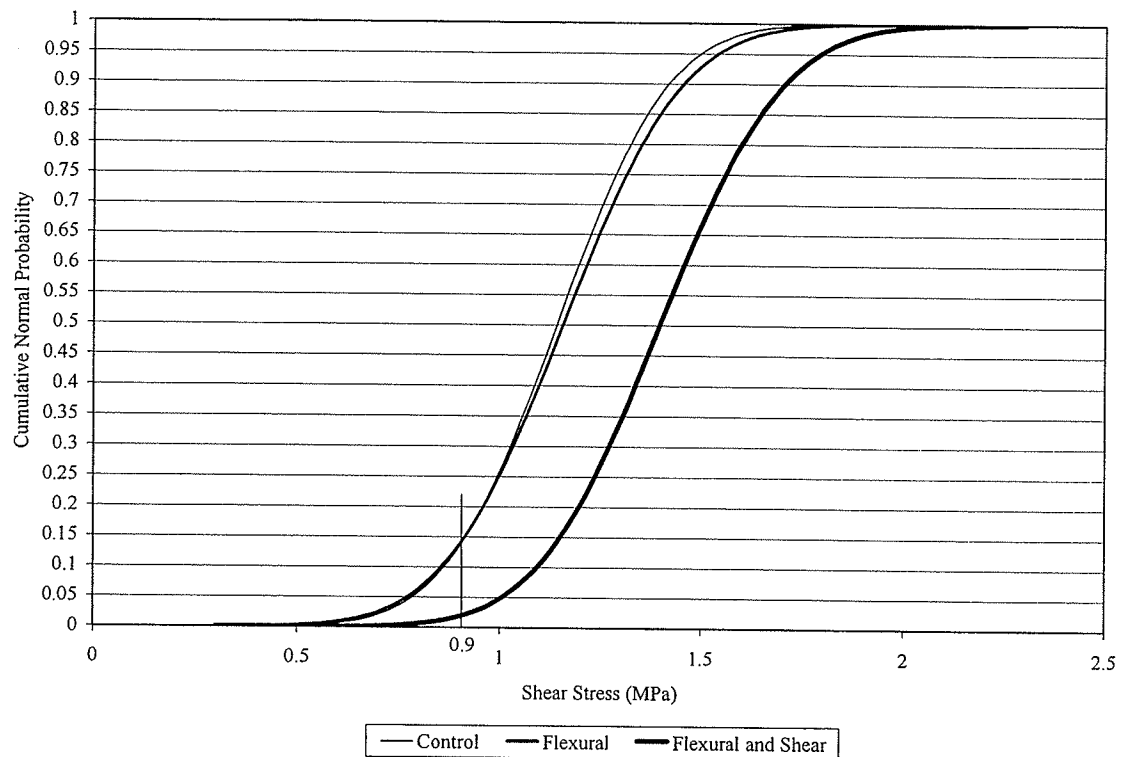


Figure 5.4 – Shear Stress for the Current Study

The timber stringers used in this study were shear deficient. This could be a result of the weathering effects the stringers were subjected to and a result of the presence of daps. By adding shear reinforcement the stringers were able to obtain a shear stress of 1 MPa, at the 5th percentile level. Since the mode of failure of the flexural and shear reinforced specimens was compression the shear stress was not the limiting factor. The load and shear stress calculations are presented in Table 5.3. The nominal values of the moment of inertia and the neutral axis depth were considered since they made the calculations

easier and gave results within 3% of the actual shear stress. The values of moment of inertia (I), neutral axis depth (y_{bar}), the beam width (b), the area above the location at which the shear stress is to be calculated (A'), and the distance from the centroid of A' to the neutral axis (y') are $533.3 \times 10^6 \text{ mm}^4$, 200 mm, 100 mm, $10 \times 10^3 \text{ mm}^2$, 100 mm respectively.

Table 5.3 – Shear Stresses

Specimen	Load (kN)	V (kN)	τ (MPa)
C1	153	76.5	1.43
C2	82	41	0.76
C3	125	62.5	1.17
C4	146	73.0	1.38
C5	127	63.5	1.19
C6	123	61.5	1.15
C7	103	51.5	0.96
C8	115	57.5	1.08
Mean	121.8	60.9	1.14
Standard Deviation	22.6	11.3	0.2
Coefficient of Variation (%)	18.6	18.6	18.9
F1	132	66.0	1.24
F2	139	69.5	1.30
F3	125	62.5	1.17
F4	125	62.5	1.17
F5	108	54.0	1.01
F6	103	51.5	0.97
F7	171	85.5	1.60
F8	94	47.0	0.88
F9	86	43.0	0.81
F10	116	58.0	1.09
F11	159	79.5	1.49
F12	121	60.5	1.13
Mean	123.3	61.7	1.16
Standard Deviation	24.9	12.5	0.2
Coefficient of Variation (%)	20.2	20.2	20.1
FD1	136	68.0	1.28
FD2	158	79.0	1.48
FD3	127	63.5	1.19
FD4	162	81.0	1.52
FD5	189	94.5	1.77
FD6	122	61	1.15
Mean	149	74.5	1.40
Standard Deviation	25.4	12.7	0.2
Coefficient of Variation (%)	17.1	17.1	16.9

5.2.4 Compressive Stress

The compressive stress was calculated using Equation 5.3.

$$[5.3] \quad \sigma_c = \frac{P}{A_b}$$

where σ_c is the compressive stress

P is the applied load

A_b is the bearing area

The compressive stresses are presented in Figure 5.5. CSA (1994) gives a design compressive stress when the load is perpendicular to the grain of 7 MPa. Since the control and flexurally reinforced specimen failed in shear they were not expected to achieve a compressive stress of 7 MPa. The flexural and shear reinforced specimen did fail in compression but as seen in Figure 5.5 the compressive stresses obtained from the testing did not come close to the design value. The stringers were unable to achieve the design compressive stress due to the weathering effects the beams had been exposed to. The surface of the stringers has become somewhat soft and worn. Despite this the flexural and shear reinforced specimens were able to obtain a 30% increase in the ultimate load when compared to the control specimen. Thus the compressive strength of the timber stringer remains sufficient to achieve the desired ultimate load increase. The calculation of the compressive stresses are presented in Table 5.4. The bearing area used to calculate the compressive stress is 100x400 mm.

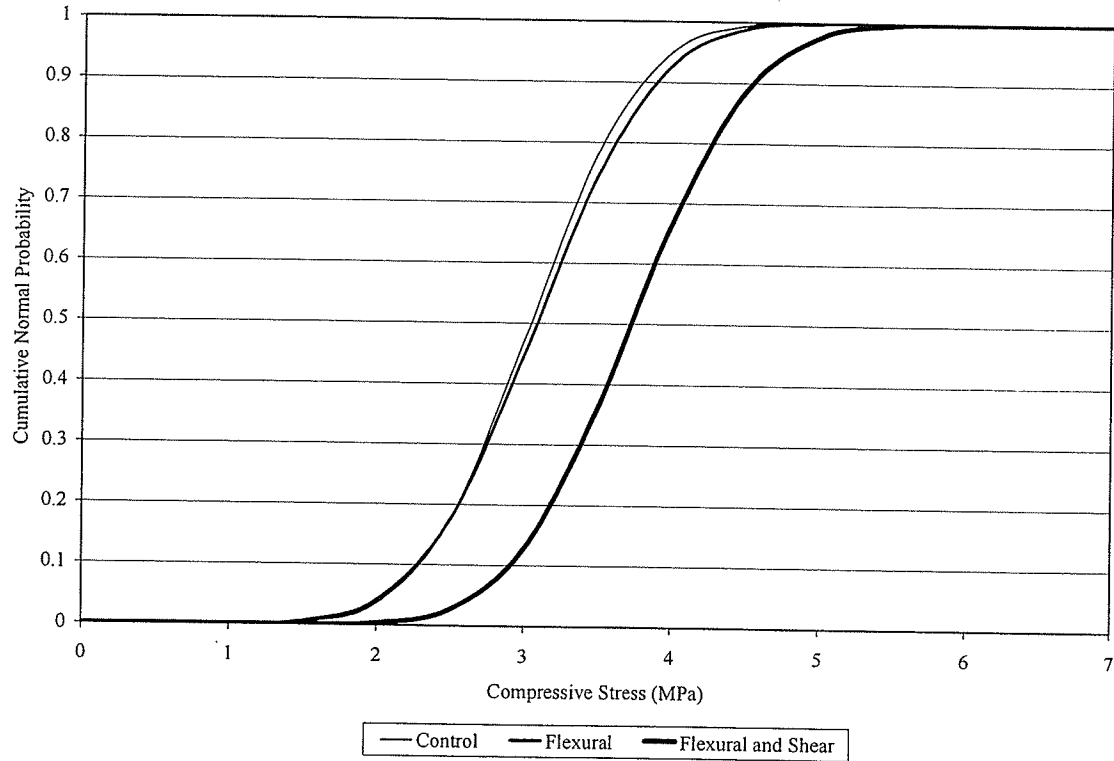


Figure 5.5 – Compressive Stress Distribution for the Current Study

The bearing area at the supports is 100x200 mm, which is half the size of the bearing area under the load point, but the load is also 50% of the load at the loading point, thus the compressive stress at under the load point or at the supports is the same.

Table 5.4 – Compressive Stresses

Specimen	Load (kN)	Compressive Stress Perpendicular to the Grain (MPa)
FD1	136	3.40
FD2	158	3.96
FD3	127	3.17
FD4	162	4.05
FD5	189	4.73
FD6	122	3.05
Mean	149	3.73
Standard Deviation	25.4	0.6
Coefficient of Variation (%)	17.1	17.1

The expected failure load due to the design stresses for tension, shear and compression are 61.5, 96, and 280 kN respectively. Thus the expected failure mode would be tensile. If the beam is strong enough in tension the next failure mode would be shear, and if strong enough in shear the failure mode would be compression. Although the loads vary from those obtained from the design stresses the progression from one failure mode to another was achieved. The tension failures were avoided by adding the flexural reinforcement along with the shear reinforcement and thus forcing the beam to fail in compression. By failing in compression, the timber beam will obtain the largest ultimate load it can achieve since timber is strongest in compression.

5.2.5 Reliability Analysis

The reliability analysis is based on the probability of failure. The probability failure is determined from the overlapping portion of the loading distribution and the resistance distributions, as seen in Figure 5.6. S represents the loads due to the traffic and R represents the resistance of the bridge members. This probability of failure is transformed into a safety factor.

To complete the reliability analysis a bridge configuration, shown in Figure 5.7, was assumed.

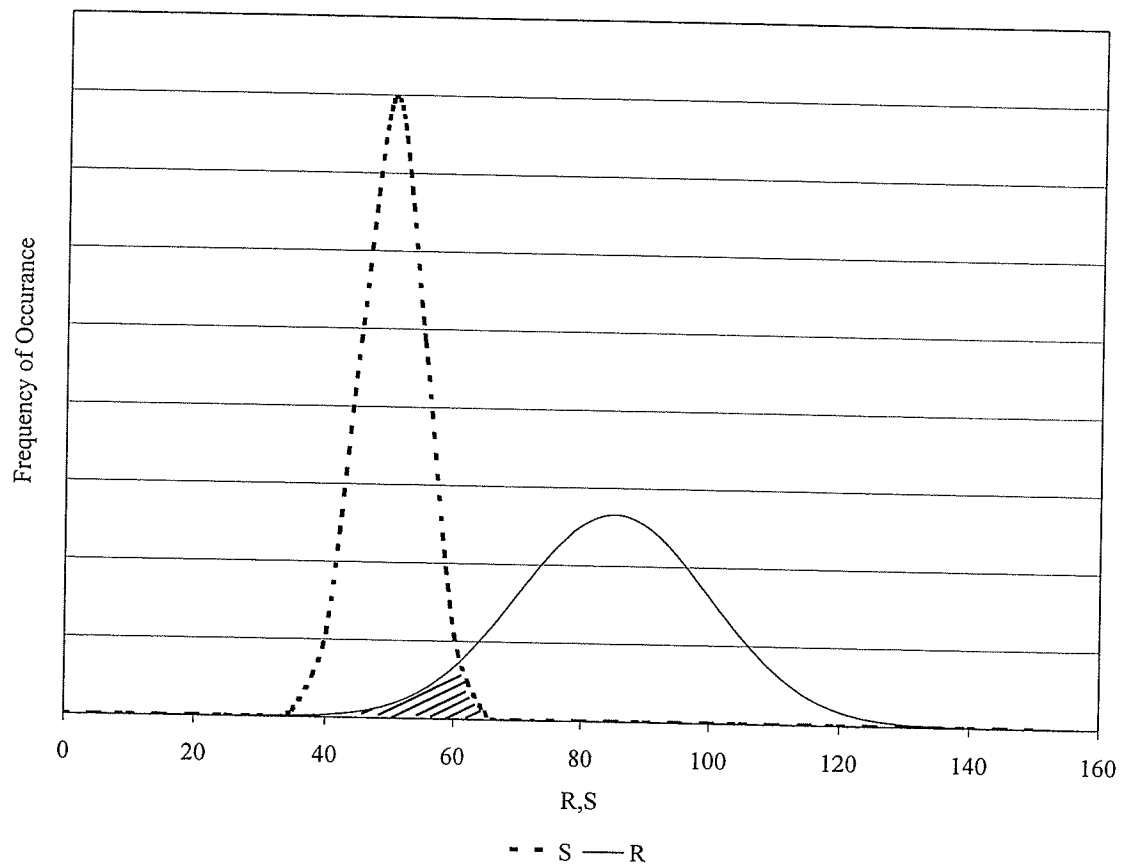


Figure 5.6 – Reliability Analysis Example

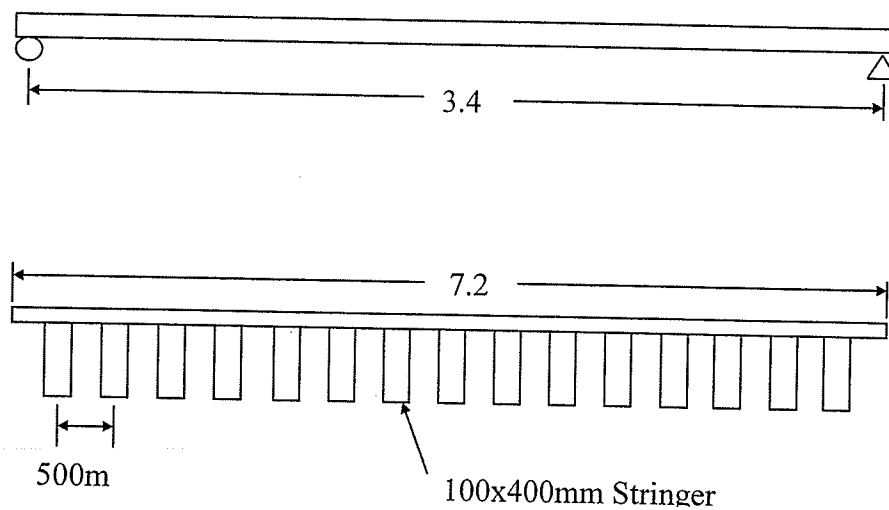


Figure 5.7 – Stringer Configuration for Typical Bridge

The only load considered on the bridge for this analysis was the live load produced by a truck as it passes over the bridge. The CL-625 truck from the Canadian Highway Bridge Design Code (CHBDC) (2000) was used to determine the loading on the bridge. Since the span of the bridge is short, the largest moment occurs when the heaviest axle is at the midspan of the bridge. The axle load is 175 kN giving a moment of 148.8 kNm. Using this moment and the theory presented in section 5.7.1.2 Longitudinal Bending Moments in Shallow Superstructures from the CHBDC (2000), as well as assuming two lanes of traffic, and a dynamic load allowance factor of 0.4 the maximum factored moment per girder was determined to be 46 kNm.

To determine the safety factor β equation 5.4 may be used, which was obtained from Mufti et al. (1996).

$$[5.4] \quad \beta = \frac{\mu_R - \mu_S}{(\sigma_R^2 - \sigma_S^2)^{0.5}}$$

where μ_R is the mean of the resistance forces

μ_S is the mean of the applied forces

σ_R is the standard deviation of the resistance forces

σ_S is the standard deviation of the applied forces

The mean and standard deviations of the resistance forces can be determined from the test data. The mean applied force is determined by multiplying the specified load, 46kNm in this case, by a bias factor obtained from table CA.4.2.1.1 of the Canadian Highway Bridge Design Code Commentary (2000). The bias values from Saskatchewan were used with a span of 3.4 m. Thus a bias value of 0.84 was determined. Therefore, the mean of the applied loads is 38.6 kNm. Using the coefficient of variation (COV) found in the

same table as the bias factor, the standard deviation of the applied loads can be determined by multiplying the COV by the mean. With the mean and standard deviation known a normal probability plot can be produced. Table 5.5 displays the means and standard deviations used in the reliability analysis.

Table 5.5 – Mean and Standard Deviation of the Moment Resistances and Applied Moments

	Mean (kNm)	Standard Deviation
C	103.4	19.7
F	104.8	21.0
FD	126.7	21.7
Loading	38.6	1.15

The safety factors determined for the CL-625 truck are displayed in Table 5.6.

Table 5.6 – Safety Factors for a CL-625 Truck Loading

Specimen	β
C	3.3
F	3.1
FD	4.1

A minimum safety factor of 3.5 is usually desired. The control and flexurally reinforced specimens did not obtain this safety factor, however the flexural and shear reinforced stringers satisfies the requirements currently used for design. This means it is possible to re-use timber stringers damaged by previous use if they are strengthened using both flexural and shear reinforcement.

Since a CL-700 truck is discussed within the CHBDC the safety factors for this truck were determined following the same process as for the CL-625. The safety factors for the CL-700 truck loading are presented in Table 5.7.

Table 5.7 – Safety Factors for a CL-700 Truck Loading

Specimen	β
C	2.7
F	2.6
FD	3.5

The flexural and shear reinforced specimens maintained a safety factor of 3.5 while the other specimens obtained a safety factor significantly lower than 3.5. The normal distributions for the moment resistances of the tested stringers and the loading effects of the CL-625 and CL-700 trucks are presented in Figures 5.8 and 5.9 respectively.

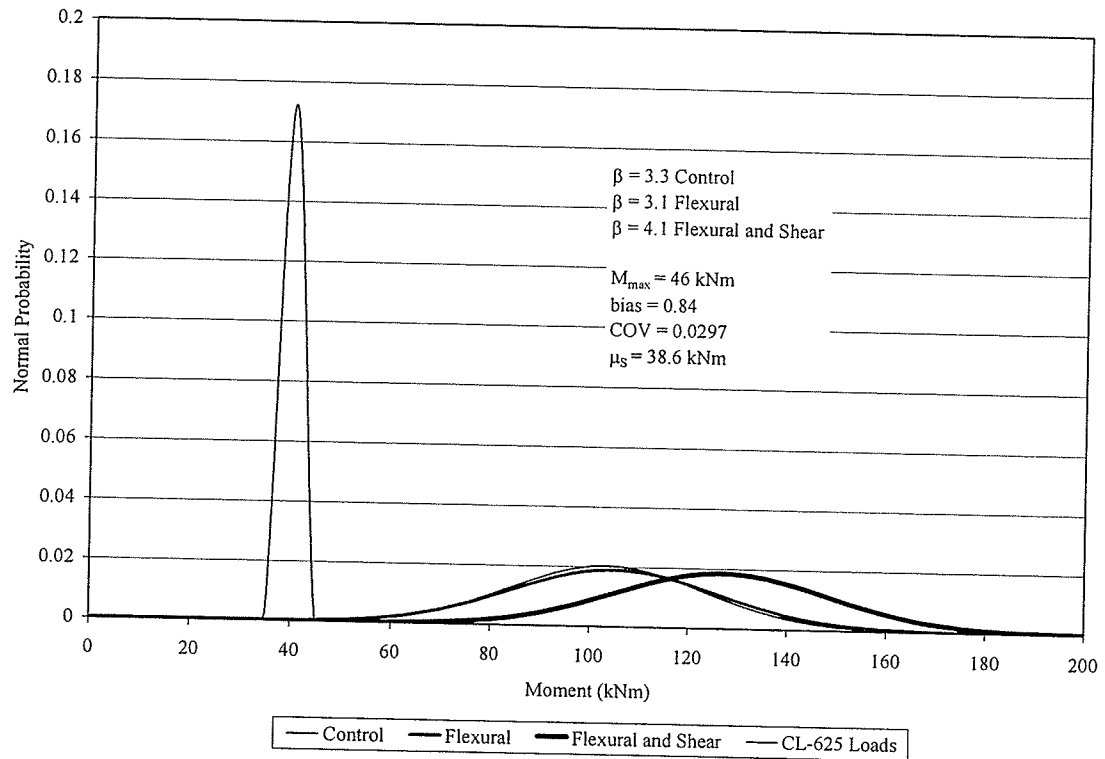


Figure 5.8 – Normal Distributions of the Moment Resistances and the CL-625 Load Effects

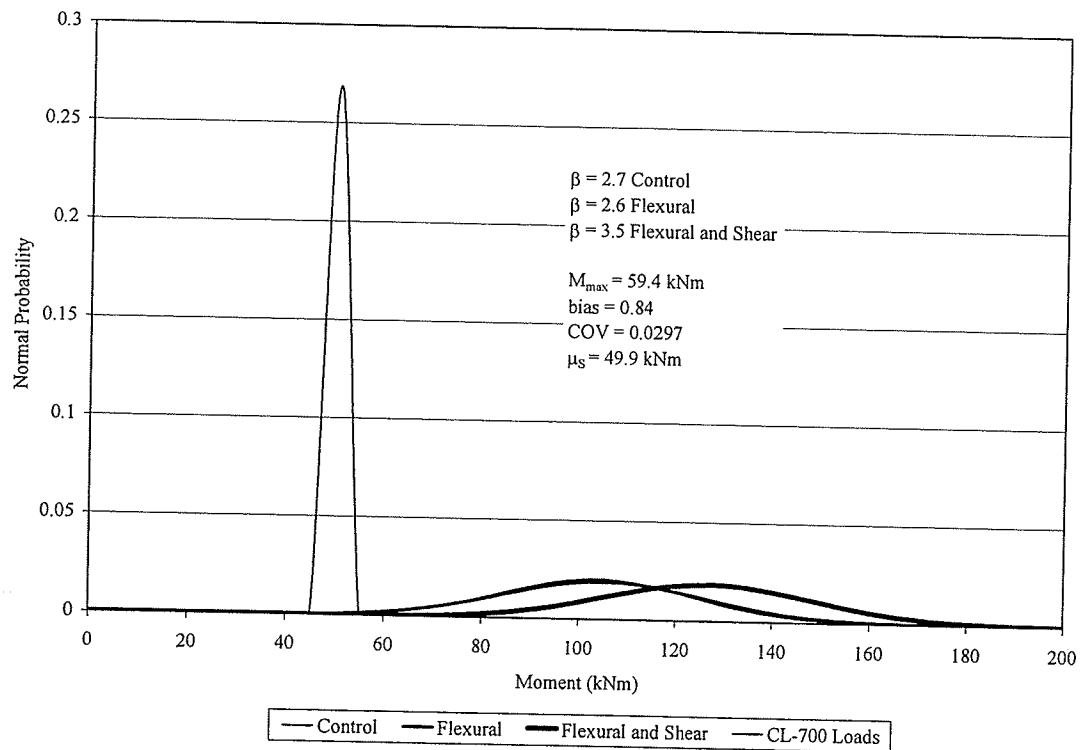


Figure 5.9 - Normal Distributions of the Moment Resistances and the CL-700 Load Effects

5.3 Analysis of the Results for the Combined Data

The test results for the combined data set were analyzed in terms of the MOE and the modulus of rupture (MOR).

5.3.1 Modulus of Elasticity for the Combined Data

MOE was determined for all the stringers and presented in a normal distribution plot. From Figure 5.10 there is an 81% increase in the 10th percentile MOE value for the flexurally reinforced specimens when compared to the control specimens.

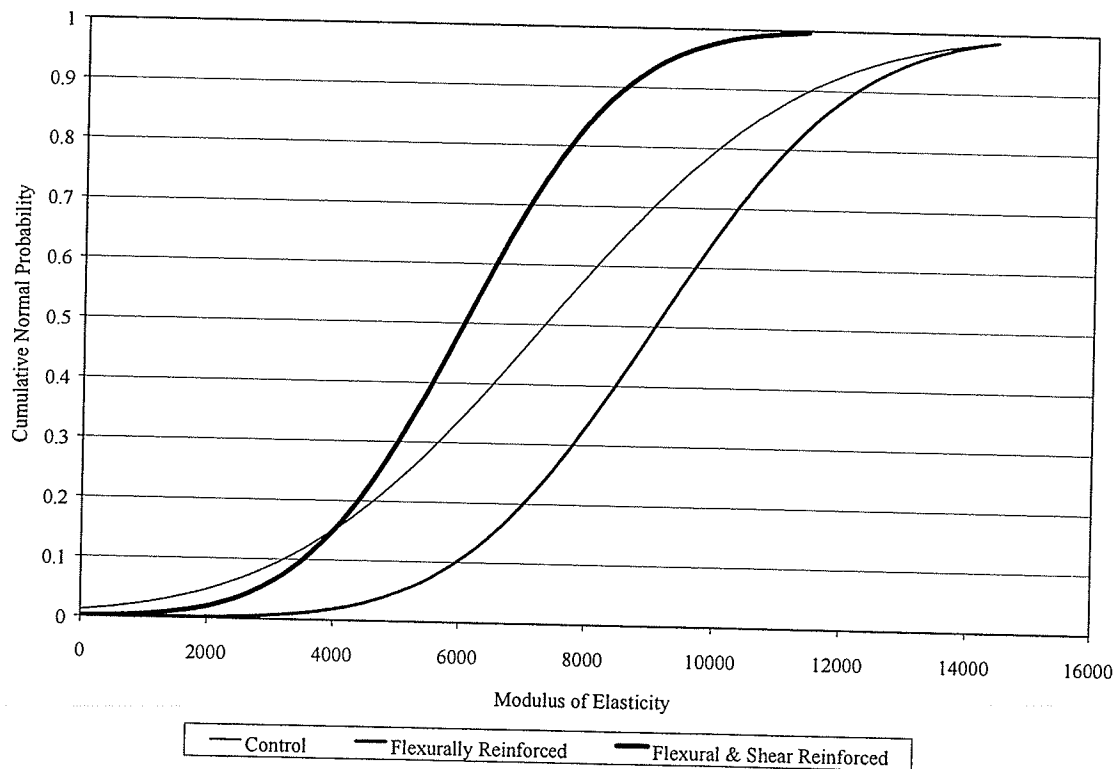


Figure 5.10 – MOE Results for the Combined Data Set

A slight increase in the 10th percentile MOE value was obtained for the flexural and shear reinforced specimens when compared to the control specimens. The discrepancy between the results is due to a span difference between the specimens tested by Gentile et al. (2002), Svecova and Eden (2004) and the current study. As stated earlier, Svecova and Eden (2004) used a test span of 1800 mm as compared to 4000 and 3400 mm used by Gentile et al. (2002) and the current study, respectively. Data obtained from testing of four different beam sizes as well as different spans is presented in Figure 5.11. According to Madsen (1992) the length of the specimen affects the MOE with shorter beams exhibiting a smaller MOE compared to longer beams. This conclusion is clearly supported by the test results presented in Figure 5.11.

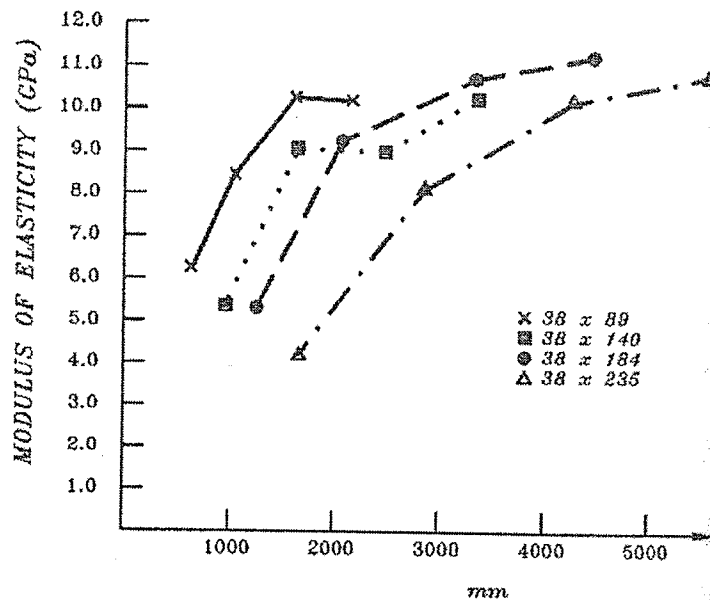


Figure 5.11 – Length Effect on MOE (Madsen 1992)

A comparison of the results obtained by Gentile et al. (2002), Svecova and Eden (2004) and the current study, shown in Figure 5.12. Figure 5.12 demonstrates, as Madsen (1992)

did, an increase in the MOE with an increase in length. Since 22 test results for the specimens reinforced for flexure and shear were from Svecova and Eden (2004) as compared to the 6 tested in this study, the MOE for these specimens appears low due to the short length of the specimens tested by Svecova and Eden (2004). All beams tested were used to create Figure 5.12, control, flexurally reinforced, and flexure and shear reinforced.

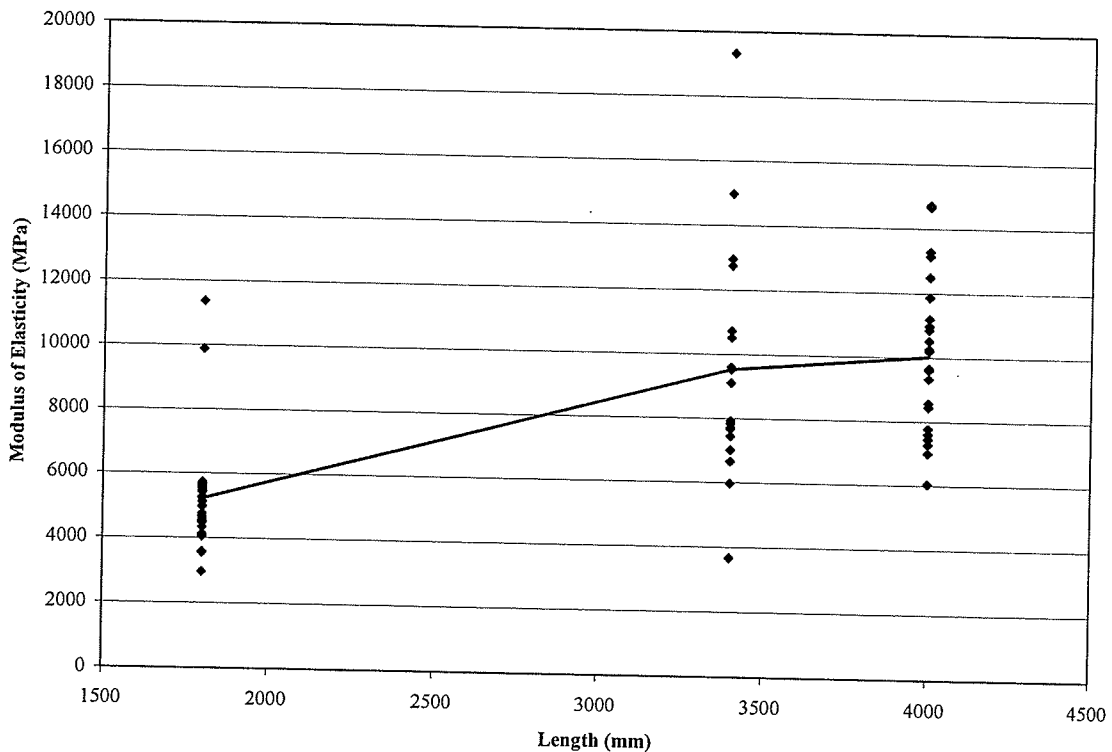


Figure 5.12 - MOE Trend for Timber Beams of Different Lengths

The flexurally reinforced specimen results were not affected since the spans used were comparable in both studies. The MOE results of the control specimens may also have been affected since 9 of the 26 test results used were obtained using the shorter spans of 1.8 m. This could indicate a larger increase in the MOE when comparing the

specimen reinforced for flexure only and the control specimens. Despite adjustments for shear deflection the increase in MOE with an increase in length remains, and therefore, there must be at least one other phenomenon that remains unknown (Madsen 1992). Definite conclusions could not be reached as to the effect of GFRP reinforcing bars on the MOE of timber stringers based on these test results.

Gentile et al. (2002) obtained no significant increase in the 10th percentile MOE value as did Svecova and Eden (2004) when comparing just their own results.

The amount of GFRP bars needed to obtain the desired strength increase is small, with a reinforcement ratio of 0.53% used in this study. Considering the low MOE of GFRP (approximately 47 GPa), and the test results, it can be stated that GFRP reinforcing bars have a negligible effect on the MOE of timber stringers. If an increase in the MOE is required, use of carbon fibre reinforced polymer (CFRP) bars or external prestressing strands may be suggested.

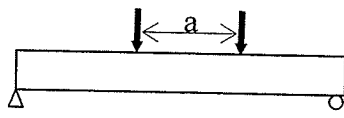
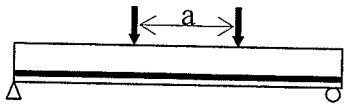
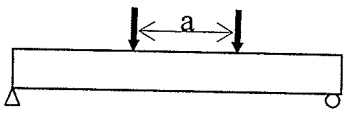
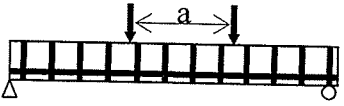
5.3.2 Strength Results of the Combined Data Set

To increase the sample size, results from Gentile (2000) and Eden (2002) were incorporated giving a total of 78 beams (26 control, 24 flexurally reinforced, and 28 reinforced for flexure and shear) as shown in Table 5.8. The beams were tested in three-point, or four-point bending with lengths ranging from 1800 mm to 4000 mm, the details are presented in Table 5.9.

Table 5.8 – Number of Stringer used for Statistical Analysis by Type and Author

Beam Type	Current Study	Gentile (2000)	Eden (2002)	Total
C	8	9	9	26
F	12	12	0	24
FD	6	0	22	28

Table 5.9 – Details of Beams used in Statistical Analysis

Beam	Diagram	Length (mm)	Depth (mm)	Width (mm)	a (mm)	# of beams
Gentile (2000)	C 	4000	300	100	600	9
	F 					12
Eden (2002)	C 	1800	300	100	600	9
	FD 					22

The beams tested by Gentile (2000) and Eden (2002) did fail in tension and thus the MOR is reported here. The beams tested in the current study did not fail in tension and thus the tensile stress at failure is reported in this section. Despite this the results of the current study were used thus increasing the number of results available and ensuring the analysis is conservative since 26 out of the 78 test results of the combined data set

would have achieved slightly higher tensile stresses if the mode of failure had been tension. For the following analysis all the tensile stresses at failure for all the specimens used in the combined data set will be considered the MOR of that particular specimen.

The experimental data had to be adjusted for depth and length effects, because the beams had varying depth and load configuration schemes. The reference beam chosen was, a "2x10" beam in bending.

The tensile stress at failure for all 78 beams were compared using a histogram shown in Figure 5.13. The peak MOR ranges were found to be 30-35 MPa for the control specimens, 36-41 MPa for the flexurally reinforced specimens and 42-47 MPa for the specimens reinforced for flexure and shear. The specimens reinforced for flexure and shear have the highest peak MOR range of 42-47 MPa as anticipated. A smaller than anticipated increase in the peak strength range between the flexurally reinforced and control beams occurred, based on the results reported by Gentile (2000), which was primarily due to the fact the beams tested by Gentile et al. (2002) did not have a dap and were graded as No. 1 or No. 2, and therefore were able to withstand higher loads before failure even without shear reinforcement. It is clear based on the present test results that when beams with dapped ends are used, it is essential to incorporate the shear reinforcement, at least in the vicinity of the dap, to prevent dap and horizontal shear failures that may be initiated when the flexural capacity of the beam is increased by the addition of flexural reinforcement.

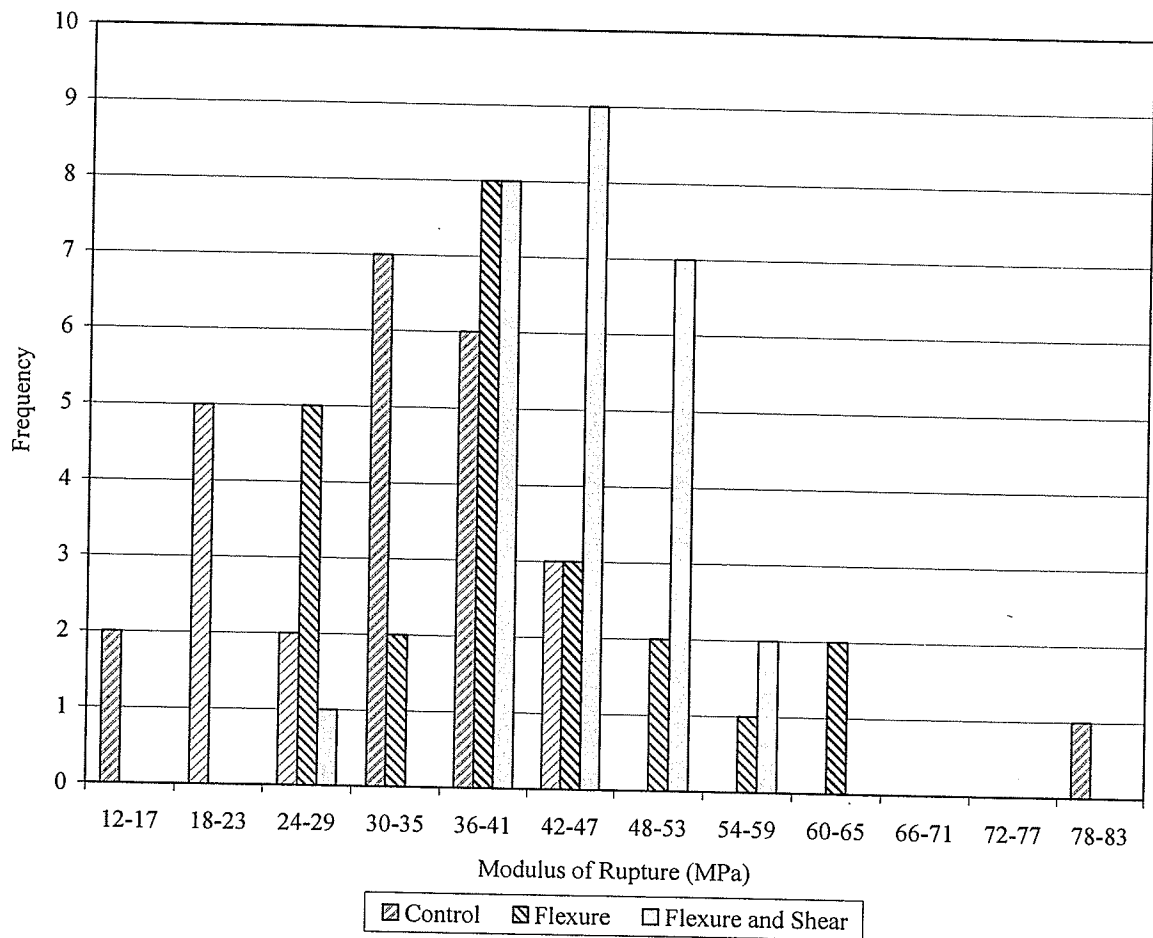


Figure 5.13 - Combined Modulus of Rupture Histogram

A 3-parameter Weibull distribution analysis was completed on the combined data set, and the cumulative probability graphs for the MOR values are given in Figure 5.14. The analysis shows a 22% increase in the 10th percentile MOR value of the flexurally reinforced specimens compared to the control specimens. Note that the stringers used in the current study were dapped and those used by Gentile et al. (2002) and Svecova and Eden (2004) were not dapped. This may have effected the results slightly since the stringers from the previous studies did not have any possiblty of a dap failure mode.

A 70% increase in the 10th percentile MOR value of the specimens reinforced for both shear and flexure compared to the control specimens was obtained, as shown in Figure 5.15. This increase is much larger than the required 30%, as stated previously. The fact that some of the stringers had daps would have had very little if any effect on these results since the dowel bars effectively eliminated dap failures. None of the beams tested failed due to rupture of GFRP reinforcement thus, all stringers reinforced with flexural and shear reinforcement had the possibility of similar failure modes.

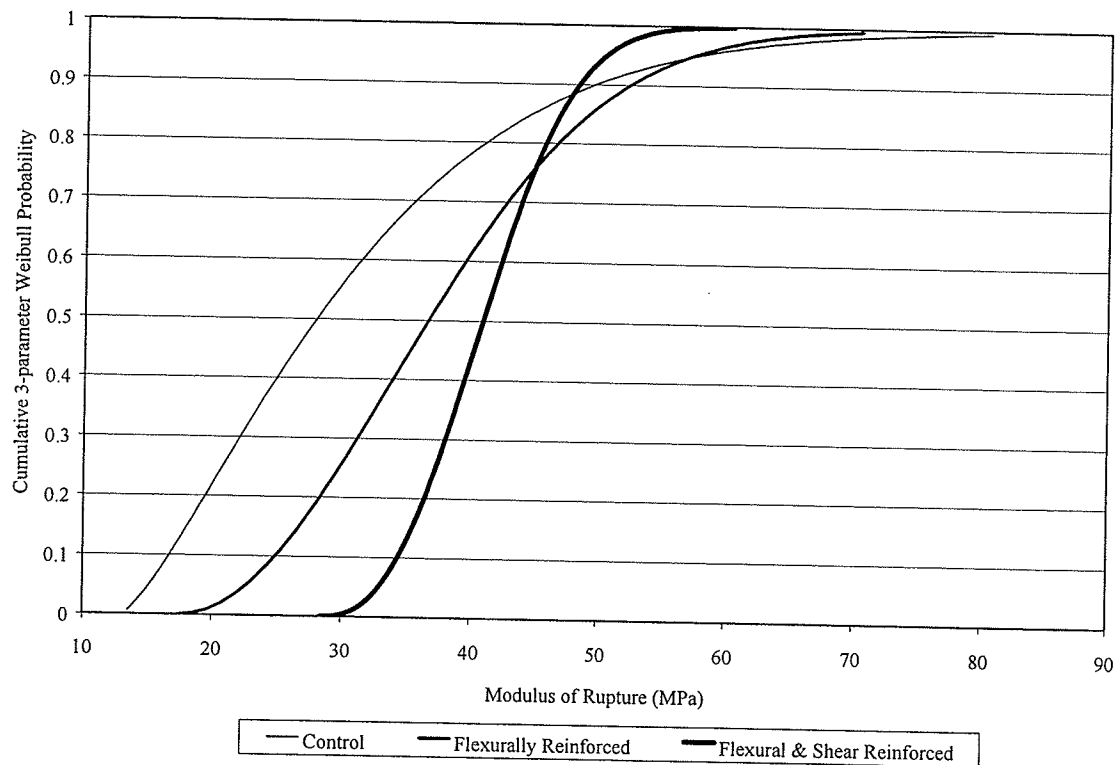


Figure 5.14 – Combined 3-parameter Weibull Probability Results for MOR Adjusted to a 38x256 mm size

The Weibull parameters obtained for the combined data set analysis are presented in Table 5.10.

Table 5.10 – Weibull Parameters from Combined Data Set Analysis

Specimen	Shape (k)	Scale (m_1)	Location (x_0)
CWC (No.1) (1994)	1.34	19.58	13.04
C	1.08	15.00	17.83
F	2.01	23.00	17.37
FD	2.58	14.00	28.38

To compare the results of the CWC and the control specimens an arbitrary Weibull curve was created with strength values ranging from 13 to 90 MPa and is presented in Figure 5.15. It demonstrates how close the results from the CWC and the control stringers actually are, especially for higher values of MOR. Thus, the control stringers are considered equivalent to No.1 grade timber, which does fit with the previously discussed visual grading scheme. All other grades of CWC douglas fir 38 x 256 mm Weibull parameters for the MOR were used and compared to the control results. From this analysis the No.1 grade parameters were found to give the best fit to the experimental results.

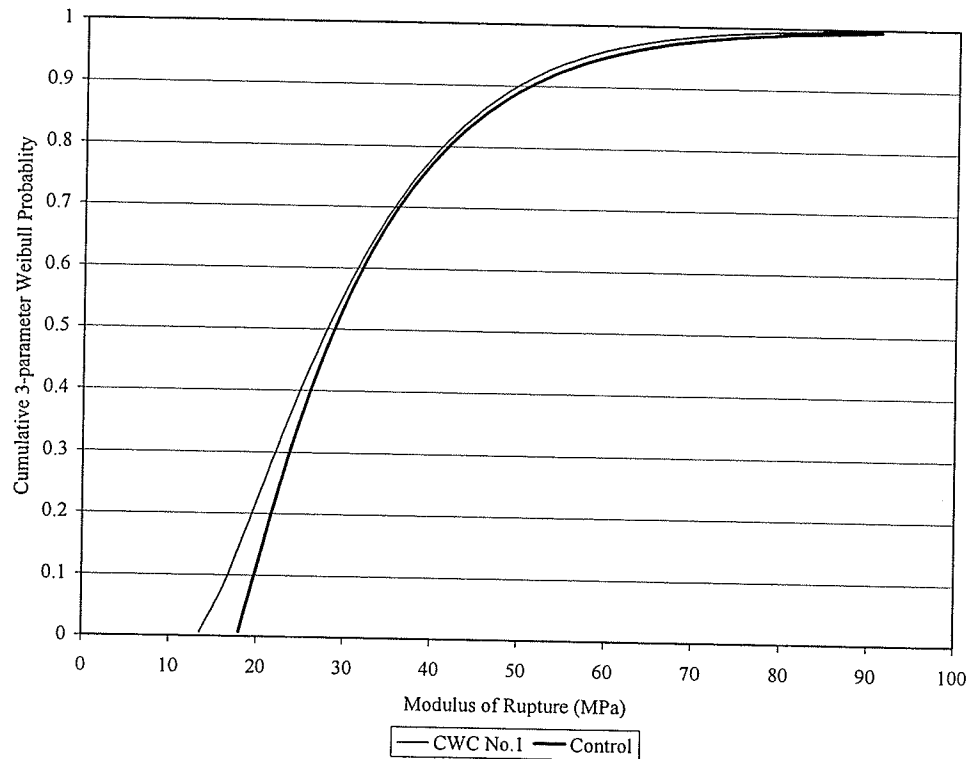


Figure 5.15 – Comparison of CWC No.1 Grade Results and the Combined Data for Control Stringers

Figure 5.16 displays the Weibull distribution results obtained for all the specimens adjusted to the size of the stringers of this current study, as opposed to the previous analysis which adjusted all the stringers to a 38 x 256 mm size. This was done since the CSA design value for timber stringers is only valid for stringer 101.6 mm (4") wide or larger (CSA 1995). Since all the stringers tested are approximately 100 mm wide, the beams of this current study were chosen to be the reference beams and thus be able to compare the results of this analysis directly to the CSA design value. The size effect factor used to adjust the strength results so as to make direct comparisons with the results of the current study are presented in Table 5.11.

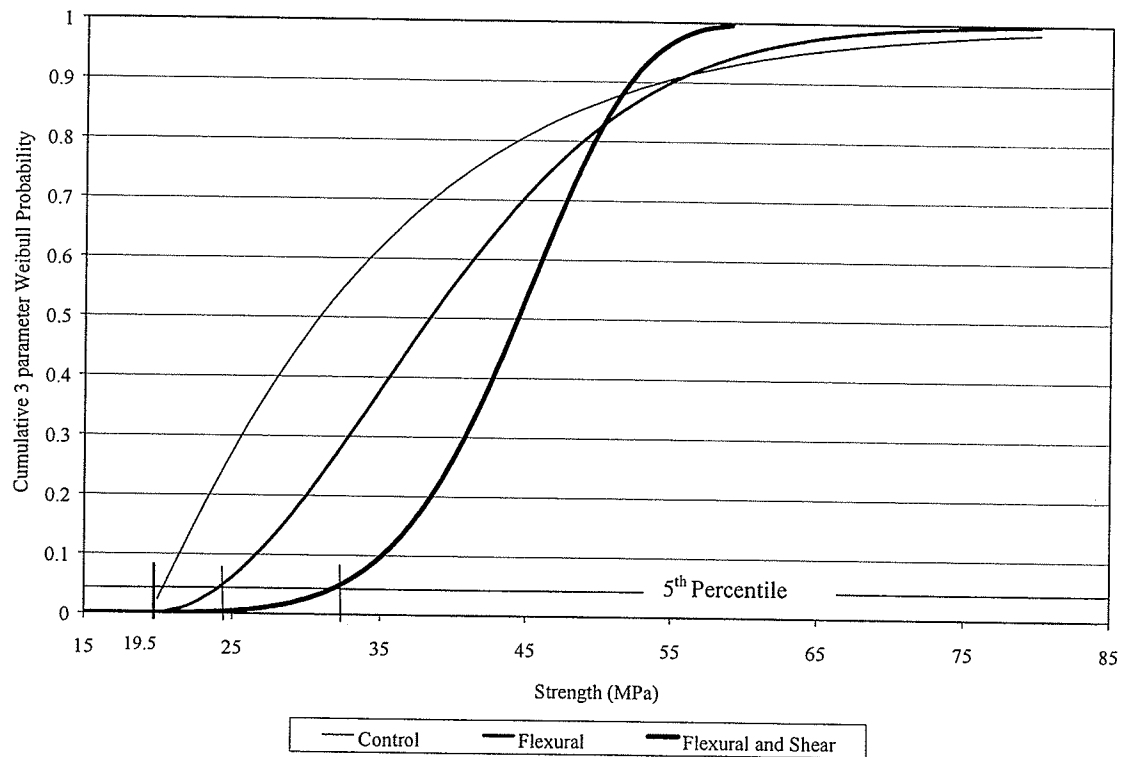


Figure 5.16 – Weibull Distribution for Combined Data Set Showing the CSA Design Value 19.5 MPa

Table 5.11 – Size Effect Factors to Obtain Equivalent Sized Stringers to the Current Study

Source	Size Effect Factors		
	Stressed Length	Depth	Overall
Current Study	1.000	1.000	1.000
Eden (2002)	1.079	0.923	0.996
Gentile (2000)	1.145	0.923	1.056

The CSA design value for select structural timber stringers is 19.5 MPa. It can be derived from Figure 5.16, there is a 26% increase of the 5th percentile strength of the flexurally reinforced specimens and a 66% increase in strength of the flexural and shear reinforced specimens as compared to the CSA design value. The control specimens are

only a few percent higher than this value despite being graded from No.1 to reject. The grading used was visual and may not always exactly represent the way in which a particular stringer will react to the applied load. Thus, the control stringers tested do in fact match very closely to the CSA design value for select structural timber beams. The 5th percentile is discussed here since the CSA design value is a 5th percentile value and a direct comparison was to be made. If the 10th percentile value was used, as discussed earlier, a comparison between the CSA value and those obtained from testing could not be compared directly.

5.4 Strength Models

The applicability of the strength model developed by Buchanan (1984) and modified by Gentile (2000) was investigated. A new strength model was developed based on the work of Buchanan (1984) and using a modified stress distribution to account for the addition of the flexural reinforcement. As discussed in Chapter 2, the equations developed by Buchanan (1984) and Gentile (2000) are for plain stringers and for stringers reinforced with GFRP flexural bars, respectively.

The parameters required to determine the predicted strength values using the strength models presented in the following sections are presented in Tables 5.12 through 5.15.

Table 5.12 - Weibull Distribution Parameters for Select Structural Douglas-Fir (Barrett and Lau 1994)

	UCS	UTS
Shape (k)	2.79	1.86
Scale (m_1)	24.13	20.62
Location (x_0)	14.9	10

Table 5.13 - Sizes of the Tension and Compression Specimens (Barrett and Lau 1994)

Specimen Type	Length (mm)	Depth (mm)
Tension	3683	235
Compression	4267	235

Table 5.14 - Length and Depth Factors for Tensile and Compression Strengths (Barrett and Lau 1994)

	k_1	k_2
Tension	5.9	4.4
Compression	10	9.1

Table 5.15 - Modulus of Elasticity Results (Barrett and Lau 1994)

	Modulus of Elasticity (MPa)
Mean	12914
5 th percentile	8860

5.4.1 Plain and Flexurally Reinforced Strength Models

The theory presented in Chapter 2 for Buchanan's (1984) plain timber strength model was used to calculate the theoretical strength values of the tested control timber stringers. The results of this analysis are presented in Figure 5.17. Buchanan's (1984) strength equation gave very good correlation between the tested strength of control stringers and the theoretical strength. Only 3 stringer strengths, or 11.5%, were over estimated, the rest were exactly predicted or underpredicted making the model somewhat conservative.

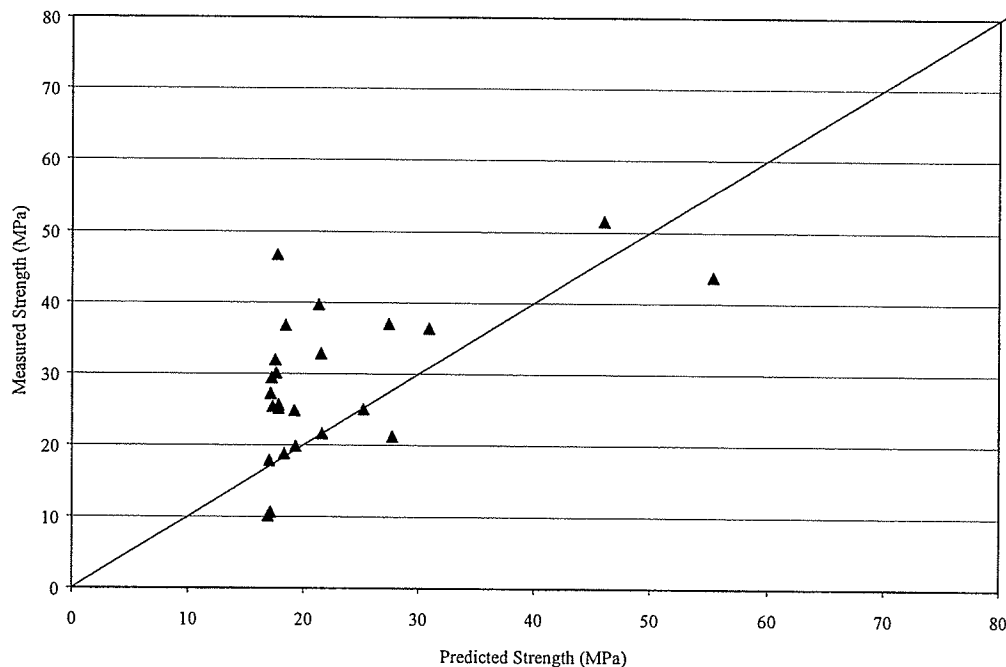


Figure 5.17 – Strength Results for the Analysis of the Control Specimens

Gentile (2000) modified Buchanan's (1984) equation by using a parameter α , as shown in Equation 5.5. The value of α was determined to be 1.3 for flexurally reinforced specimens. α is an overall factor used to adjust the Buchanan's (1984) plain

timber strength equation to fit the strength results of the flexurally reinforced stringers. To determine if this value fit the combined data sets for all beams reinforced in flexure, various values of α were used in the calculations of the theoretical strength values. The theoretical strength values were then compared to the actual test data to determine the best fit. The equation developed by Gentile (2000) was presented in Equation 2.15 and again in Equation 5.5.

$$[5.5] \quad f_m = \alpha \left(\frac{k_3 + 1}{c} \right)^{\frac{1}{k_3}} f_u$$

Figure 5.14 displays the results of using an α factor equal to 1.3 as determined by Gentile (2000). A k_3 value of 10 was used as for the plain timber model.

As seen in Figure 5.18, the α value of 1.3 over predicts the strengths of 42% flexurally reinforced timber stringers. This is because Gentile (2000) had limited data to base his conclusions on. With the addition of 12 more test results from this study a more refined α factor can be decided upon.

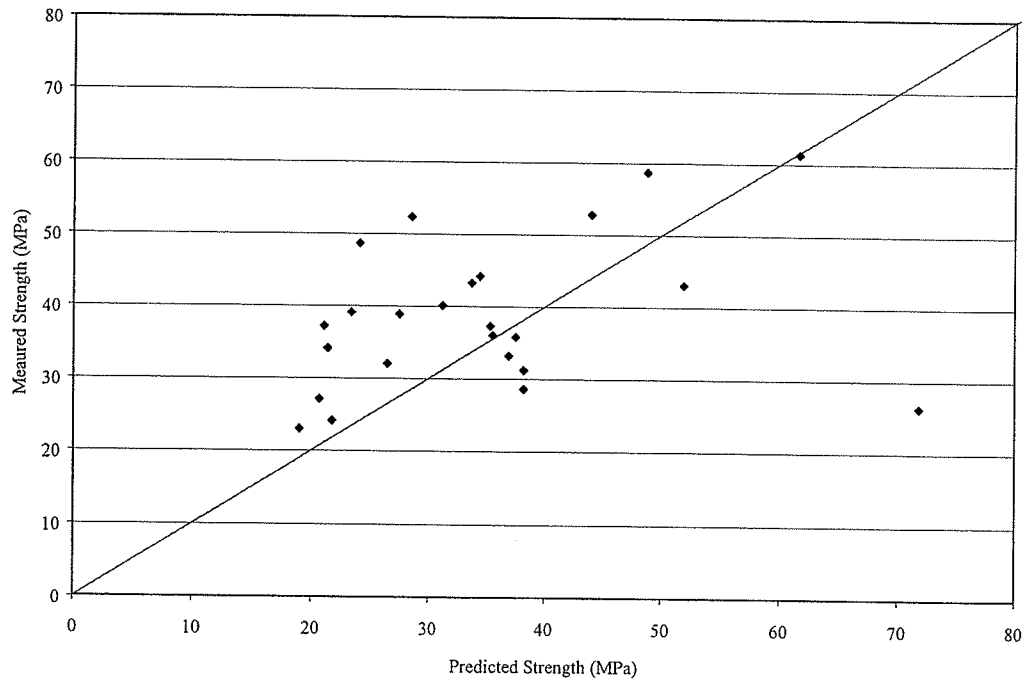


Figure 5.18 - Strength Results for the Analysis of the Flexurally Reinforced Specimens with $\alpha=1.3$

Figure 5.19 displays the calculated strength values versus the experimental values using an α value of 1.1 for the flexurally reinforced specimens. Except for the outlier, which will be ignored, the predicted and measured values fit well when using an α value of 1.1. The majority of the values were underpredicted, thus making the model somewhat conservative. This model over estimated 6 strengths, or 25% of the beams. This is not as conservative as Buchanan's (1984) but still gives a fairly accurate representation of the actual strength of a timber stringer reinforced with GFRP bars for flexure if the original value of α is changed based on the larger number of the sample to 1.1. It must be expected to over predict some of the terms since timber gives such varying results. A sample calculation of the predicted strength is presented in the Appendix A.

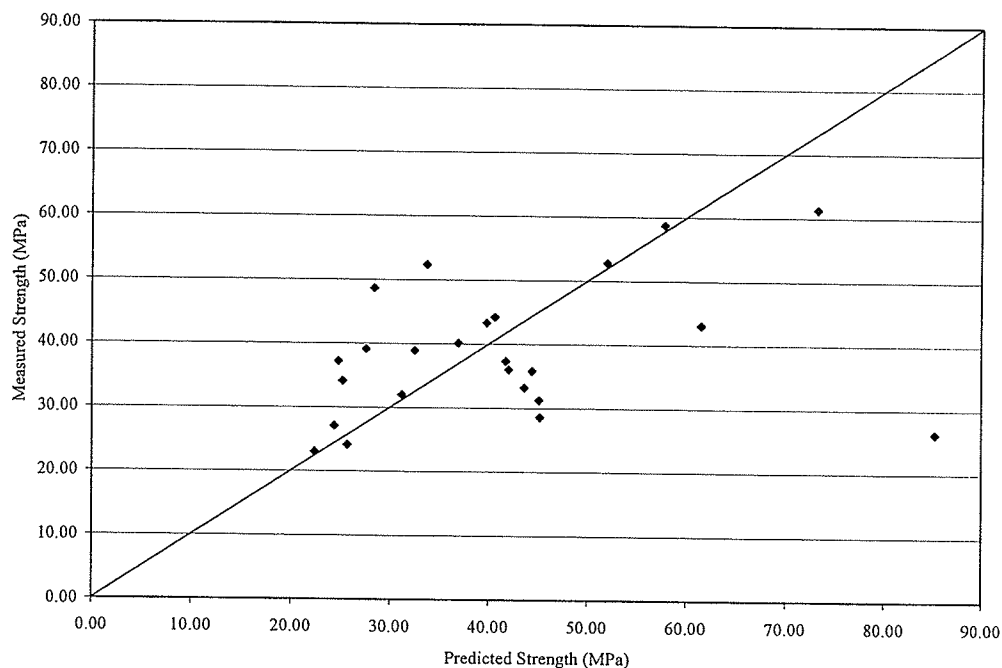


Figure 5.19 – Strength Results for the Analysis of the Flexurally Reinforced Specimens with $\alpha=1.1$

Figure 5.20 displays the predicted versus measured strength values for the specimens reinforced for flexure and shear using an α of 1.3. An α value of 1.6 was determined to give the best fit between the measured and predicted strength values and is presented in Figure 5.21. The flexural and shear reinforced specimen results have much less spread and therefore are easier to fit the strength equation to. All the data points in Figure 5.21 are underpredicted or predicted exactly thus making this model conservative, yet not too conservative since the spread in the data is significantly less than with the control and flexurally reinforced specimens.

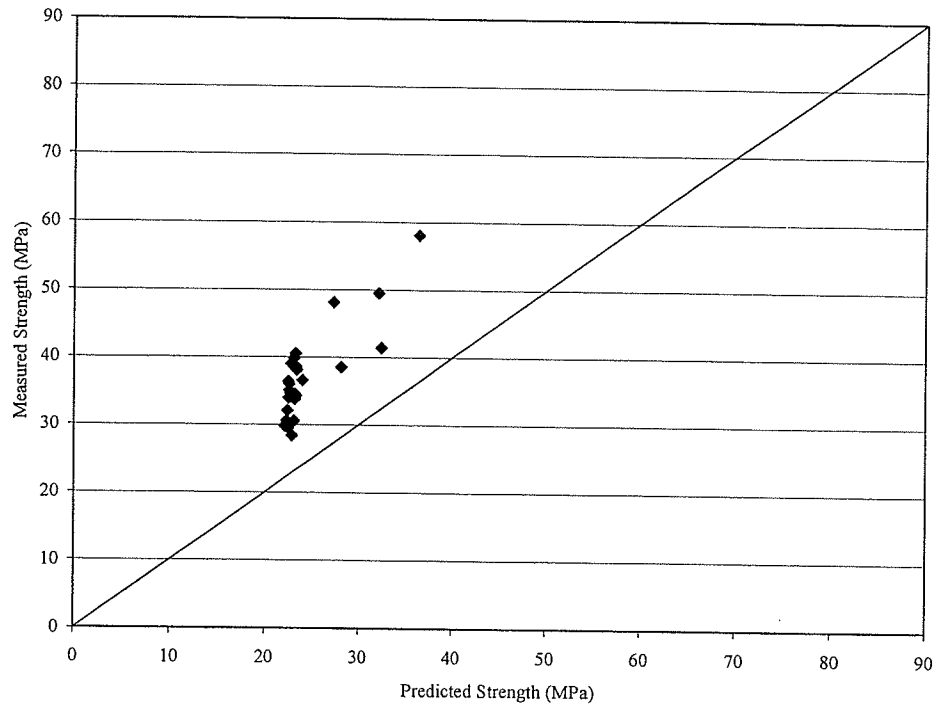


Figure 5.20 - Strength Values for Flexural and Shear Reinforced Specimens with $\alpha=1.3$

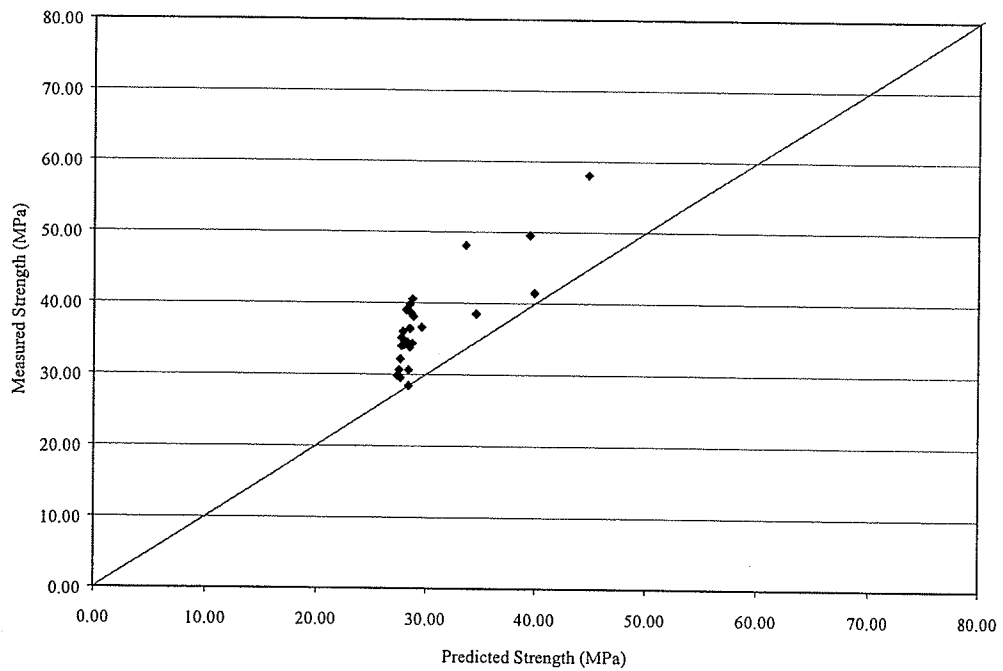


Figure 5.21- Strength Values for Flexural and Shear Reinforced Specimens with $\alpha=1.6$

5.4.2 Strength Model using Modified Stress Distributions

The modular ratio was used to increase the stress at the location of the FRP reinforcement to depict a more accurate stress distribution with the addition of the FRP bars. Figure 5.22 depicts the new stress distributions.

The same process used to derive the bending strength equation for a plain timber beam will be used to derive a bending strength equation for a reinforced timber beam.

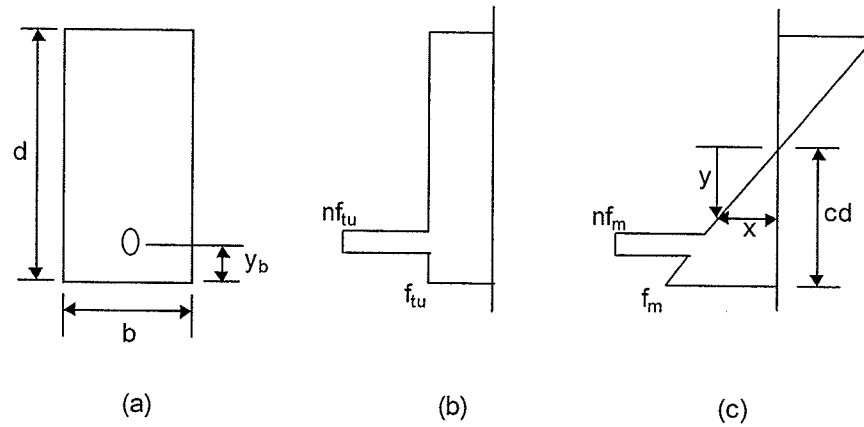


Figure 5.22 – a) Cross-section b) Axial Tension Stress Distribution of Reinforced Section
c) Bending Stress Distribution of Reinforced Section

Using equation 2.8 the Weibull probability function for the tension stresses is

$$[5.6] \quad F(f_{tu}) = 1 - e^{\left(-\frac{1}{d_1} \left[\int_d \left(\frac{f_{tu}}{m} \right)^{k_3} dy + \left(\frac{f_{tu}(n-1)}{m} \right)^{k_3} d_b \right] \right)}$$

where: f_{tu} is the tensile strength

n is the modular ratio

d_b is the diameter of the reinforcing bar

all other terms are the same as in equation 2.8

By completing the integral in equation 5.6 and simplifying, equation 5.7 is obtained.

$$[5.7] \quad F(f_{tu}) = 1 - e^{\left(-\frac{1}{d_1} \left[\left(\frac{f_{tu}}{m} \right)^{k_3} (d + (n-1)^{k_3} d_b) \right] \right)}$$

The Weibull probability equation for the bending stresses is as follows

$$[5.8] \quad F(x) = 1 - e^{\left(-\frac{1}{d_1} \left[\int_d^x \left(\frac{y}{m} \right)^{k_3} dy + \left(\frac{x_1(n-1)}{m} \right)^{k_3} d_b \right] \right)}$$

where, from Figure 5.15c)

$$[5.9] \quad x = \frac{y f_m}{cd}$$

and at the level of FRP reinforcement

$$[5.10] \quad x_1 = f_m \left(1 - \frac{y_{bfrp}}{cd} \right)$$

Substituting equations 5.9 and 5.10 into equation 5.7 gives

$$[5.11] \quad F\left(\frac{y f_m}{cd}\right) = 1 - e^{\left(-\frac{1}{d_1} \left[\int \left(\frac{y f_m}{mcd} \right)^{k_3} + \left(\frac{f_m \left(1 - \frac{y_{bfrp}}{cd} \right) (n-1)}{m} \right)^{k_3} d_b \right] \right)}$$

By completing the integral in equation 5.11 from 0 to cd and simplifying, equation 5.12 is obtained.

$$[5.12] \quad F\left(\frac{y f_m}{cd}\right) = 1 - e^{\left(-\frac{1}{d_1} \left[\left(\frac{f_m}{m} \right)^{k_3} \left[\left(\frac{cd}{k_3 + 1} \right) + \left(\left(1 - \frac{y_{bfrp}}{cd} \right) (n-1) \right)^{k_3} d_b \right] \right] \right)}$$

As stated previously f_m can be determined as a ratio of f_{tu} . To this end, equations 5.7 and 5.12 are equated and simplified to give

$$[5.13] \quad f_{tu}^{k_3} (d + (n-1)^{k_3} d_b) = f_m^{k_3} \left(\frac{cd}{k_3 + 1} + \left(\left(1 - \frac{y_{bfrp}}{cd} \right) (n-1) \right)^{k_3} d_b \right)$$

Thus the bending strength of a timber beam reinforced for flexure is

$$[5.14] \quad f_m = \left(\frac{d + (n-1)^{k_3} d_b}{\frac{cd}{k_3 + 1} + \left(\left(1 - \frac{y_{bfrp}}{cd} \right) (n-1) \right)^{k_3} d_b} \right)^{\frac{1}{k_3}} f_{tu}$$

The results of using equation 5.14 are presented in Figures 5.23 to 5.25. Figure 5.22 displays the scatter plot of the measured versus predicted strength values for the flexurally reinforced specimens using the modified stress distribution equation. The fit of the results of equation 5.14 is much like the fit of the control specimens to the equation developed by Buchanan (1984). Equation 5.14 is not too conservative, as there are 4 or 17% over estimated, but at the same time it is not unconservative as the majority of the specimens are underpredicted. If the one outlier is ignored, only 3 strengths were over predicted or 12.5%. Equation 5.14 gives good correlation between the measured and predicted strengths for the high strength specimens as well as the lower strength specimens, as shown in Figure 23. The one outlier is an anomaly and was caused by determining a very large stiffness from testing but measuring a low strength. The outlier is stringer F9 that failed in tension originating at a crack and in the general vicinity of a knot. This failure was discussed at length in the section 4.4. The tension failure mode caused an abnormally low strength result and thus could not be predicted by any of the strength models. Normally a large stiffness would indicate a high strength specimen. This erroneous result is ignored during discussions of the results of this equation and in any conclusions made.

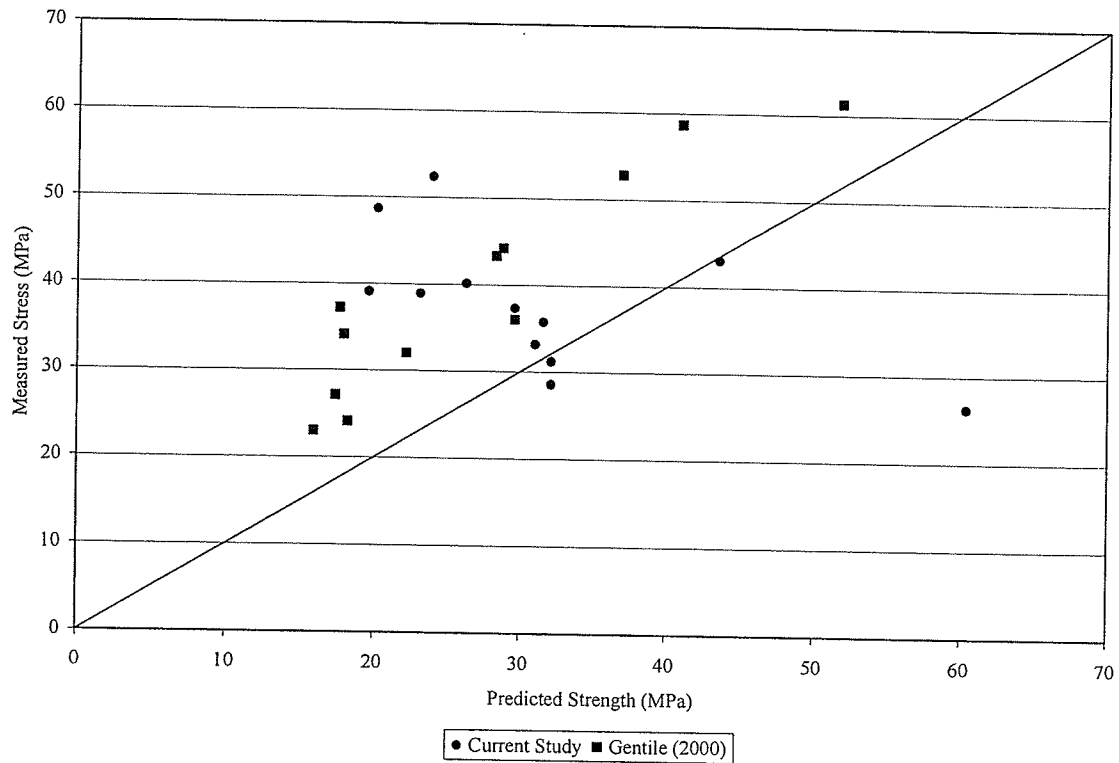


Figure 5.23 – Strength Results for the Flexurally Reinforced Timbers Stringers using the Modified Stress Distribution Equation

Equation 5.14 was also used to predict the results of the flexurally and shear reinforced specimens. As seen in Figure 5.24, the results are conservative and linear in nature with very little scatter as would be expected since the tension and shear failures were eliminated.

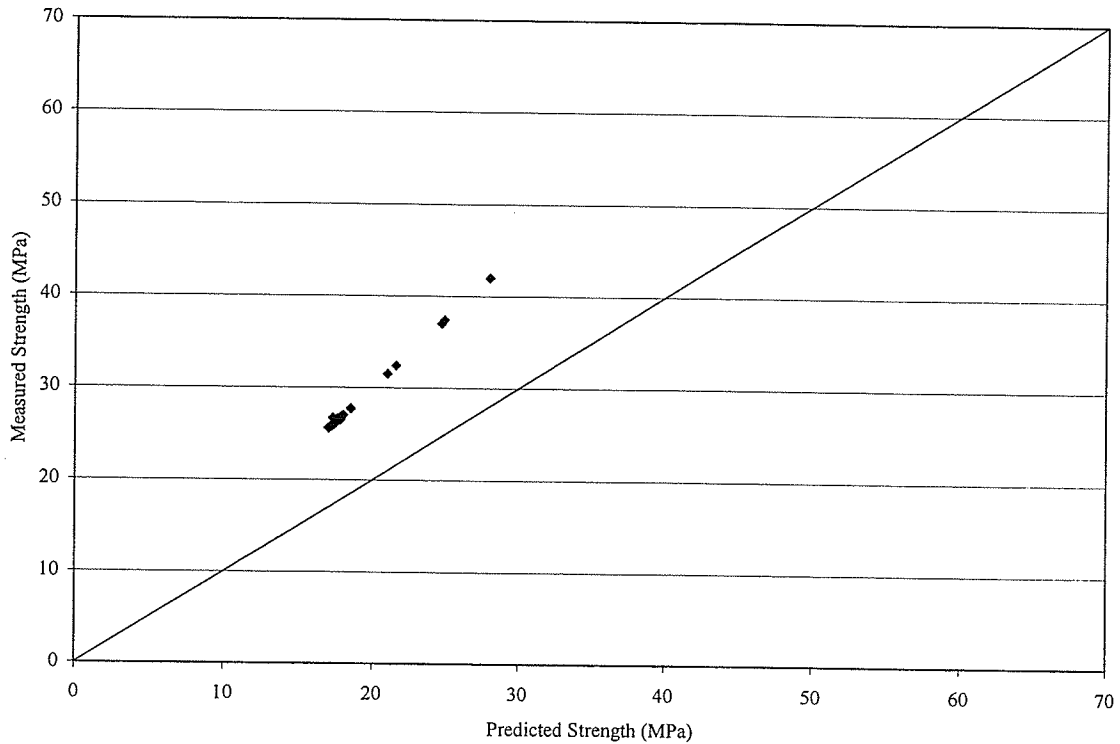


Figure 5.24 –Strength Results for the Flexural and Shear Reinforced Timber Stringers using the Modified Stress Distribution Equation

The conservative nature of this equation with the FD specimens would indicate an additional adjustment must be made to account for the shear reinforcement. To determine the magnitude of this adjustment, the results were multiplied by a factor until a good fit could be found. Figure 5.25 displays the result of this analysis. It was determined a factor of 1.5 gave exact correlation between the measured and predicted value. Thus, it appears the addition of shear reinforcement has increased the strength of the stringers by 50% when using equation 5.14 to predict the strength values.

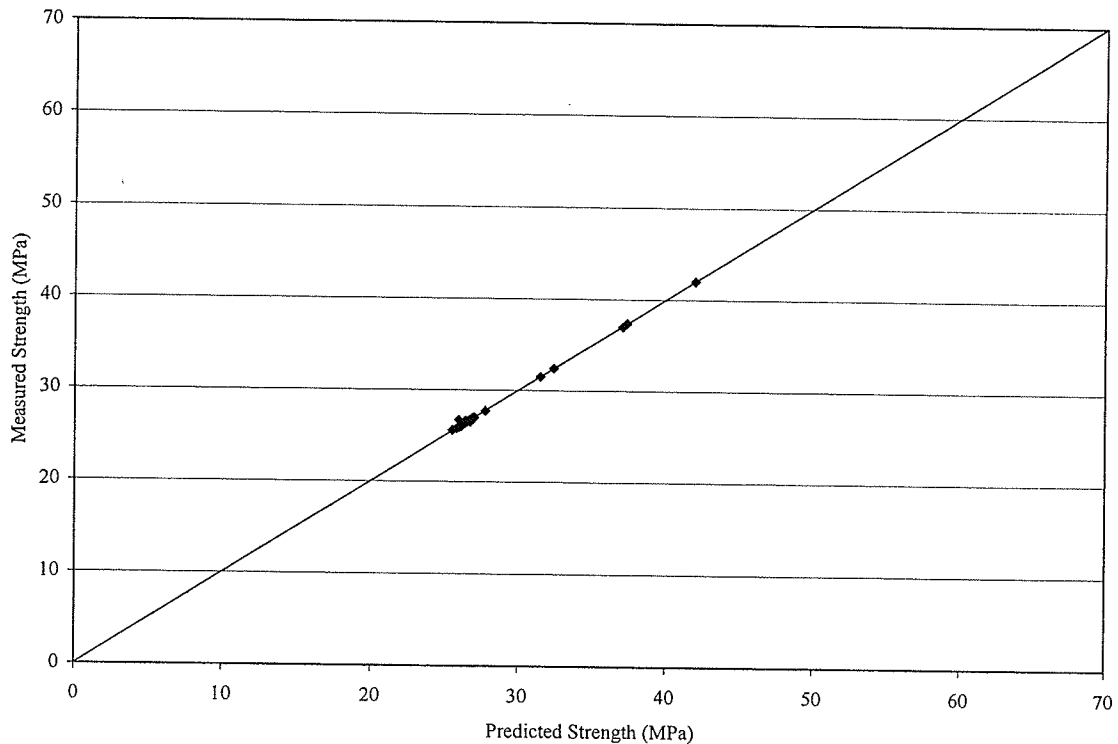


Figure 5.25 - Strengths of Flexural and Shear Reinforced Timber Stringers using the Modified Stress Distribution Equation and a Factor of 1.5

Further investigation is required to determine the exact effects of adding shear reinforcement and to determine an appropriate alteration to equation 5.14. This alteration should include the material properties of both the timber and shear reinforcement, much like equation 5.14 does for flexural reinforcement. By including the properties of the shear reinforcement the equation is not specific for a particular type of reinforcement and suitable for use with a variety of reinforcing bars. Although conservative, Equation 5.14 can be safely used for predicting the strength of timber beams reinforced for both flexure and shear.

CHAPTER 6 SUMMARY AND CONCLUSIONS

Experimental program was carried out at the University of Manitoba to investigate the behaviour of timber beams, pressure treated with creosote and strengthened using GFRP bars. Two types of beams were tested – rectangular beams and beams with dapped ends. It is the conclusion of this investigation that dapped ends significantly decrease the strength of the beams and therefore are not recommended for future use in practice unless the ends are strengthened. The existing dapped beams may be sufficiently strengthened using the methods presented in this thesis.

It is feasible to use GFRP bars to reinforce dapped timber stringers. The use of only flexural reinforcement is not recommended for dapped timber beams as dap failures occur and reduce the ultimate strength of the beam significantly. The use of both flexural and shear reinforcement for dapped timber beams was proved to increase the strength significantly. If both forms of reinforcement are used an increase of 66% in the 5th percentile MOR value could be achieved when compared to the CSA design value for timber stringers, based on the 78 large to medium scale stringers tested to date. The addition of both the flexural and shear reinforcement bridges the natural defects present in the timber beams. This results in less dispersion of the test results and increased strength.

The ductility of the stringers is increased with the addition of GFRP reinforcement. With the addition of only flexural reinforcement the increase in ductility is smaller compared to the stringers with both flexural and shear reinforcement.

The bond between the timber, epoxy and GFRP was good throughout the test and was not the cause of failure in any specimen.

A minimum safety factor (β) of 3.5 can be obtained if both flexural and shear reinforcement are used. A safety factor (β) of 3.5 cannot be obtained by the addition of just the flexural reinforcement.

The strength model developed by Gentile (2000) needed to be adjusted to fit the test data obtained in this study. This is a result of the use of different GFRP bars used in this study as well as increased number of test beams. Thus, if this model is to be used an investigation to determine the proper α term to be applied to the theoretical strength value must be completed. This is a result of the discrepancy between the results obtained in this study and those obtained by Gentile (2000). Further testing would refine the α and make it suitable for use.

The strength model developed in this thesis is using a modified stress distribution to account for the addition of the flexural reinforcement fit the test data for the flexurally reinforced stringers very well. This equation is recommended for use with flexurally reinforced timber stringers, however this model must be adjusted to account for the effects of adding shear reinforcement. Currently a factor of 1.5 is used for this purpose based on the 28 timber stringers tested to date. Further refinement of the model is needed.

The use of GFRP bars to reinforce dapped timber stringers is a viable rehabilitation scheme, as long as both flexural and shear reinforcement is used. The shear reinforcement is needed to control the dap failures as well as to prevent the propagation of shear cracks.

REFERENCES

- ASTM 1992. Standard test methods for use and calibration of hand-held moisture meters, ASTM D4444-92 (reapproved 1998). American Society for Testing and Materials, Philadelphia, PA.
- ASTM 1999. Standard practice for establishing structural grades and related allowable properties for visually graded lumber, ASTM D245-99. American Society for Testing and Materials, Philadelphia, PA.
- ASTM 1999. Standard methods for static tests of timber in structural sizes, ASTM D198-99. American Society for Testing and Materials, Philadelphia, PA.
- Barrett, J.D., and Lau, W. 1994. "Canadian Lumber Properties. Edited by E.D. Jones, Canadian Wood Council, Ottawa, Ontario, Canada.
- Buchanan, Andrew. 1984. "Strength Model and Design Methods for Bending and Axial Load Interaction in Timber Members" thesis presented to the University of British Columbia, Vancouver, British Columbia, Canada, in partial fulfillment of the requirements for the degree of Doctor of Philosophy in Civil Engineering.
- Buchanan, Andrew. 1990. Bending Strength of Lumber. ASCE Journal of Structural Engineering, Vol.116, No.5, 1213-1229.
- CSA.2000. Canadian Highway Bridge Design Code, S6.1-00. Canadian Standards Association, Toronto, Ontario, Canada.
- CSA.2000. Canadian Highway Bridge Design Code Commentary, S6.1-00. Canadian Standards Association, Toronto, Ontario, Canada.
- CSA. 1994. Engineering Design in Wood (Limit States Design) Structures (Design), CSA O86.1-94. Canadian Standards Association, Etibicoke, Ontario, Canada.
- Dagher, Habib J., and Abdel-Magid, Beckry. 1994. The Effect of Composite Reinforcement on Structural Wood. Proceedings of the 3rd Materials Engineering Conference, San Diego, CA. pp. 1338-1345.
- Dagher, H.J., and Lindyberg, R. 2000. Strengthening of Wood Beams Using FRP Composites Composites Fabricators Association Conference
- Eden, Ruth. 2002. "Strengthening of Timber Bridge Stringers Using GFRP" thesis present to the University of Manitoba, Winnipeg, Manitoba, Canada, in partial fulfillment of the requirements for the degree of Master of Science in Civil Engineering.

- Forest Products Laboratory. 1999. Wood Handbook – Wood as an Engineering Material. U.S. Department of Agriculture, Forest Service, Forest Products Laboratory Madison, Wisconsin.
- Gentile, C., Svecova, D., and Rizkalla, S. H. 2002. Timber Beams Strengthened with GFRP Bars – Development and Application. ASCE Journal of Composites for Construction, Vol. 6, No.1, 11-20.
- Gentile, Chris J. 2000. “Flexural Strengthening of Timber Bridge Beams Using FRP” thesis presented to the University of Manitoba, Winnipeg, Manitoba, Canada, in partial fulfillment of the requirements for the degree of Master of Science in Civil Engineering.
- ISIS Canada. 2001. Design Manual No. 3 Reinforcing Concrete Structures with Fibre Reinforced Polymers. ISIS Canada, University of Manitoba, Winnipeg, Manitoba, Canada
- Johns, Kenneth C. and Lacroix, Simon. 2000. “Composite Reinforcement of Timber in Bending” Canadian Journal of Civil Engineering, 27, 899-906.
- Johns, K.C., and Racine, P. 2001. Composite Reinforcement of Timber in Bending. Proceedings of the 29th Annual Conference of the Canadian Society for Civil Engineering, Victoria, British Columbia, pp.1-6
- Lantos, G. 1970. “The Flexural Behaviour of Steel Reinforced Laminated Timber Beams” Wood Science, 2, 136-143.
- Madsen, Borg. 1992. Structural Behaviour of Timber. Timber Engineering Ltd. North Vancouver, BC
- Madsen, Borg., and Buchanan, Andrew H. 1986. “Size Effects in Timber Explained by a Modified Weakest Link Theory” Canadian Journal of Civil Engineering, 13, 218-232.
- Mongomery, Douglas C, Runger, George C, and Hubele, Norma F. 1998. Engineering Statistics. John Wiley and Sons, Inc. New York
- Mufti, Aftab. A, Bakht, Baider, and Jaeger, Leslie G. 1996. Bridge Superstructures – New Developments. National Book Foundation. Pakistan.
- National Lumber Grades Authority. 2002. Standard Grading Rules for Canadian Lumber. National Lumber Grading Authority, New Westminster, British Columbia, Canada

Svecova, D., and Eden, R. 2004. "Flexural and Shear Strengthening of Timber Beams Using GFRP Bars – An Experimental Investigation" Canadian Journal of CE, Vol. 31, No. 1, pp. 45-55

Tingley, Daniel A. 1996. "High-strength Fibre-Reinforced Plastic Reinforcement of Wood and Wood Composite" 41st International SAMPE symposium, Anaheim, California, 667-673

APPENDIX A

Sample Calculation of the Theoretical Strength using the Method Developed by Gentile (2000).

Modulus of Elasticity

From CWC

Mean =	12914 MPa
5 th percentile	8860 MPa

Assume MOE follows a Normal Distribution

$$P_5 = \text{Mean} - 1.645(\text{SD})$$

$$\text{SD} = 2464.43769$$

MOE of the beam in question

$$E_w = 10969 \text{ MPa}$$

Calculate standard normal random variable (z) of E_w

$$E_w = \text{Mean} + z(\text{SD})$$

$$z = -0.78922669$$

$$F(z) = 0.214989696 \text{ From Table of Standard Normal Curve Areas}$$

From the Canadian Lumber Properties (Barrett and Lau, 1994)

which used a 3-point Weibull distribution to calculate UCS and UTS

	Table I.25 (UCS)	Table I.13 (UTS)
Shape, k	2.79	1.86
Scale, m_1	24.13	20.62
Location, x_0	14.9	10

Location Parameter or Minimum Strength, x_0

Weibull Equation

$$F(x) = 1 - e^{-\left(\frac{x-x_0}{m_1}\right)^k}$$

$$\text{UCS} = 29.41 \text{ MPa}$$

$$\text{UTS} = 19.62 \text{ MPa}$$

Calculation of Equivalent Stressed Length, L_e

$$L_e = \frac{1 + \frac{a_1 k_1}{L}}{k_1 + 1} L$$

	a_1 (mm)	k_1	L (mm)
UCS	600	10	4000
UTS	600	5.9	4000

$$\text{UCS (mm)} \quad \text{UTS (mm)}$$

$$L_e = 909.09091 \quad 1092.7536$$

L_e equation specific for four point loading

Calculation of Ultimate Compressive and Tensile Strengths

The length and depth effects must be considered and used to modify the CWC properties

	k_1	k_2
Tension	5.9	4.4
Compression	10	9.1

From the Canadian Lumber Properties, Table 3.5

$$L_{\text{UCS}} = 4267 \text{ mm}$$

From the Canadian Lumber Properties, Table 3.7

$$L_{\text{UTS}} = 3683 \text{ mm}$$

$$d_{\text{UCS}} = 235 \text{ mm}$$

$$d_{\text{UTS}} = 235 \text{ mm}$$

$$d = 300 \text{ mm}$$

depth of beam in question

$$f_{cu} = 33.42 \text{ MPa}$$

$$f_{tu} = 22.80 \text{ MPa}$$

$$f_{cu} = \text{UCS} \left(\frac{L_{\text{UCS}}}{L_{ec}} \right)^{\frac{1}{k_1}} \left(\frac{d_{\text{UCS}}}{d} \right)^{\frac{1}{k_2}}$$

$$f_{tu} = \text{UTS} \left(\frac{L_{\text{UTS}}}{L_{et}} \right)^{\frac{1}{k_1}} \left(\frac{d_{\text{UTS}}}{d} \right)^{\frac{1}{k_2}}$$

Calculation of Transformed Section Properties

$$y_b = \frac{bd \left(\frac{d}{2} \right) + (n-1)A_{frp} y_{b \text{ frp}}}{bd + (n-1)A_{frp}}$$

$$n = \frac{E_{frp}}{E_w}$$

$$n = 5.105296745$$

$$y_b = 146.0919465$$

$$y_b/d \text{ or } c = 0.486973155$$

Tensile Bending Strength, f_m

$$f_m = \left(\frac{k_3 + 1}{c} \right)^{\frac{1}{k_3}} f_{tu}$$

$$m = 1828.5323$$

$$f_m = 31.14 \text{ MPa}$$

$$\alpha = 1.3$$

$$E_{frp} = 56000 \text{ MPa}$$

$$E_w = 10969 \text{ MPa}$$

$$A_{frp} = 246 \text{ mm}^2$$

$$y_{b \text{ frp}} = 30 \text{ mm}$$

$$b = 100 \text{ mm}$$

$k_3 = 10$ from calibration of model was found to give good agreement

Yield Strain, e_y

$$\epsilon_y = 0.0030469$$

c	f _m MPa	e _t	f _t MPa	αf _m MPa	ε _c	b	a	r	f _{c,up} MPa	ε _{rip}	T _w KN	T _{rip} KN	C _{w1} KN	C _{w2} KN	C _{w3} KN
0.4870	31.14346733	0.0001	1.0969	40.48650753	0.00010535	0.5130268	0	1.0000	1.1555856	7.9465E-05	7.797986551	1.0947097	0	0	8.8926962
0.4870	31.14346733	0.0002	2.1938	40.48650753	0.0002107	0.5130268	0	1.0000	2.3111711	0.00015893	15.5959731	2.1894193	0	0	17.785392
0.4870	31.14346733	0.0003	3.2907	40.48650753	0.00031605	0.5130268	0	1.0000	3.4667567	0.00023895	23.39395965	3.284129	0	0	26.678089
0.4870	31.14346733	0.0004	4.3876	40.48650753	0.000421401	0.5130268	0	1.0000	4.6223422	0.00031786	31.1919462	4.3788387	0	0	35.570785
0.4870	31.14346733	0.0005	5.4845	40.48650753	0.000526751	0.5130268	0	1.0000	5.7779278	0.000397325	38.98993275	5.4735483	0	0	44.463481
0.4870	31.14346733	0.0006	6.5814	40.48650753	0.000632101	0.5130268	0	1.0000	6.933134	0.00047679	46.7879193	6.568258	0	0	53.356177
0.4870	31.14346733	0.0007	7.6783	40.48650753	0.000737451	0.5130268	0	1.0000	8.0890989	0.000556255	54.58590585	7.6629676	0	0	62.248873
0.4870	31.14346733	0.0008	8.7752	40.48650753	0.000842801	0.5130268	0	1.0000	9.2446845	0.00063572	62.38389241	8.7576773	0	0	71.14157
0.4870	31.14346733	0.0009	9.8721	40.48650753	0.000948151	0.5130268	0	1.0000	10.40027	0.000715185	70.18187896	9.852387	0	0	80.034266
0.4870	31.14346733	0.001	10.969	40.48650753	0.001053501	0.5130268	0	1.0000	11.555856	0.00079465	77.97986551	10.947097	0	0	88.926962
0.4870	31.14346733	0.0011	12.0659	40.48650753	0.001158851	0.5130268	0	1.0000	12.711441	0.000874115	85.77785206	12.041806	0	0	97.819658
0.4870	31.14346733	0.0012	13.1628	40.48650753	0.001264202	0.5130268	0	1.0000	13.867027	0.00095358	93.57583861	13.136516	0	0	106.71235
0.4870	31.14346733	0.0013	14.2597	40.48650753	0.001369552	0.5130268	0	1.0000	15.022612	0.001033045	101.3738252	14.231226	0	0	115.60505
0.4870	31.14346733	0.0014	15.3566	40.48650753	0.001474902	0.5130268	0	1.0000	16.178198	0.00111251	109.1718117	15.325935	0	0	124.49775
0.4870	31.14346733	0.0015	16.4535	40.48650753	0.001580252	0.5130268	0	1.0000	17.333783	0.001191975	116.9697983	16.420645	0	0	133.39044
0.4870	31.14346733	0.0016	17.5504	40.48650753	0.001685602	0.5130268	0	1.0000	18.489369	0.00127144	124.7677848	17.515355	0	0	142.28314
0.4870	31.14346733	0.0017	18.6473	40.48650753	0.001790952	0.5130268	0	1.0000	19.644955	0.001350905	132.5657714	18.610064	0	0	151.17584
0.4870	31.14346733	0.0018	19.7442	40.48650753	0.001896302	0.5130268	0	1.0000	20.80054	0.00143037	140.3637579	19.704774	0	0	160.06853
0.4870	31.14346733	0.0019	20.8411	40.48650753	0.002001652	0.5130268	0	1.0000	21.956126	0.001509835	148.1617445	20.799484	0	0	168.96123
0.4870	31.14346733	0.002	21.938	40.48650753	0.002107003	0.5130268	0	1.0000	23.11711	0.0015893	155.959731	21.894193	0	0	177.85392
0.4870	31.14346733	0.0021	23.0349	40.48650753	0.002212353	0.5130268	0	1.0000	24.267297	0.001668765	163.7577176	22.988903	0	0	186.74662
0.4870	31.14346733	0.0022	24.1318	40.48650753	0.002317703	0.5130268	0	1.0000	25.422882	0.00174823	171.5557041	24.083613	0	0	195.63932
0.4870	31.14346733	0.0023	25.2287	40.48650753	0.002423053	0.5130268	0	1.0000	26.578468	0.001827695	179.3536907	25.178322	0	0	204.53201
0.4870	31.14346733	0.0024	26.3256	40.48650753	0.002528403	0.5130268	0	1.0000	27.734053	0.00190716	187.1516772	26.273032	0	0	213.42471
0.4870	31.14346733	0.0025	27.4225	40.48650753	0.002633753	0.5130268	0	1.0000	28.889639	0.001986625	194.9496638	27.367742	0	0	222.31741
0.4870	31.14346733	0.0026	28.5194	40.48650753	0.002739103	0.5130268	0	1.0000	30.045225	0.00206609	202.7476503	28.462451	0	0	231.2101
0.4870	31.14346733	0.0027	29.6163	40.48650753	0.002844453	0.5130268	0	1.0000	31.20081	0.002145555	210.5456369	29.57161	0	0	240.1028
0.4870	31.14346733	0.0028	30.7132	40.48650753	0.002949804	0.5130268	0	1.0000	32.356396	0.00222502	218.3436234	30.651871	0	0	248.99549
0.4869	31.14419911	0.0029	31.8101	40.48745884	0.003057235	0.5115242	0.001617	0.9994	33.402819	0.002334853	226.0050732	32.164941	1.6204168	0.000457428	256.43996
0.4867	31.14508298	0.003	32.907	40.48860788	0.003165257	0.4943331	0.0189463	0.9935	33.205297	0.002415523	233.7297356	33.276245	18.873538	0.061494436	247.82162
0.4861	31.14933563	0.0031	34.0039	40.49413632	0.003277859	0.4777341	0.0362093	0.9874	32.9994	0.002496821	241.1798991	34.396204	35.846595	0.229355962	239.50015
0.4852	31.15474195	0.0032	35.1008	40.50116454	0.003395032	0.4620025	0.0527838	0.9810	32.785146	0.002578383	248.5133997	35.519802	51.915756	0.503978985	231.61347
0.4841	31.16196876	0.0033	36.1977	40.51055939	0.00351692	0.4469645	0.0689459	0.9743	32.562271	0.002660354	255.665332	36.649037	67.351021	0.88878877	224.07456
0.4827	31.17089577	0.0034	37.2946	40.5221645	0.003643639	0.4325777	0.0847173	0.9674	32.33056	0.002742735	262.6334375	37.783914	82.168721	1.386548581	216.86208
0.4811	31.18141713	0.0035	38.3915	40.53584227	0.003775316	0.4188026	0.1001187	0.9601	32.089784	0.002825524	269.4156916	38.924417	96.383632	2.000213143	209.95626
0.4792	31.19343982	0.0036	39.4884	40.55147177	0.003912086	0.4056025	0.1151697	0.9527	31.839696	0.002908719	276.0102467	40.070512	110.00905	2.732945086	203.33877
0.4772	31.20688229	0.0037	40.5853	40.56894697	0.004054091	0.3929437	0.1298889	0.9449	31.580035	0.002992316	282.4153795	41.222151	123.05684	3.588133497	196.99256

APPENDIX B

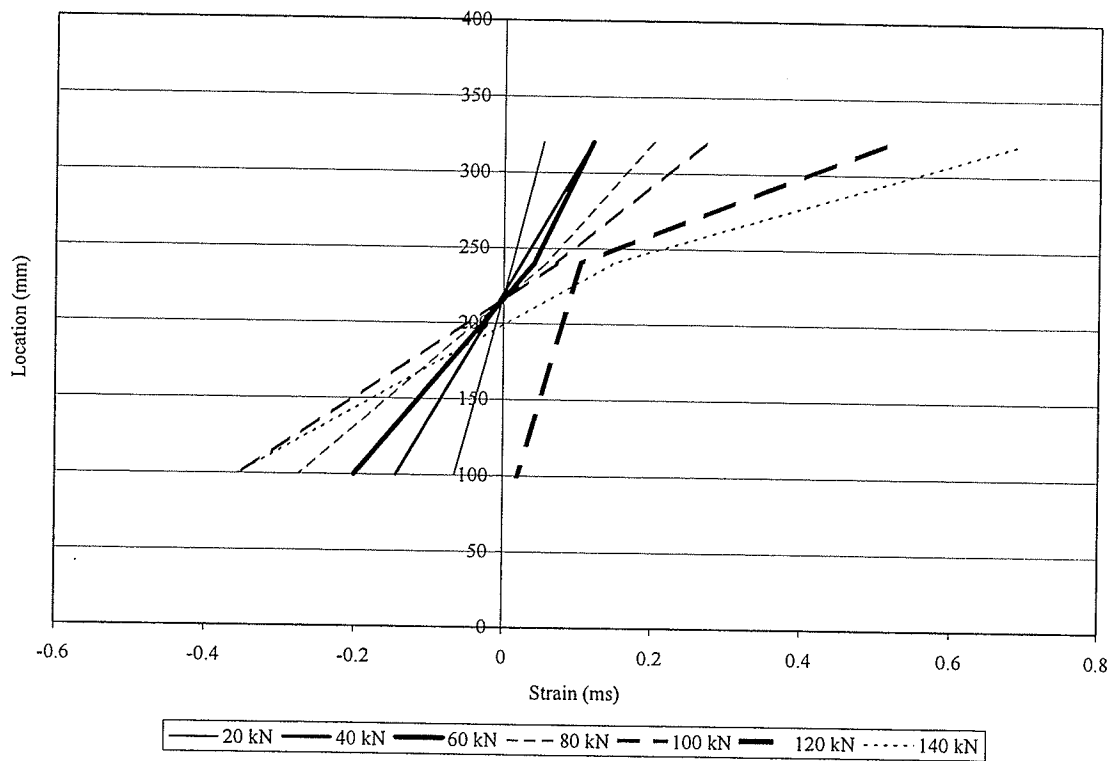


Figure B1 – Cross-sectional Strain Profile for C1

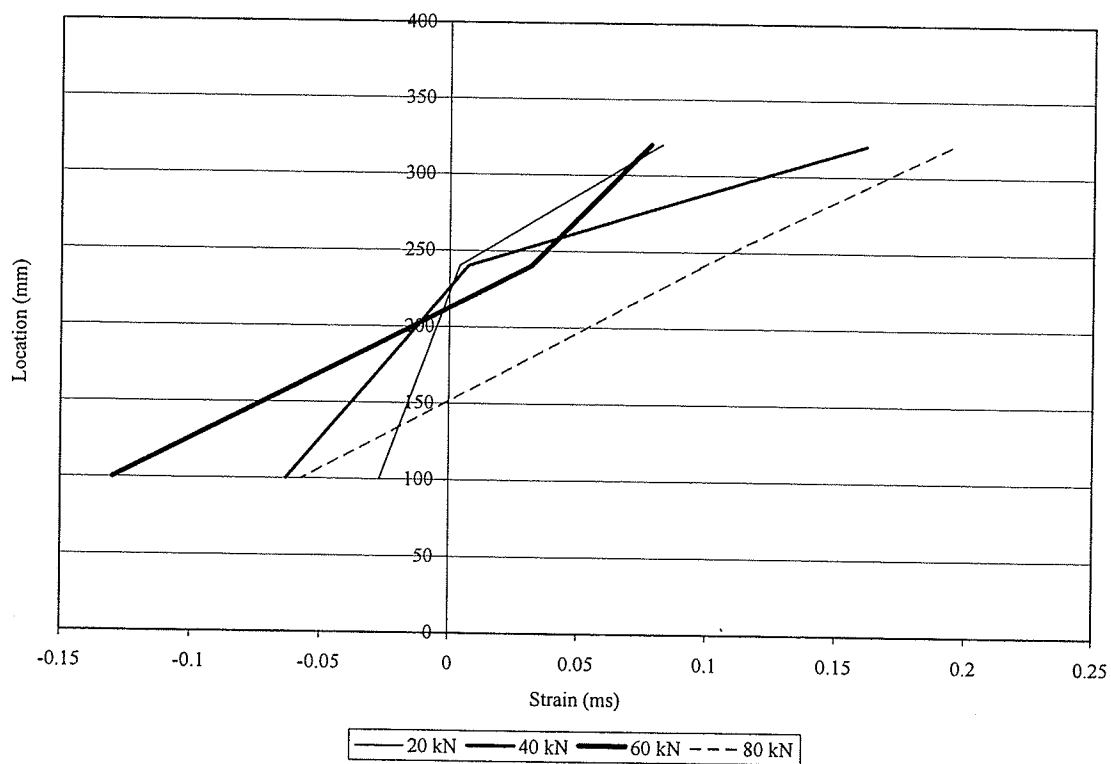


Figure B2 - Cross-sectional Strain Profile for C2

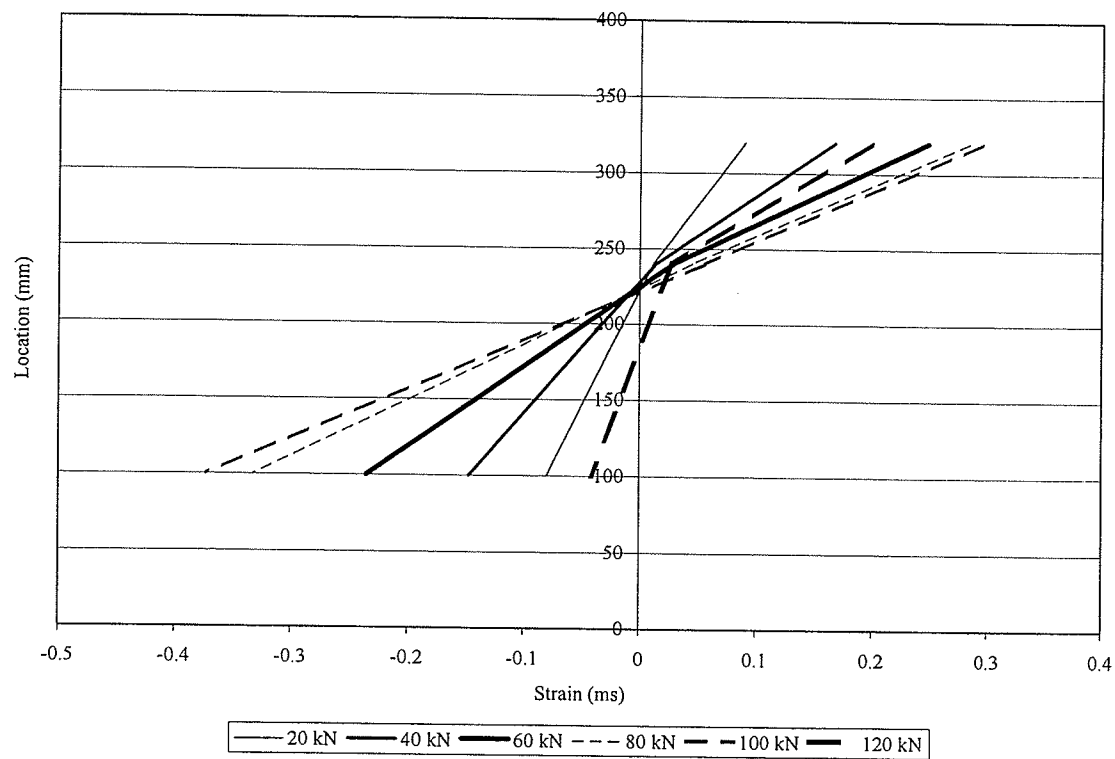


Figure B3 - Cross-sectional Strain Profile for C3

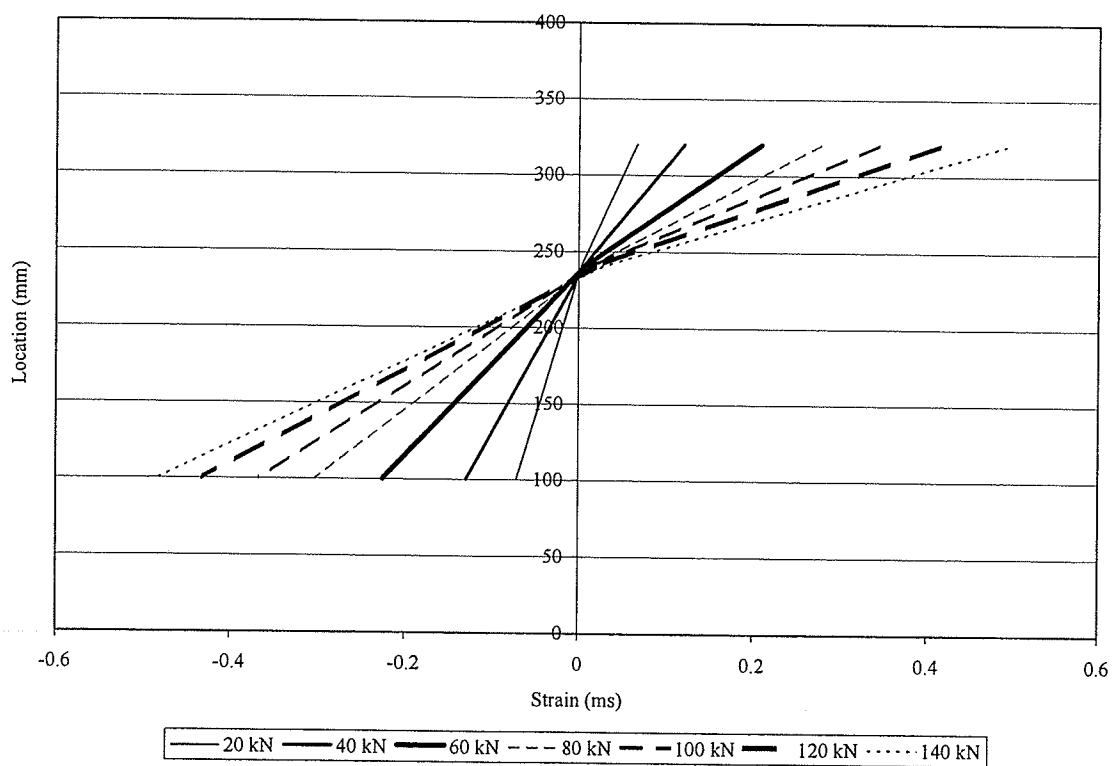


Figure B4 - Cross-sectional Strain Profile for C4

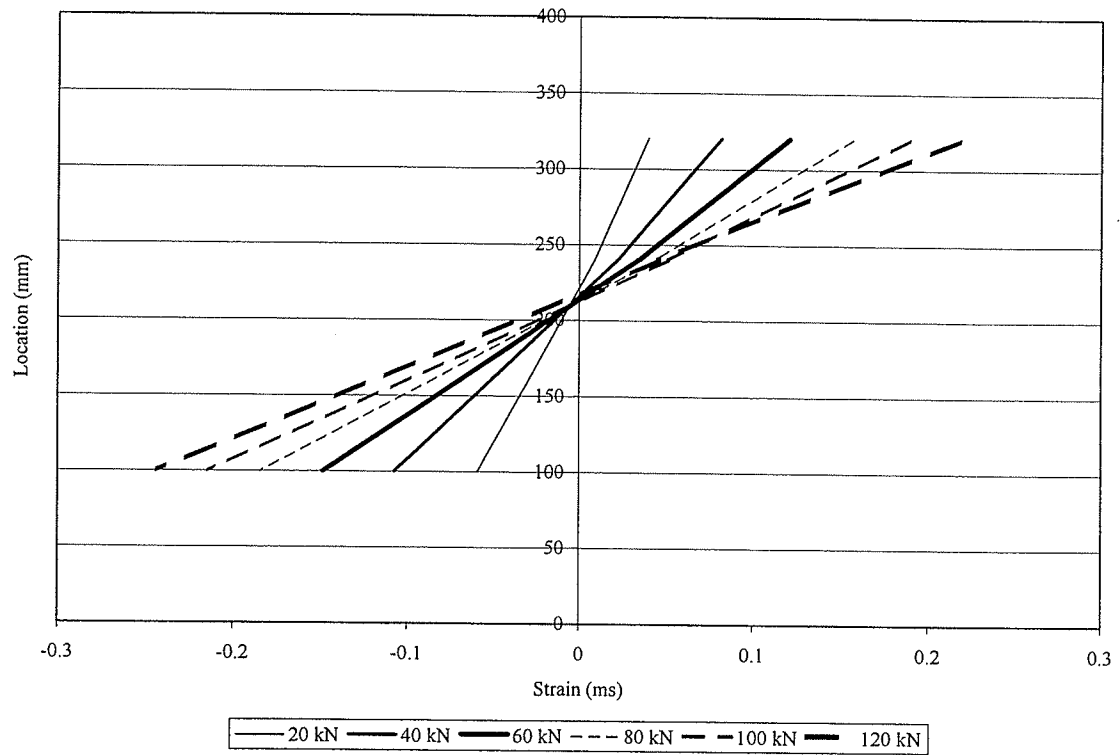


Figure B5 - Cross-sectional Strain Profile for C5

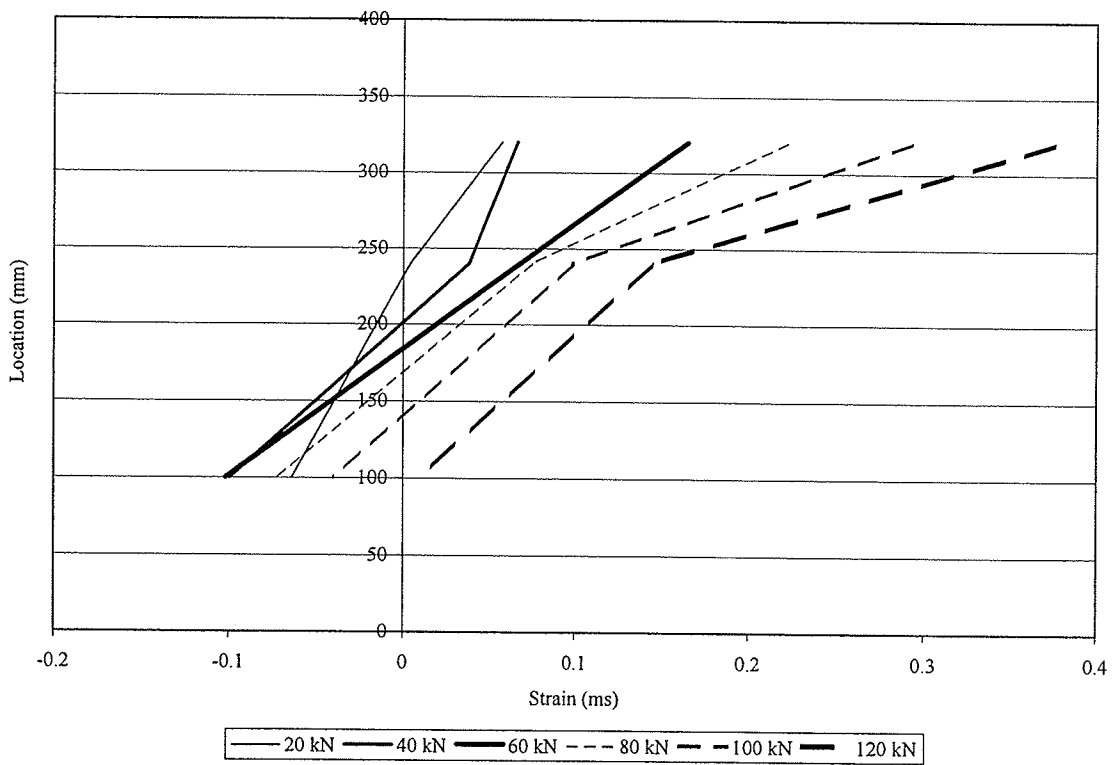


Figure B6 - Cross-sectional Strain Profile for C6

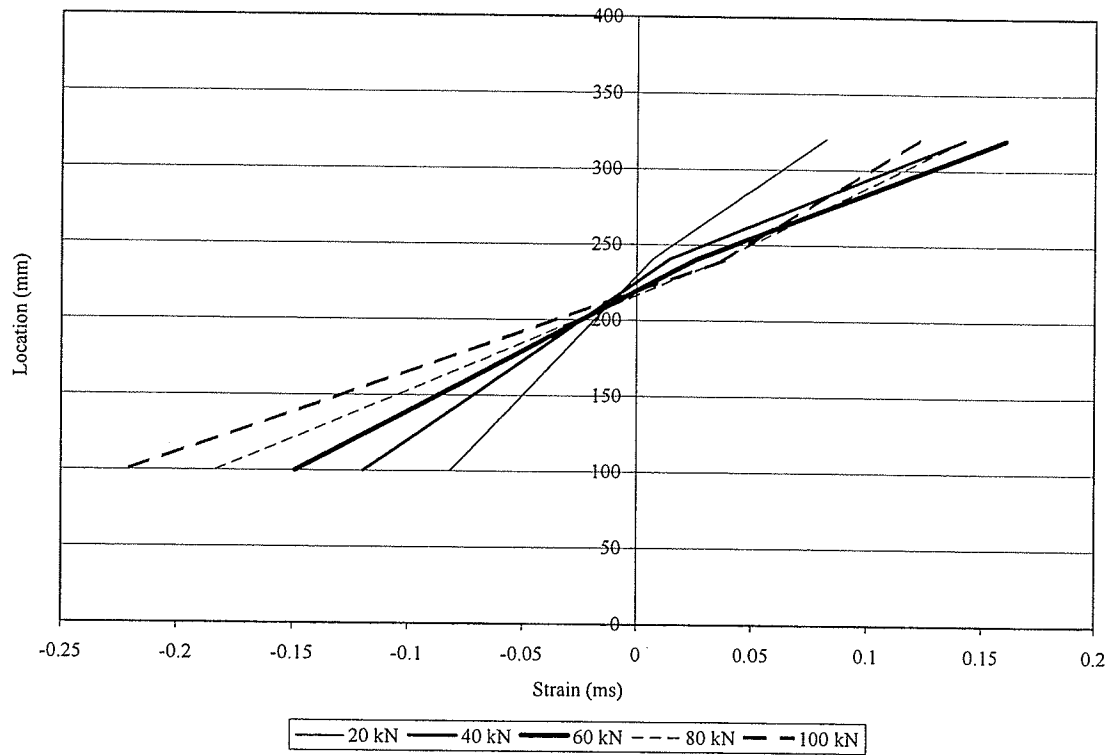


Figure B7 - Cross-sectional Strain Profile for C7

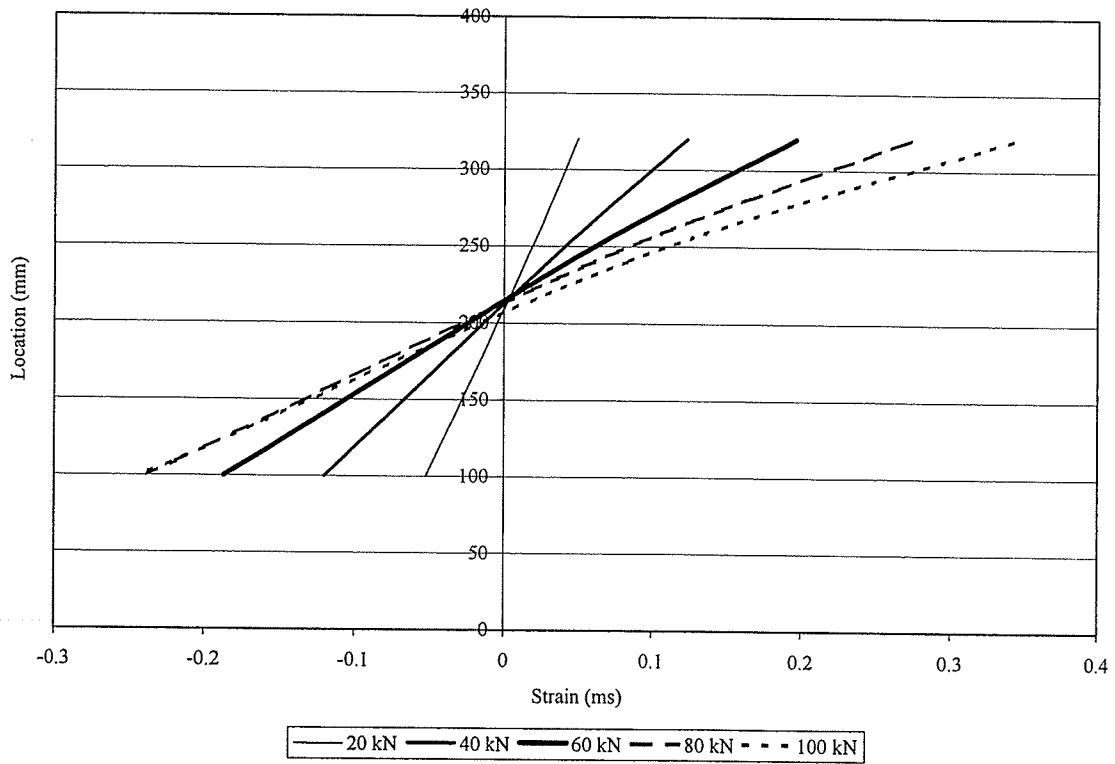


Figure B8 - Cross-sectional Strain Profile for C8

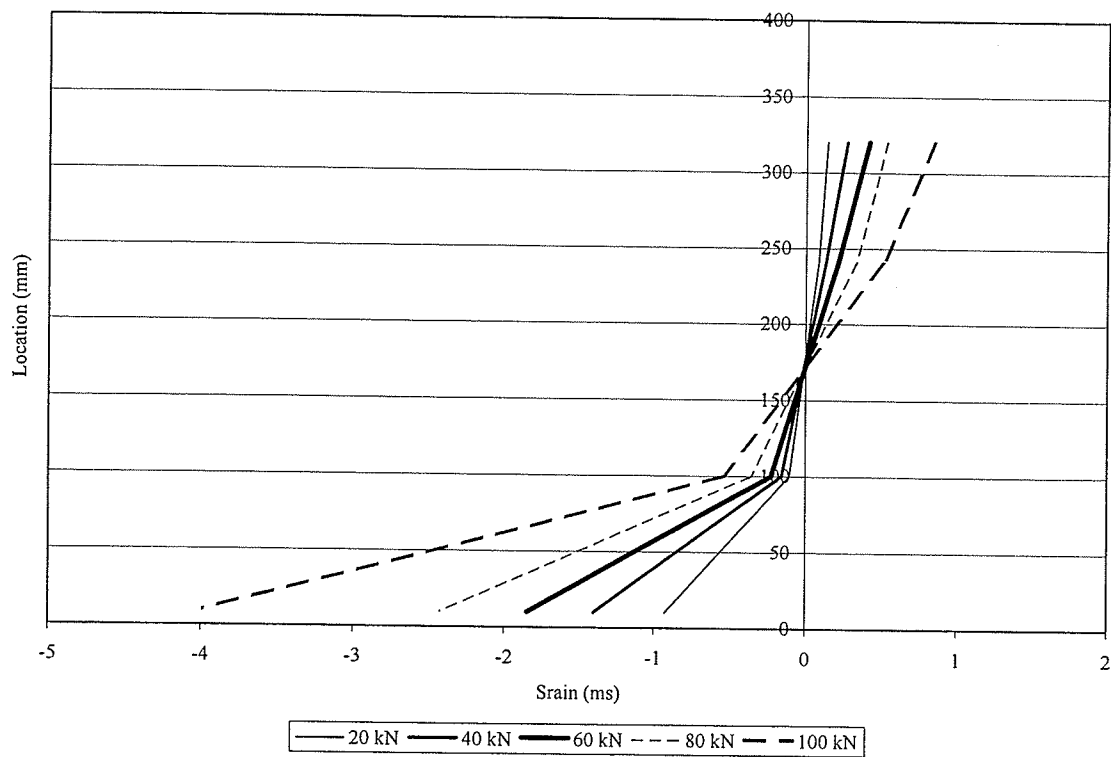


Figure B9 – Cross-sectional Strain Profile for F1

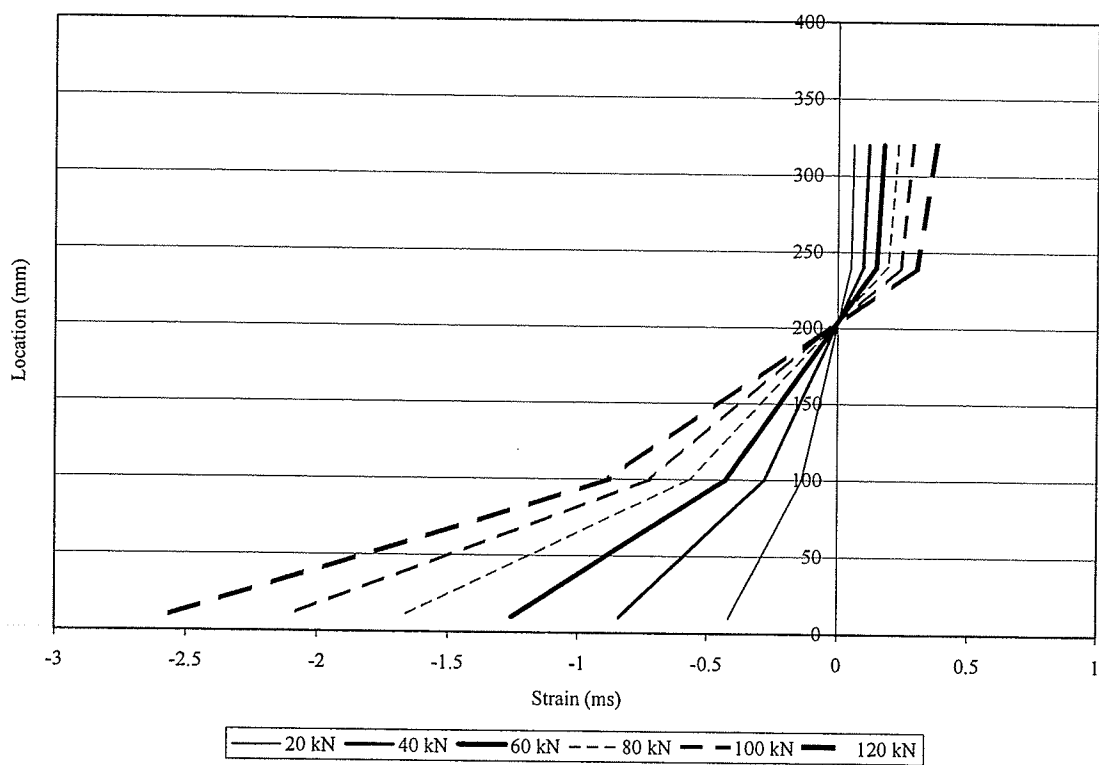


Figure B10 – Cross-sectional Strain Profile for F2

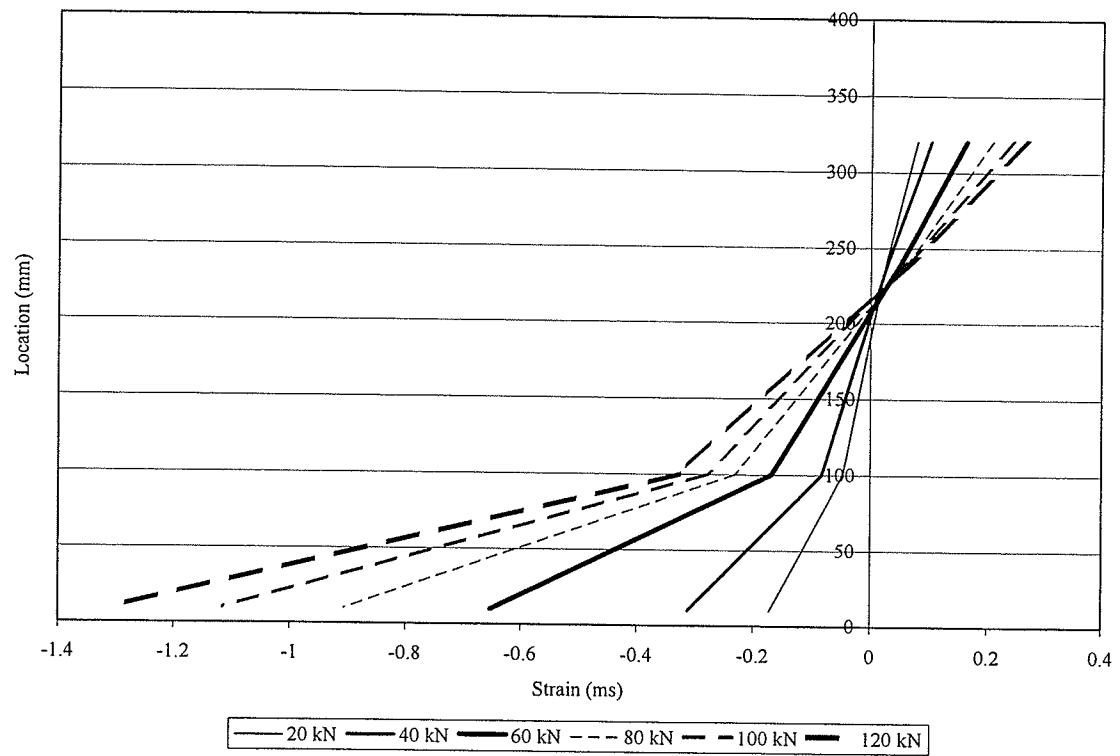


Figure B11 – Cross-sectional Strain Profile for F3

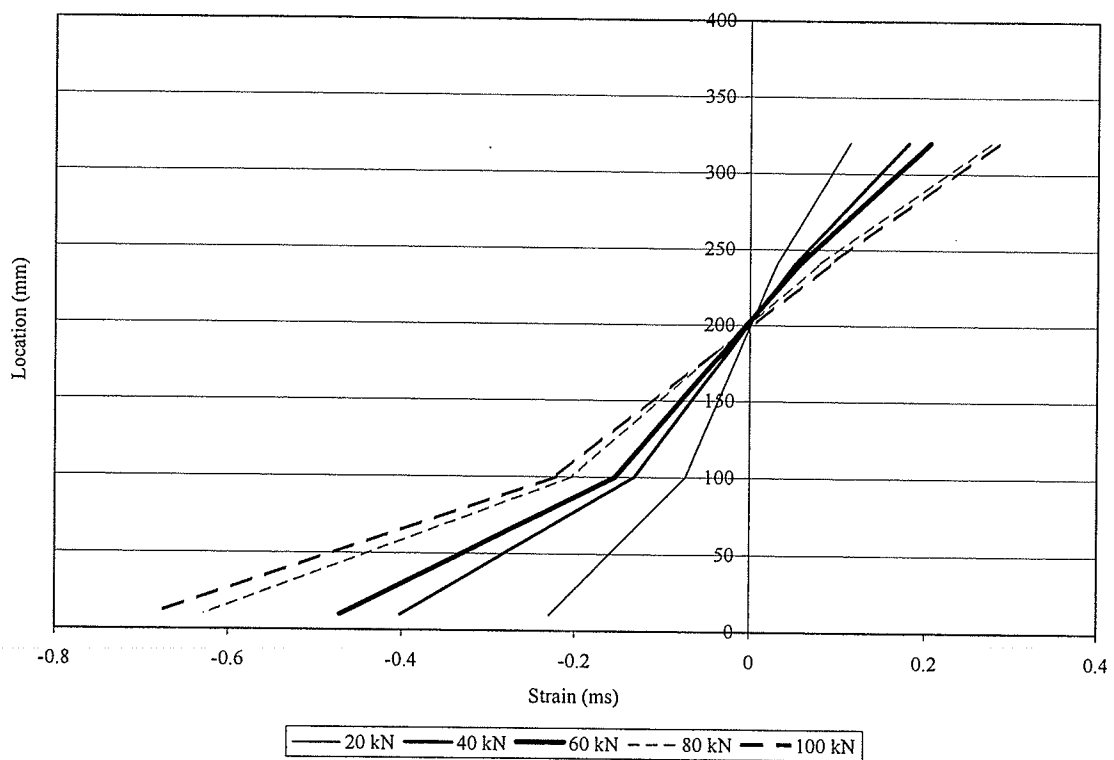


Figure B12 – Cross-sectional Strain for F4

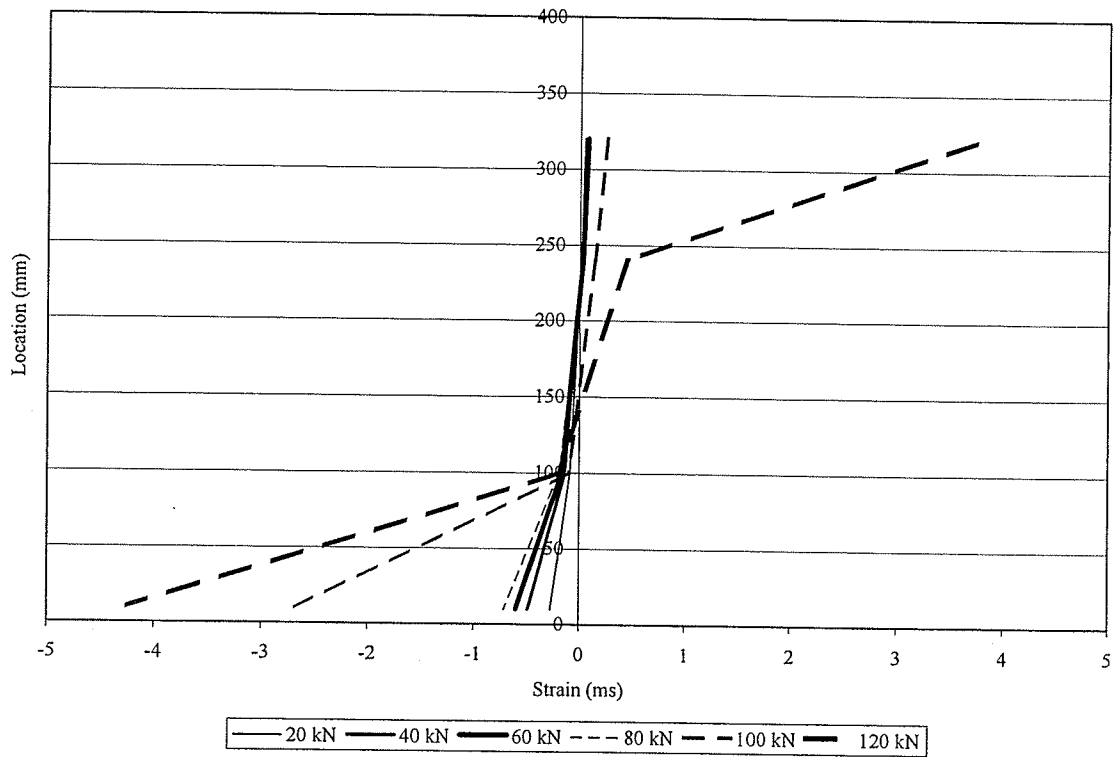


Figure B13 – Cross-sectional Strain Profile for F5

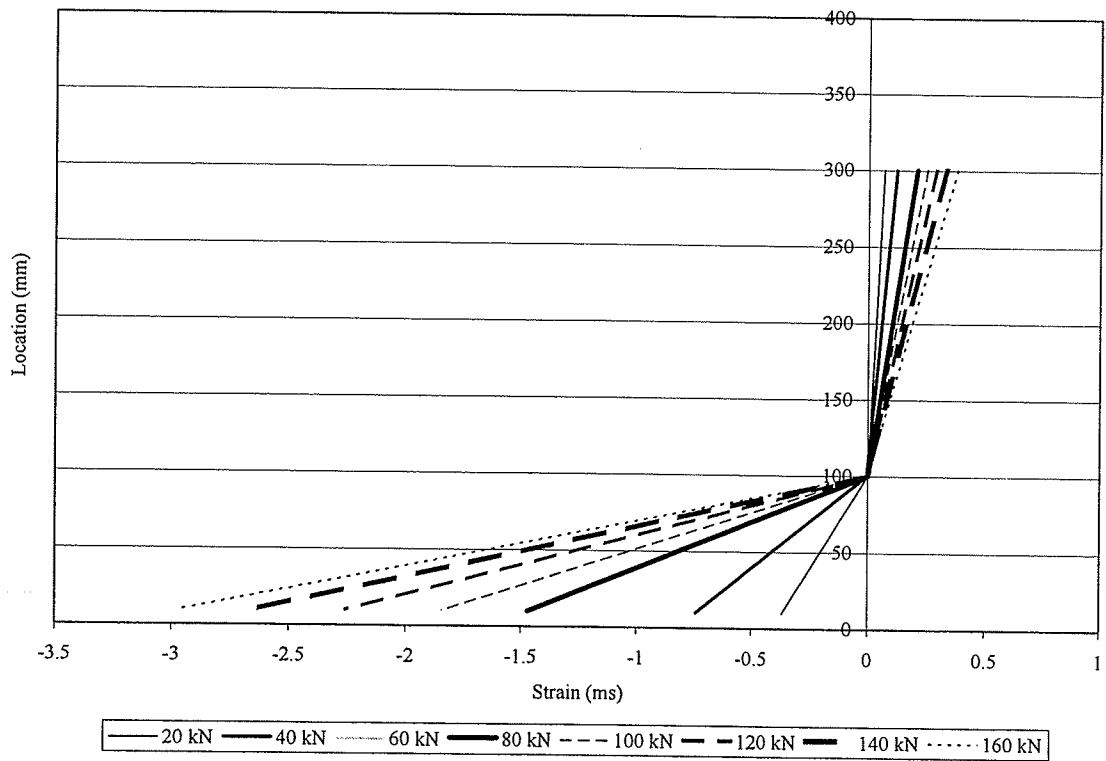


Figure B14 – Cross-sectional Strain Profile for F6

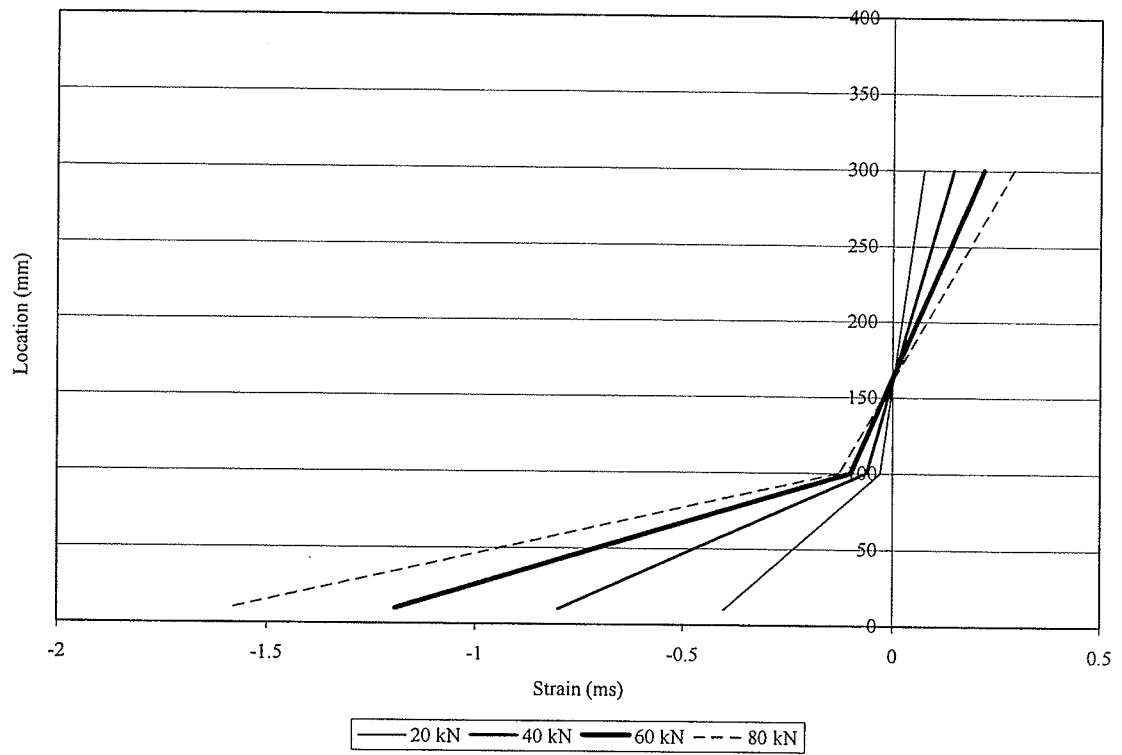


Figure B15 – Cross-sectional Strain Profile for F7

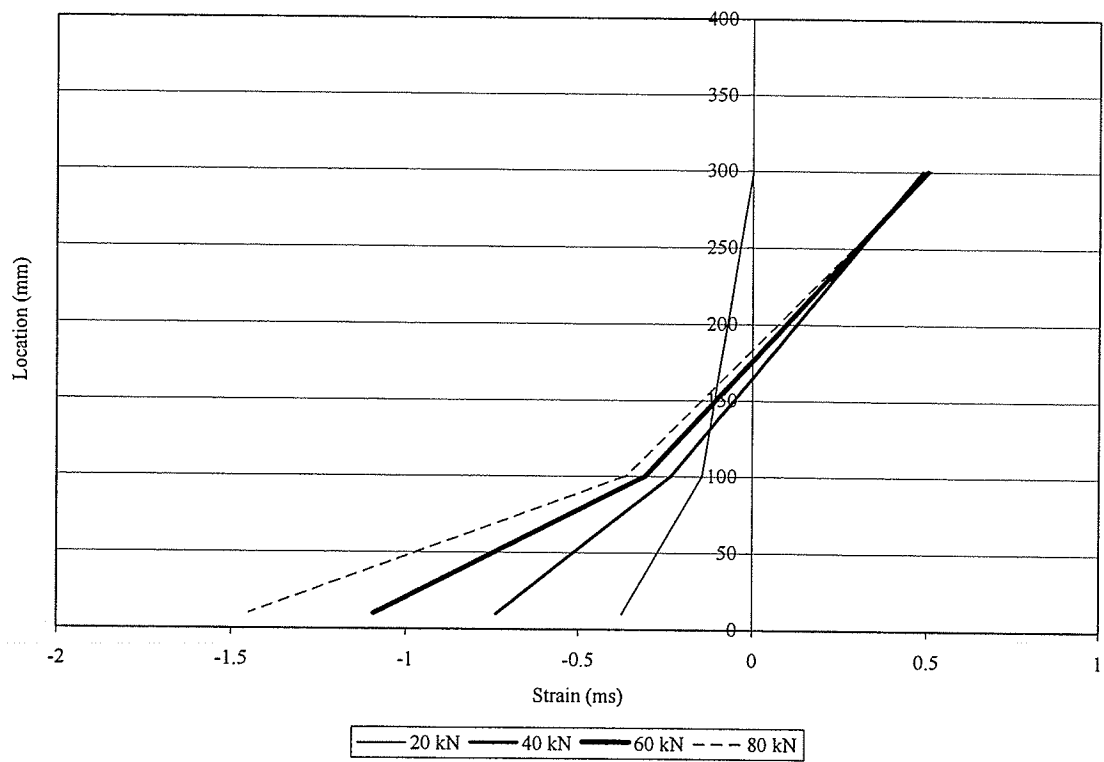


Figure B16 – Cross-sectional Strain Profile for F8

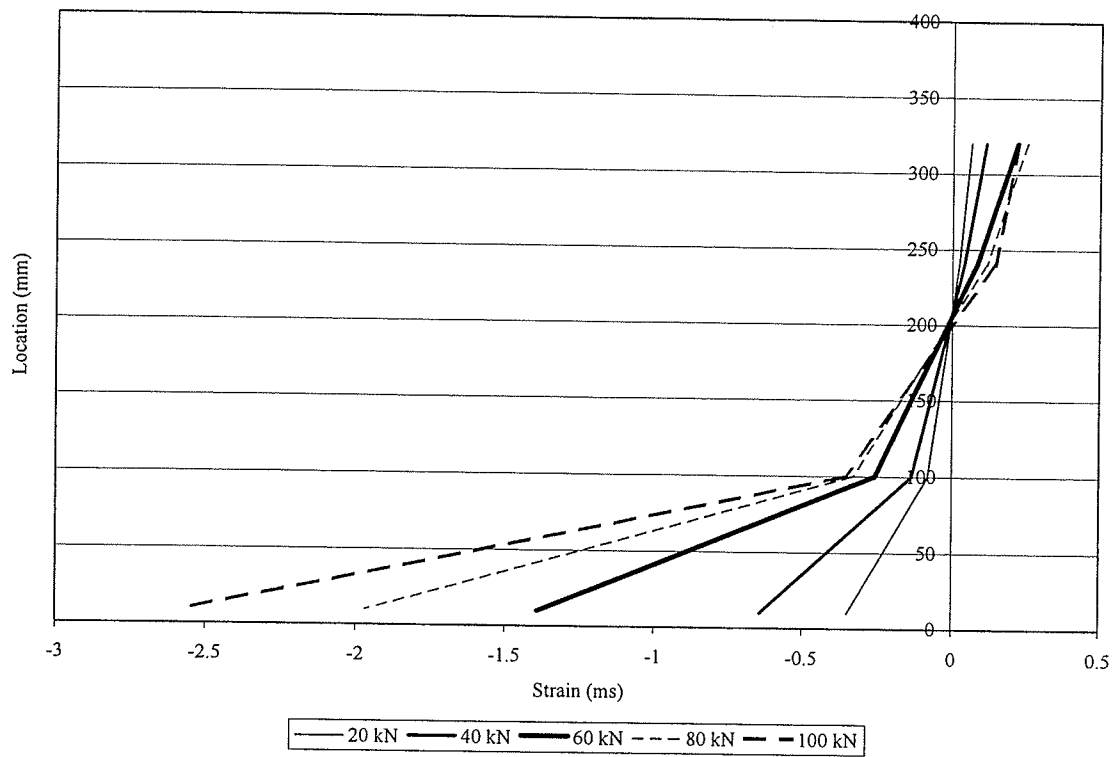


Figure B17 – Cross-sectional Strain Profile F9

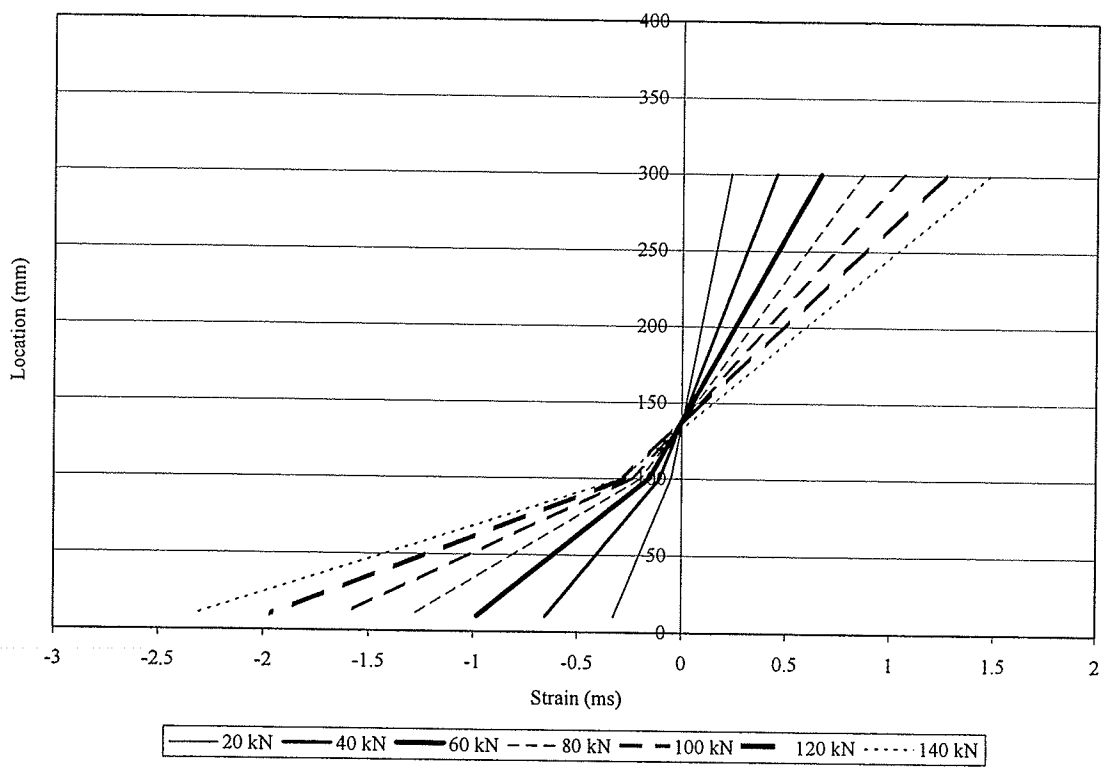


Figure B18 – Cross-sectional Strain Profile F10

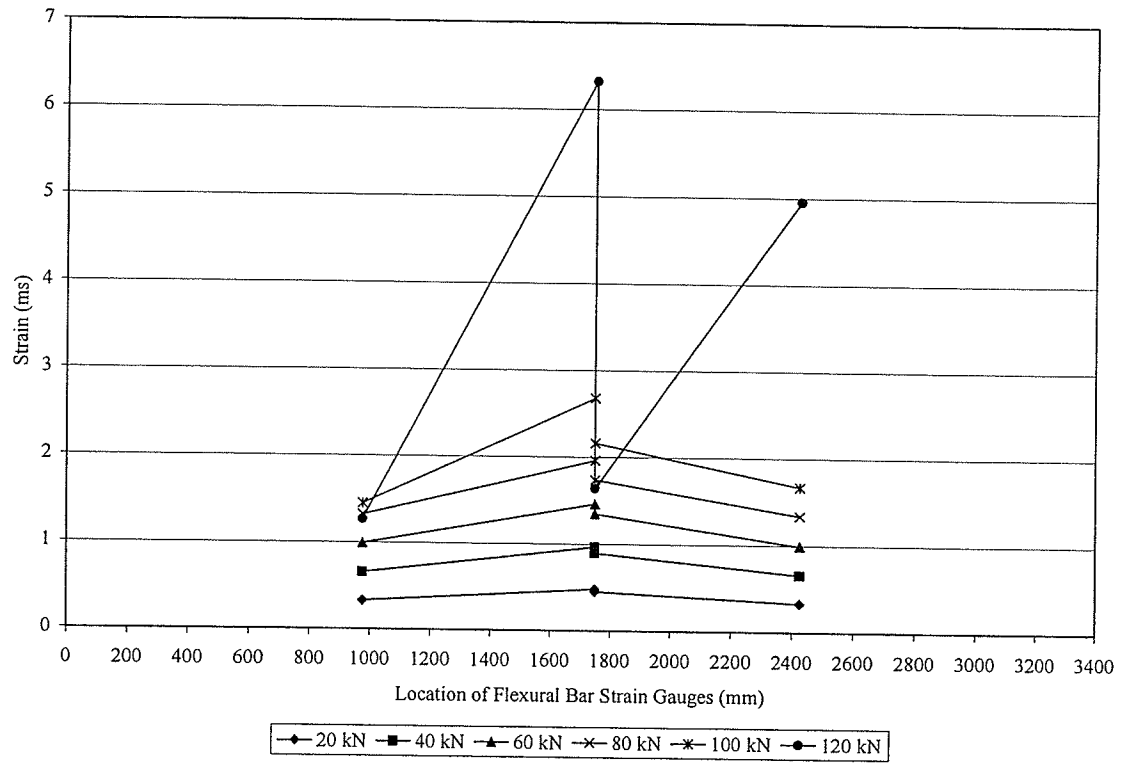


Figure B19 – Strain Profile of the Flexural Bars F1

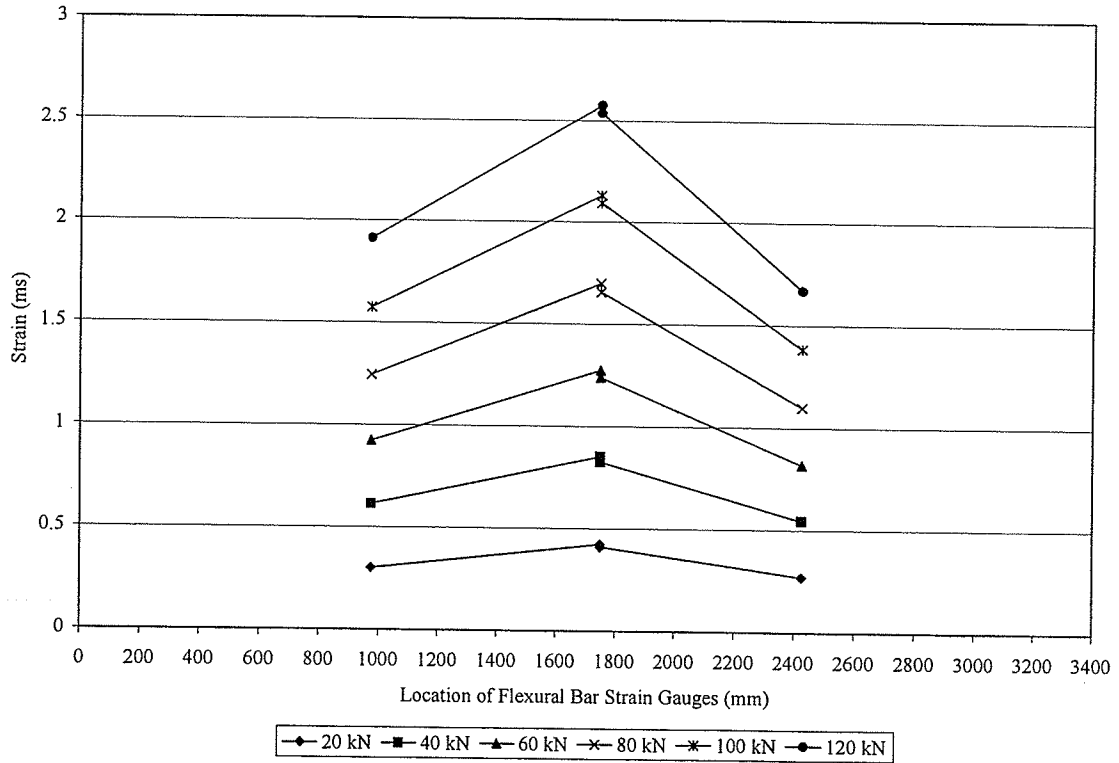


Figure B20 – Strain Profile for the Flexural Bars F2

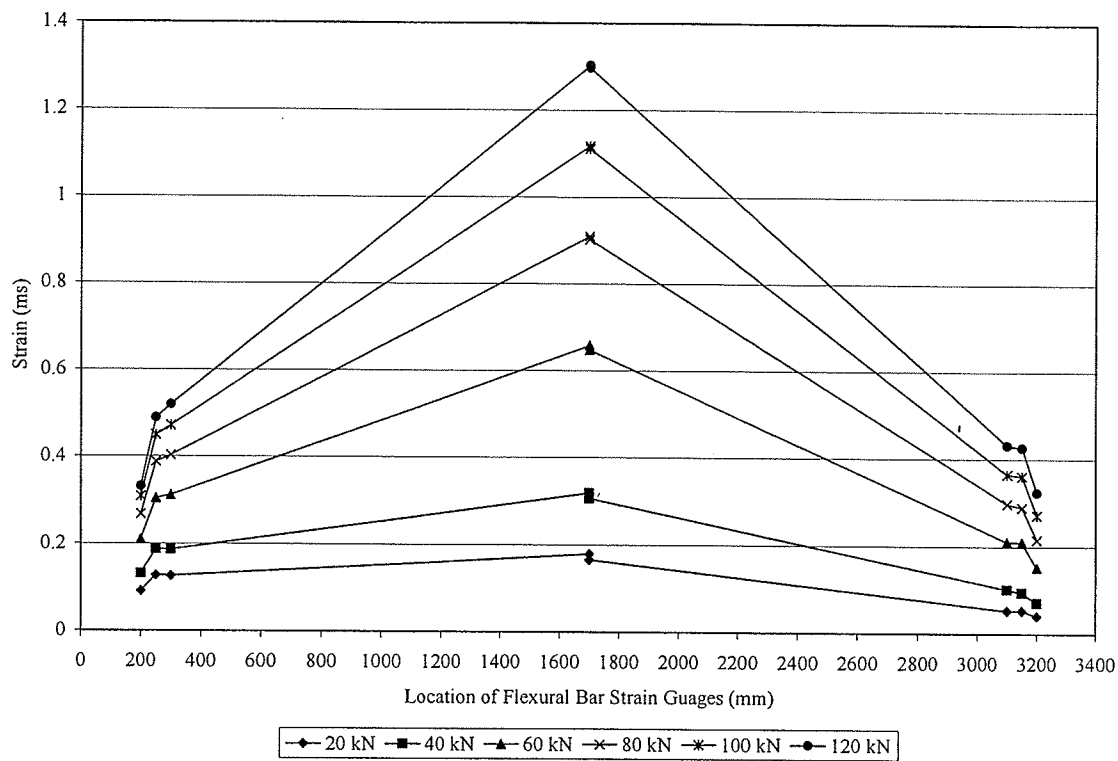


Figure B21 – Strain Profile of the Flexural Bars F3

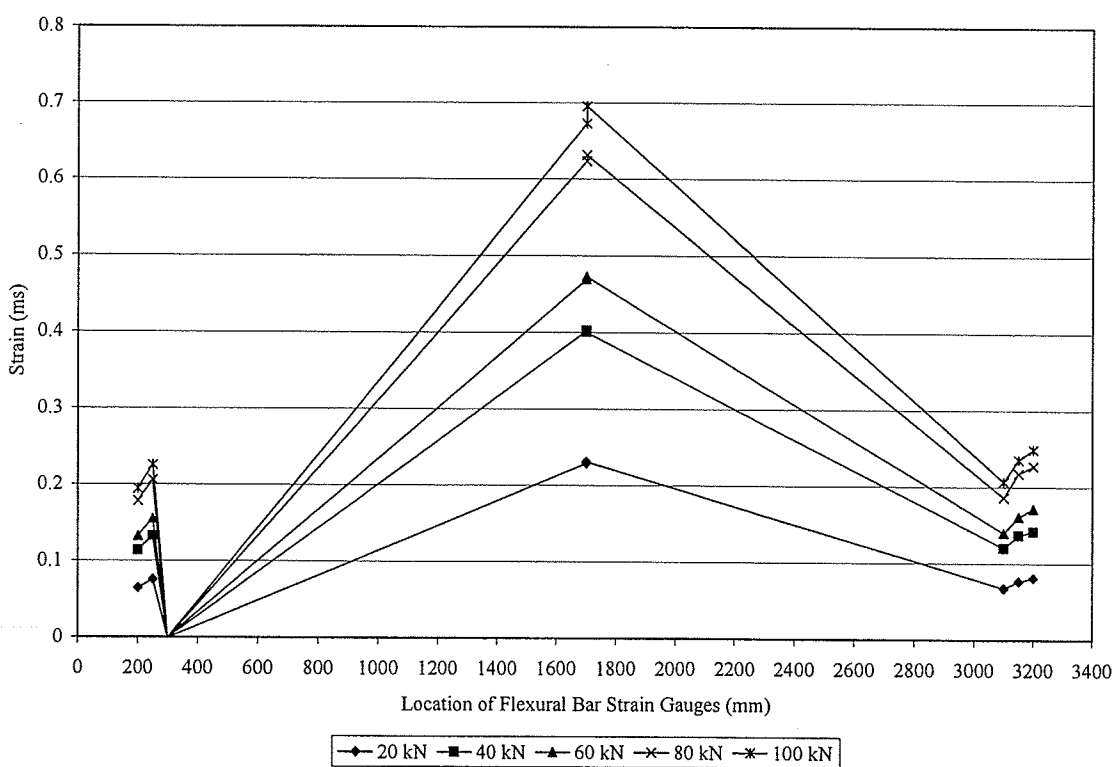


Figure B22 – Strain Profile of the Flexural Bars F4

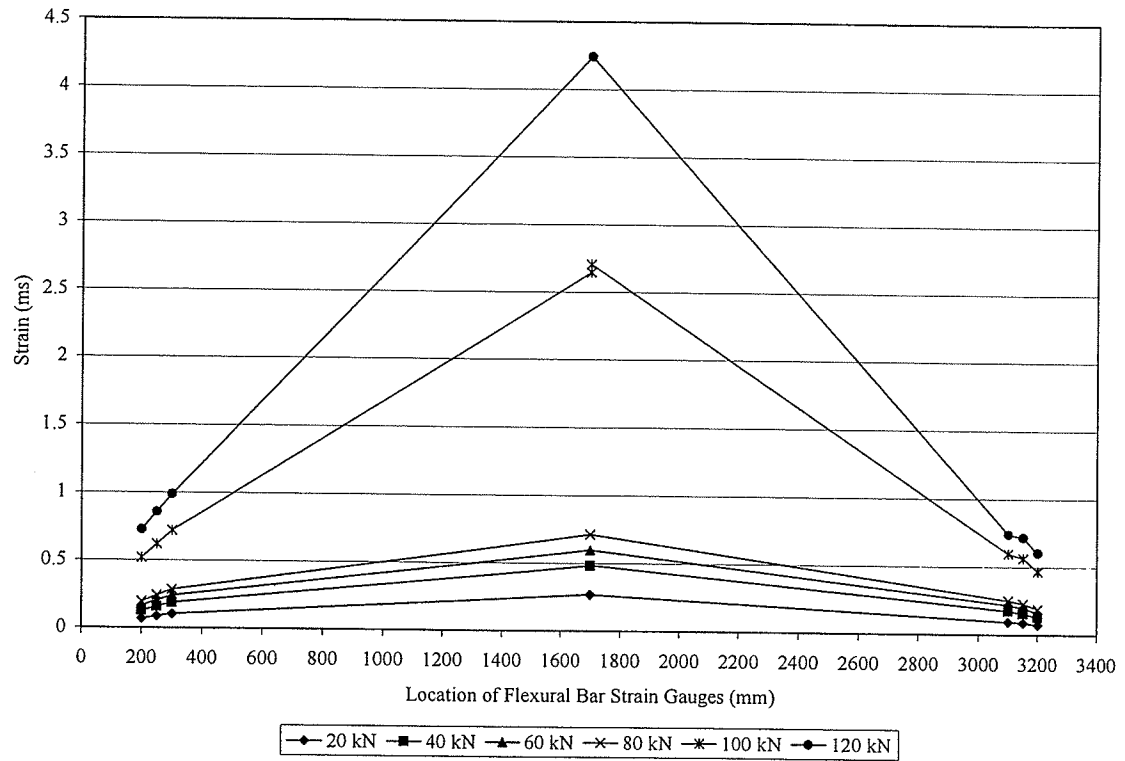


Figure B23 – Strain Profile for the Flexural Bars F5

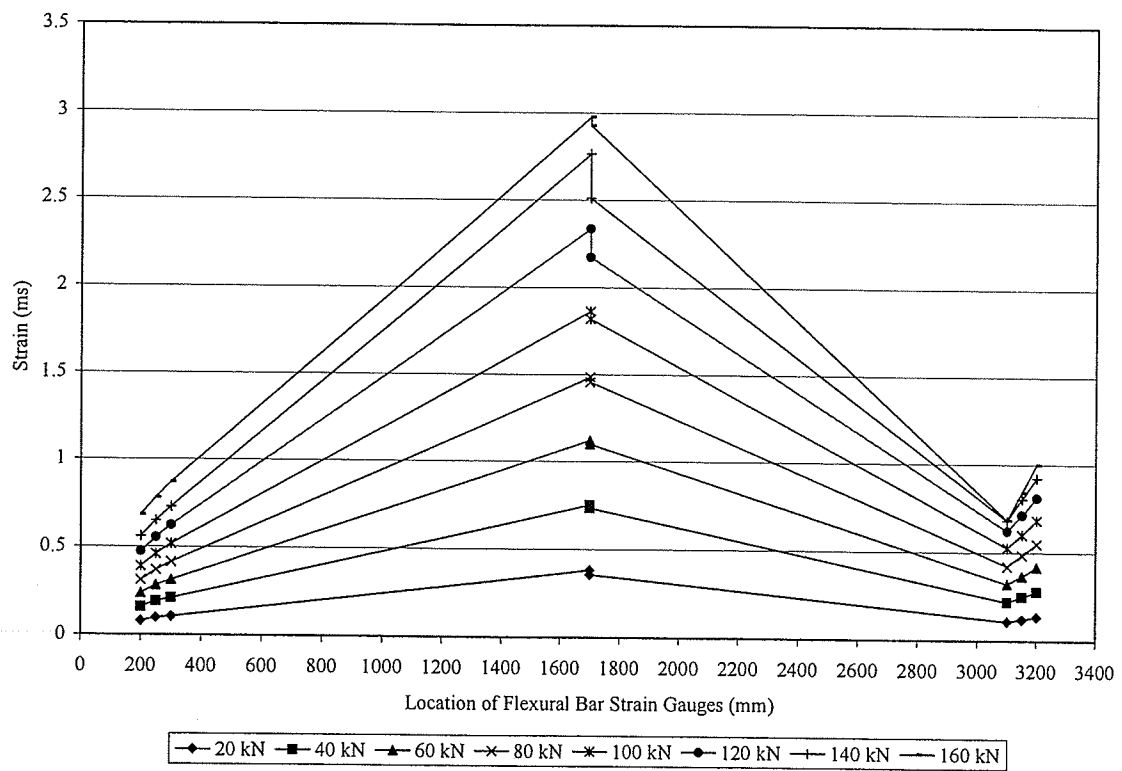


Figure B24 – Strain Profile for the Flexural Bars F6

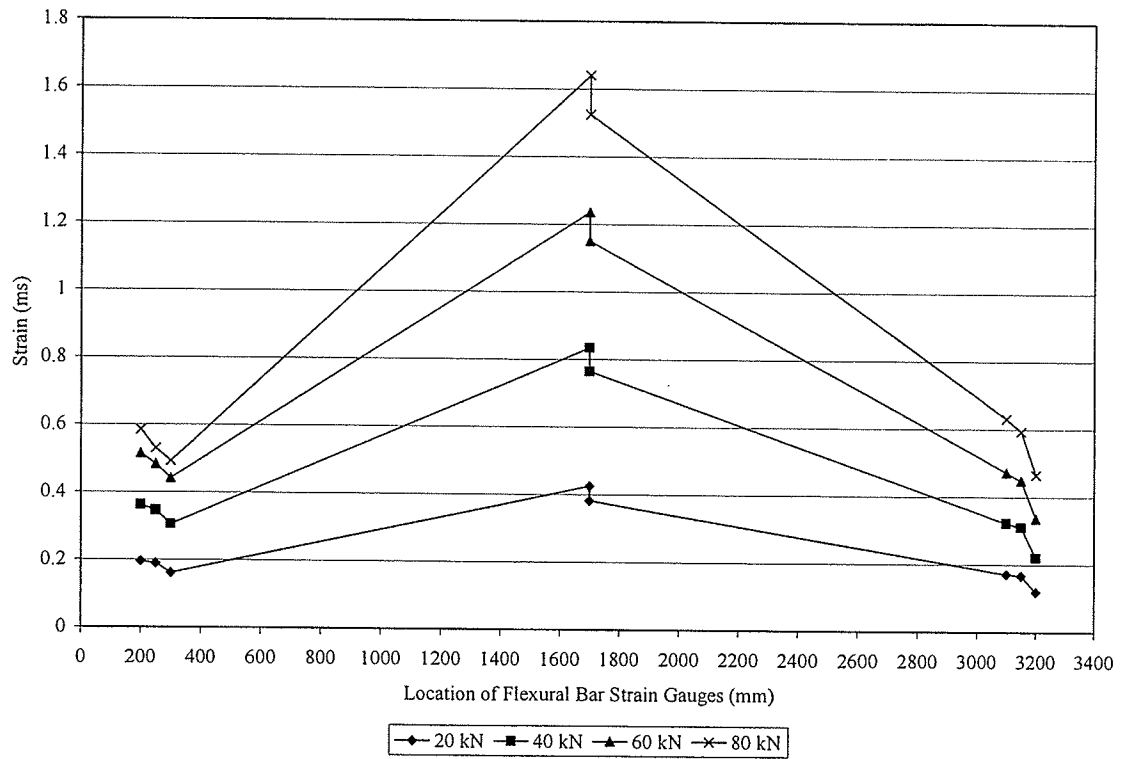


Figure B25 – Strain Profile for the Flexural Bars F7

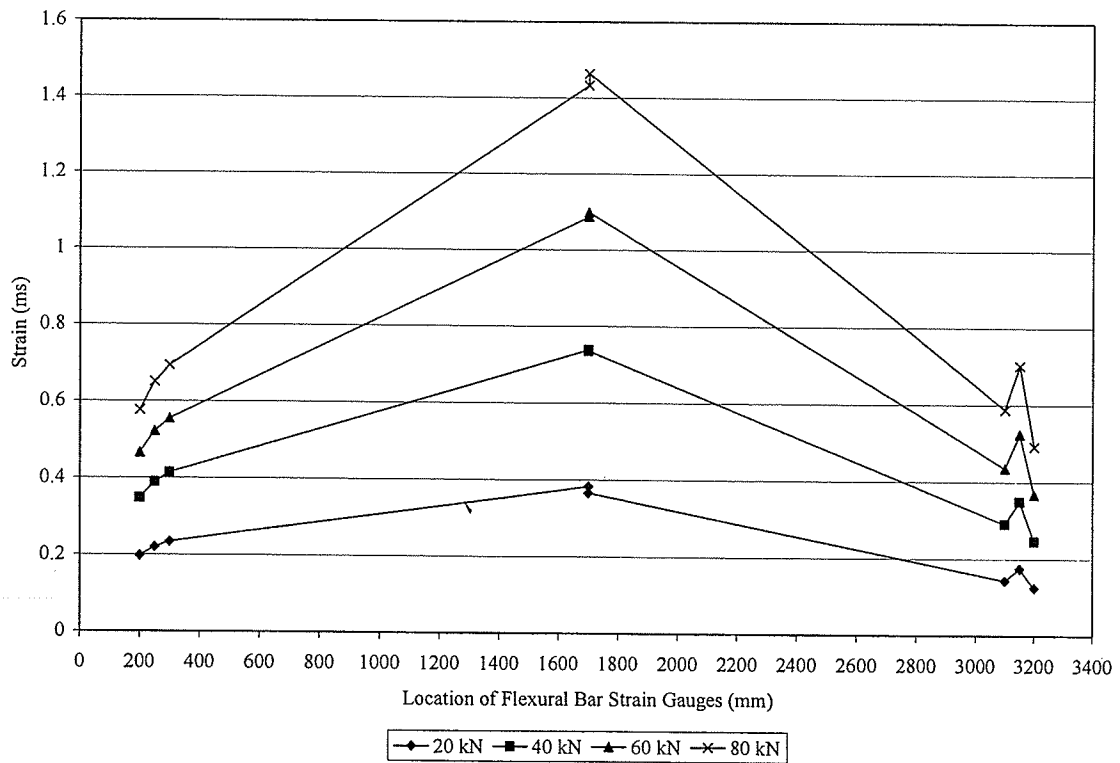


Figure B26 – Strain Profile for the Flexural Bars F8

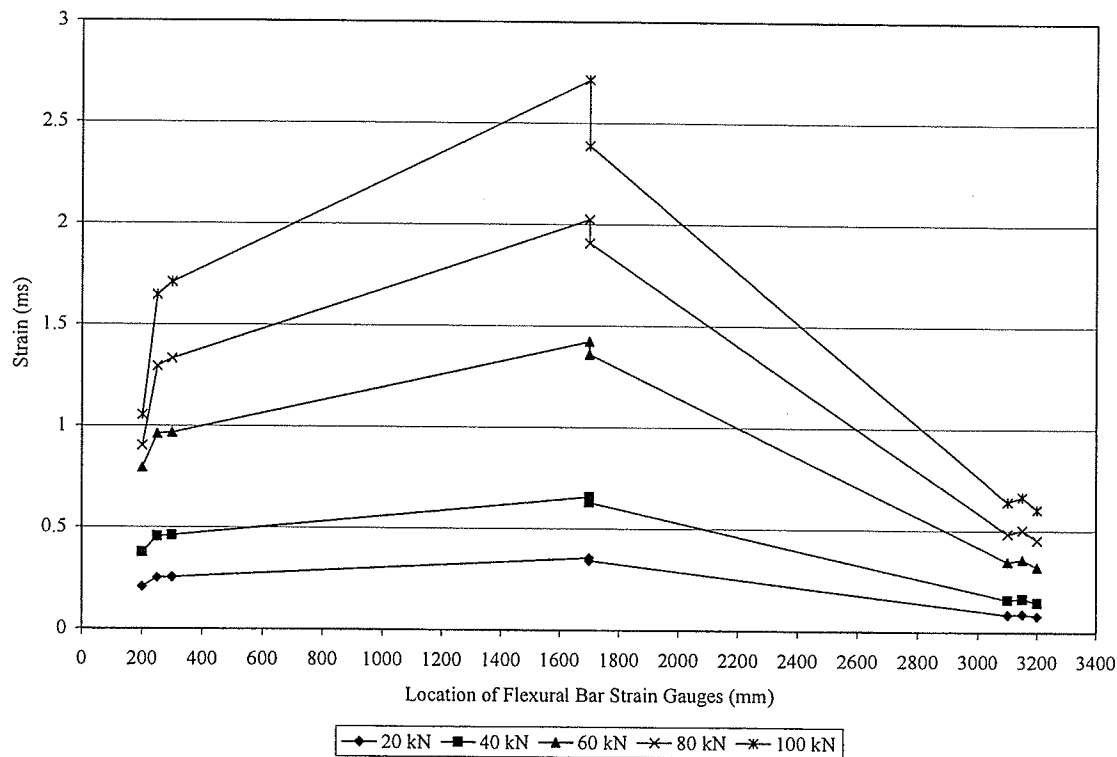


Figure B27 – Strain Profile for the Flexural Bars F9

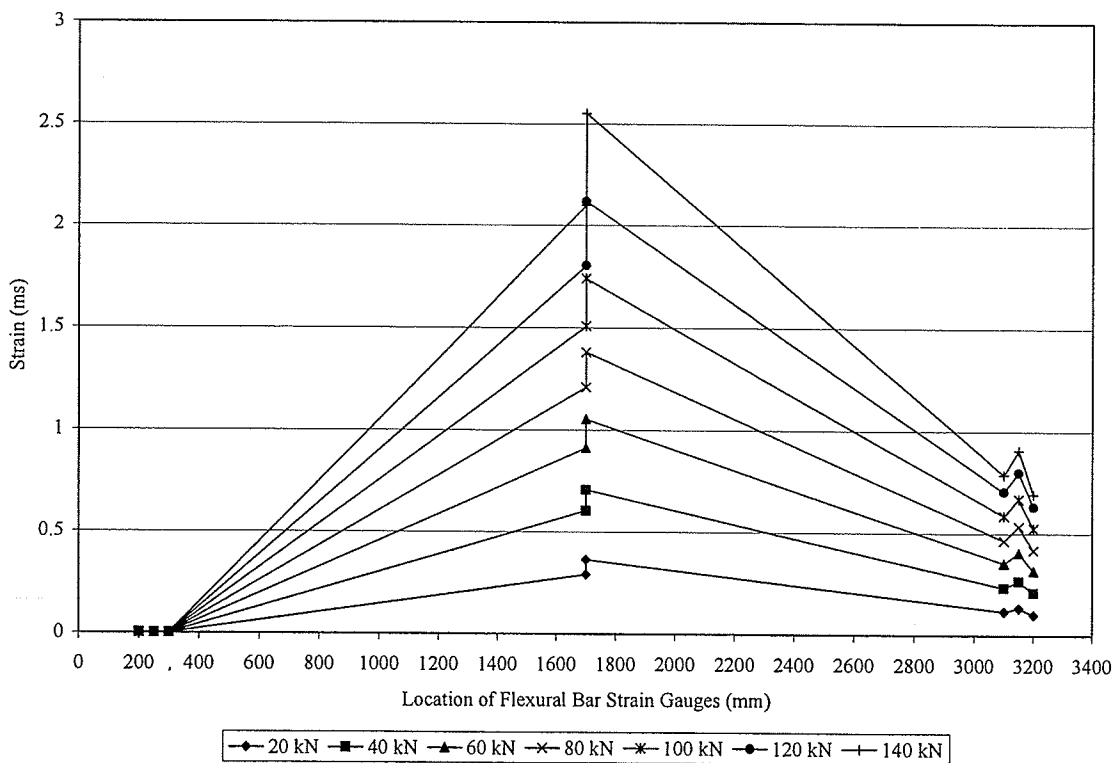


Figure B28 – Strain Profile for the Flexural Bars F10

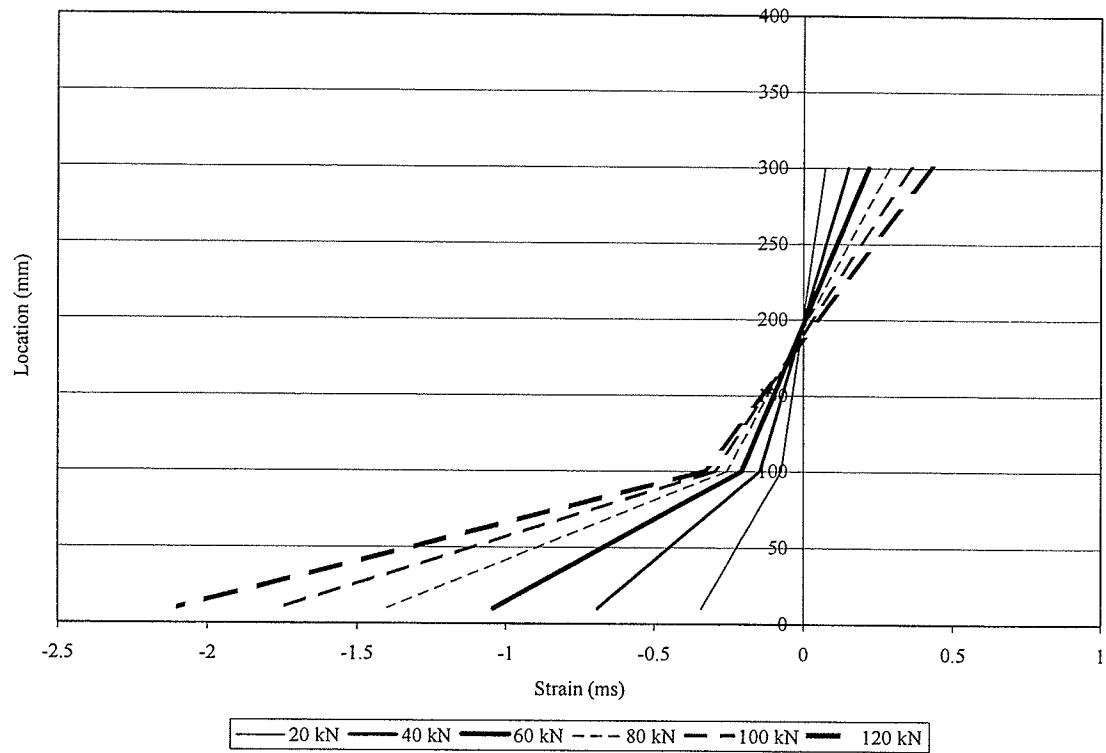


Figure B29 – Cross-sectional Strain Profile FD1

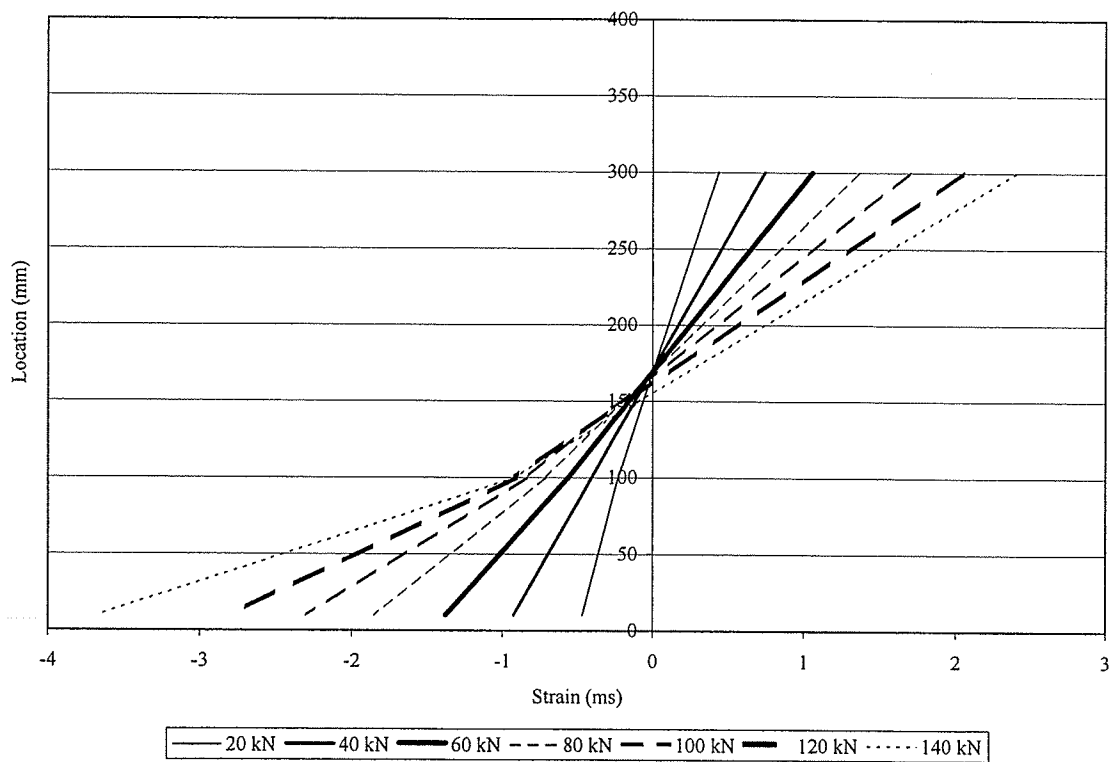


Figure B30 – Cross-sectional Strain Profile FD2

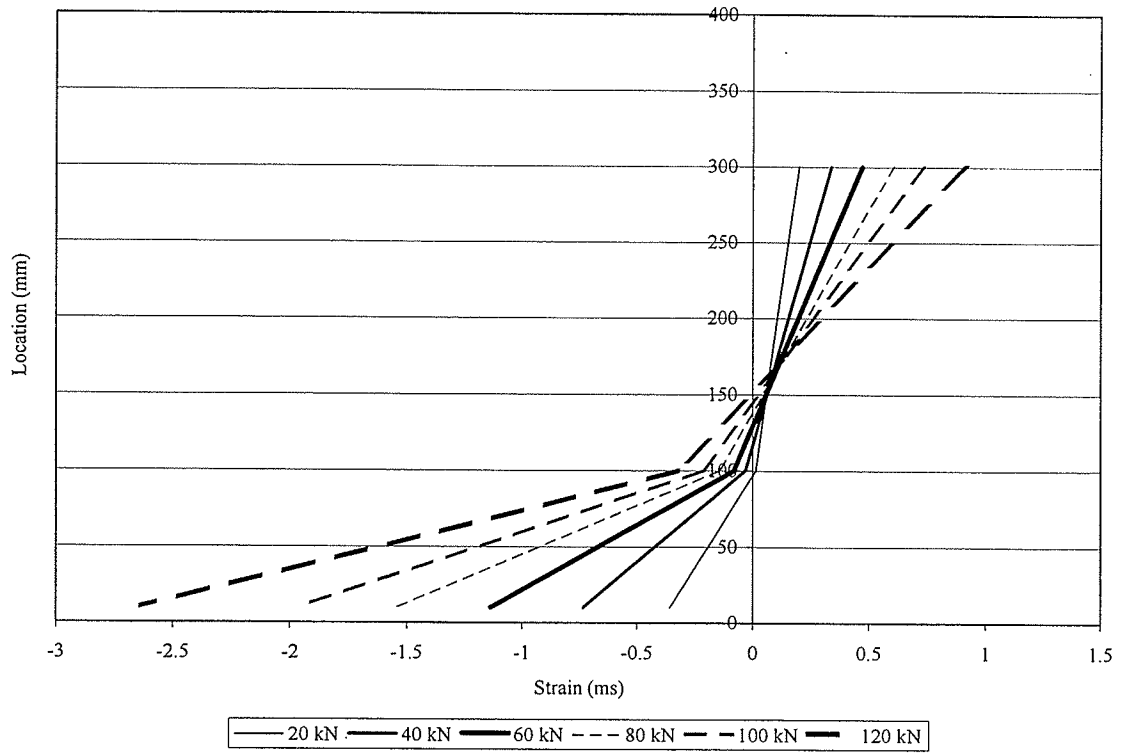


Figure B31 – Cross-sectional Strain Profile FD3

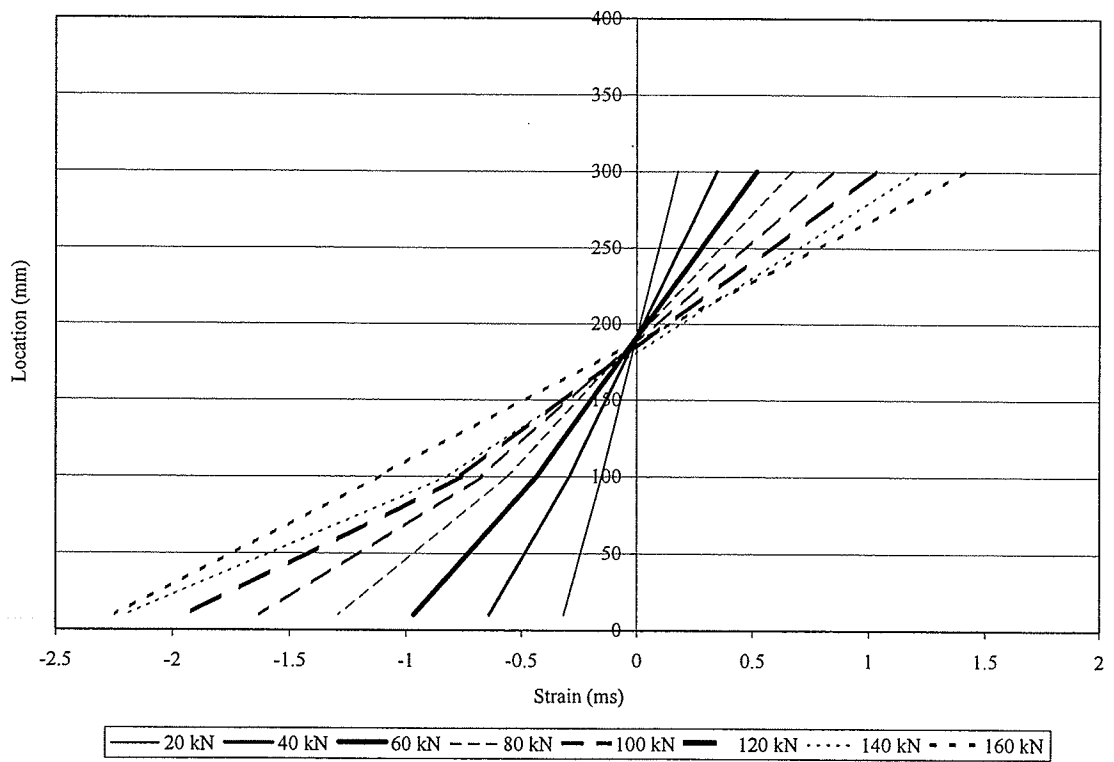


Figure B32 – Cross-sectional Strain Profile FD4

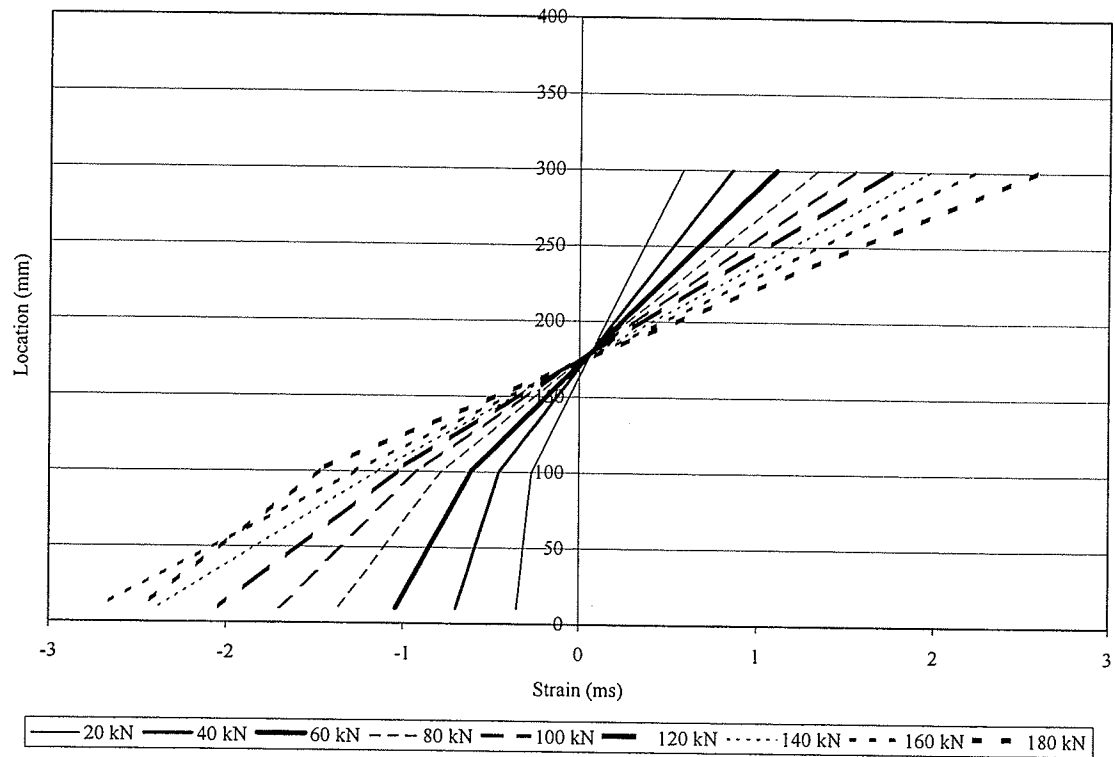


Figure B33 – Cross-sectional Strain Profile FD5

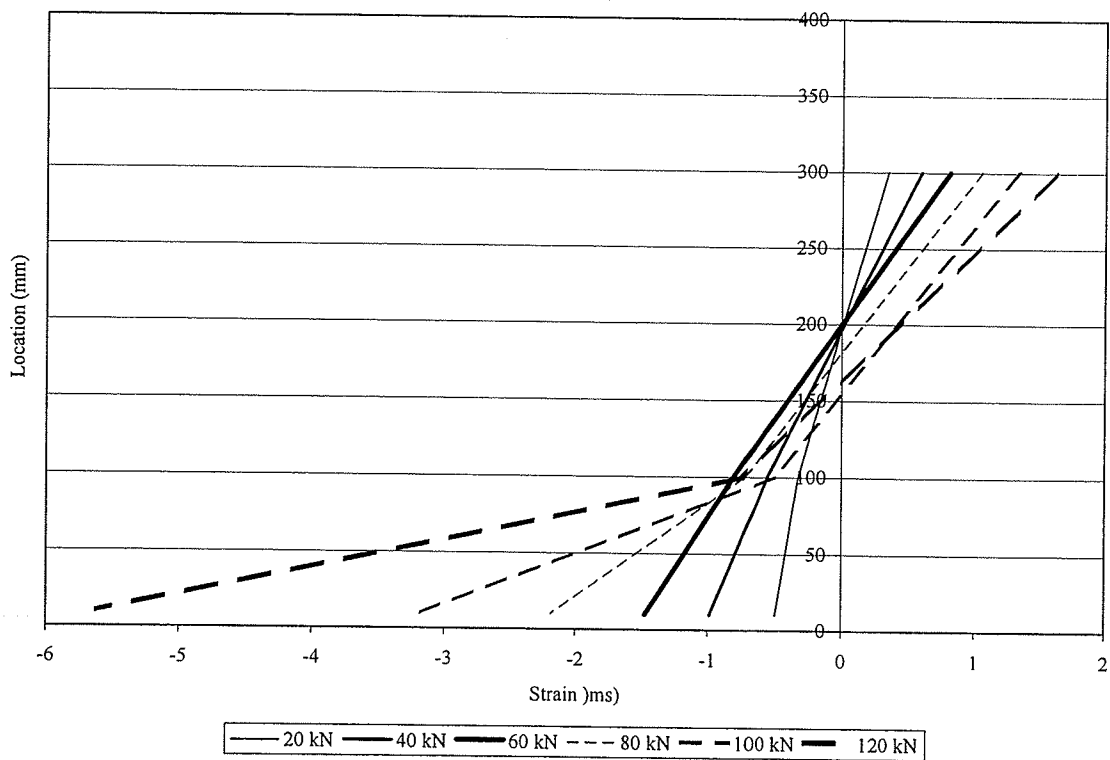


Figure B34 – Cross-sectional Strain Profile FD6

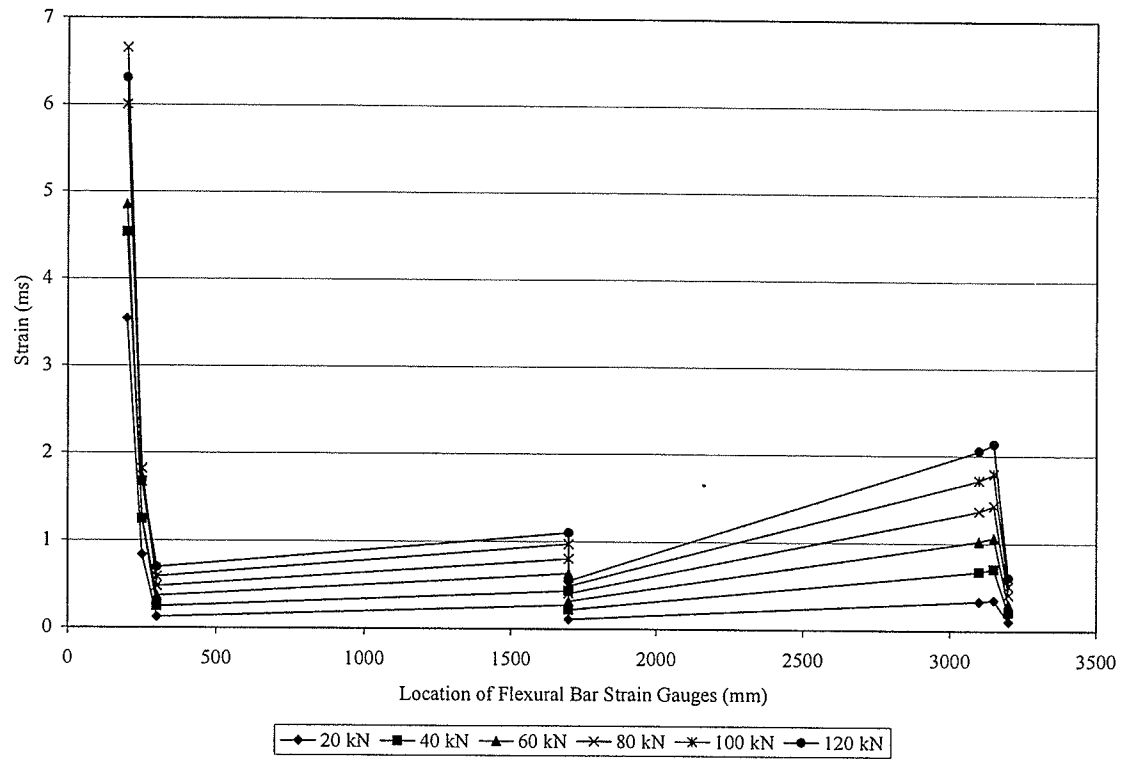


Figure B35 – Strain Profile in the Flexural Bars FD1

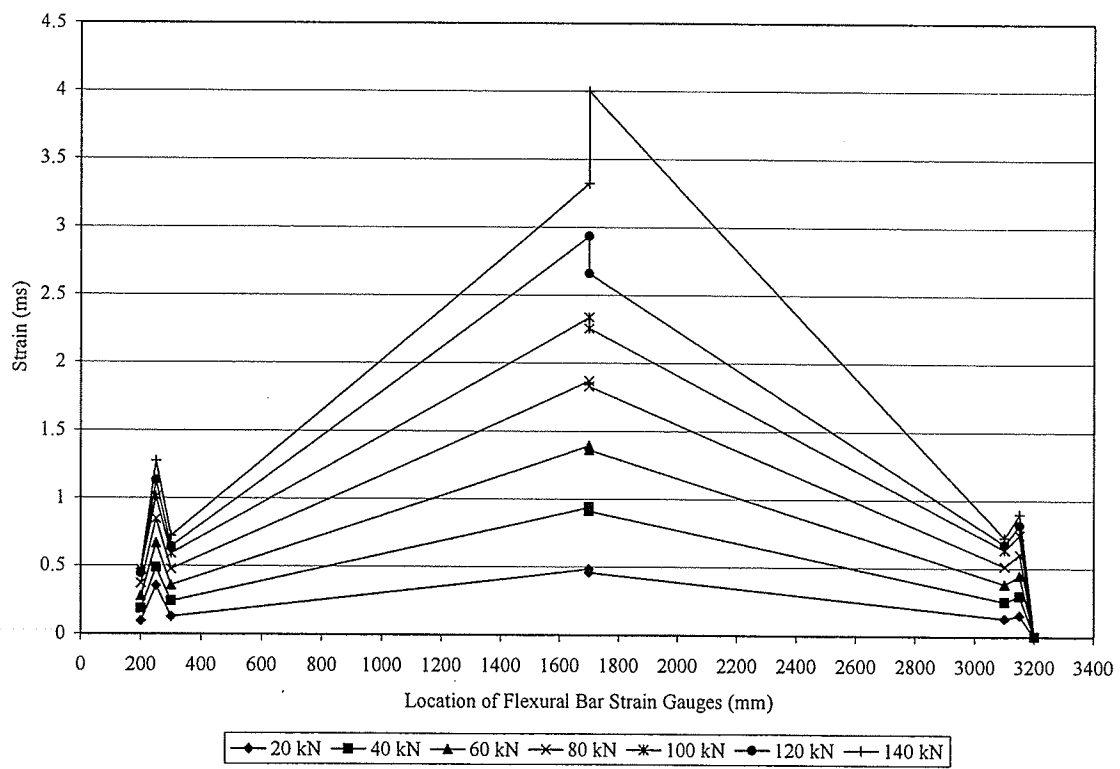


Figure B36 – Strain Profile for the Flexural Bars FD2

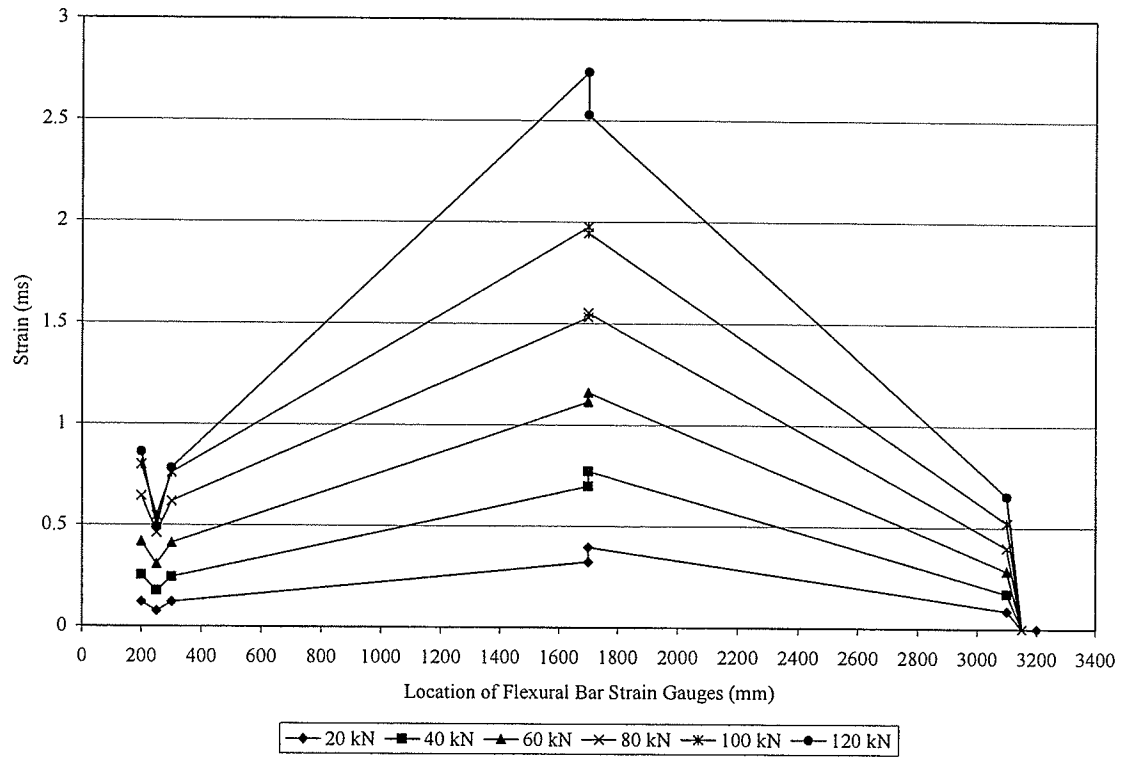


Figure B37 – Strain Profile for the Flexural Bars FD3

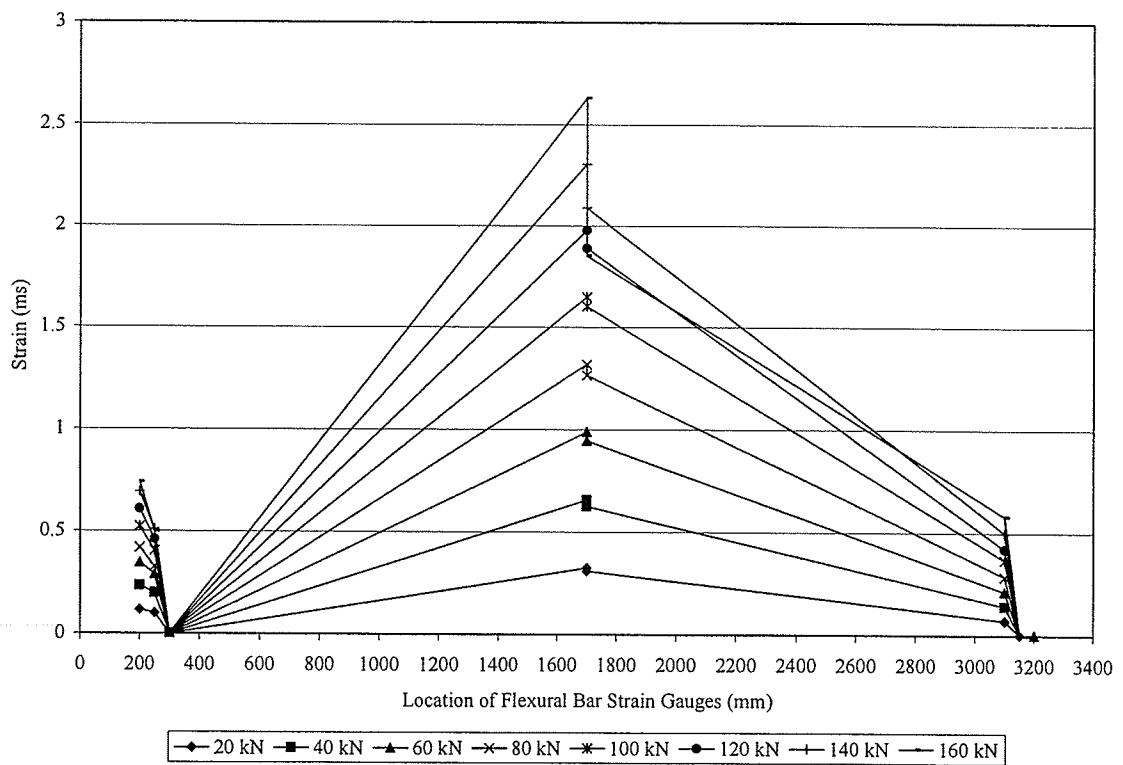


Figure B38 – Strain Profile for the Flexural Bars FD4

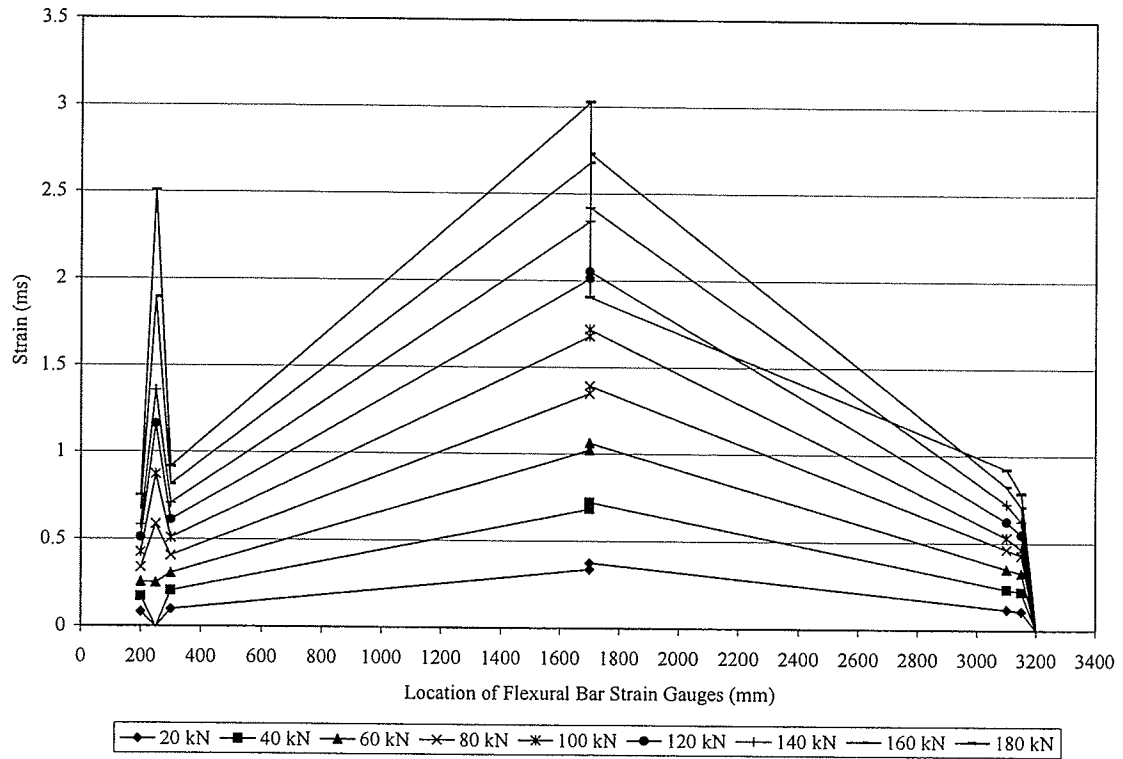


Figure B39 – Strain Profile for the Flexural Bars FD5

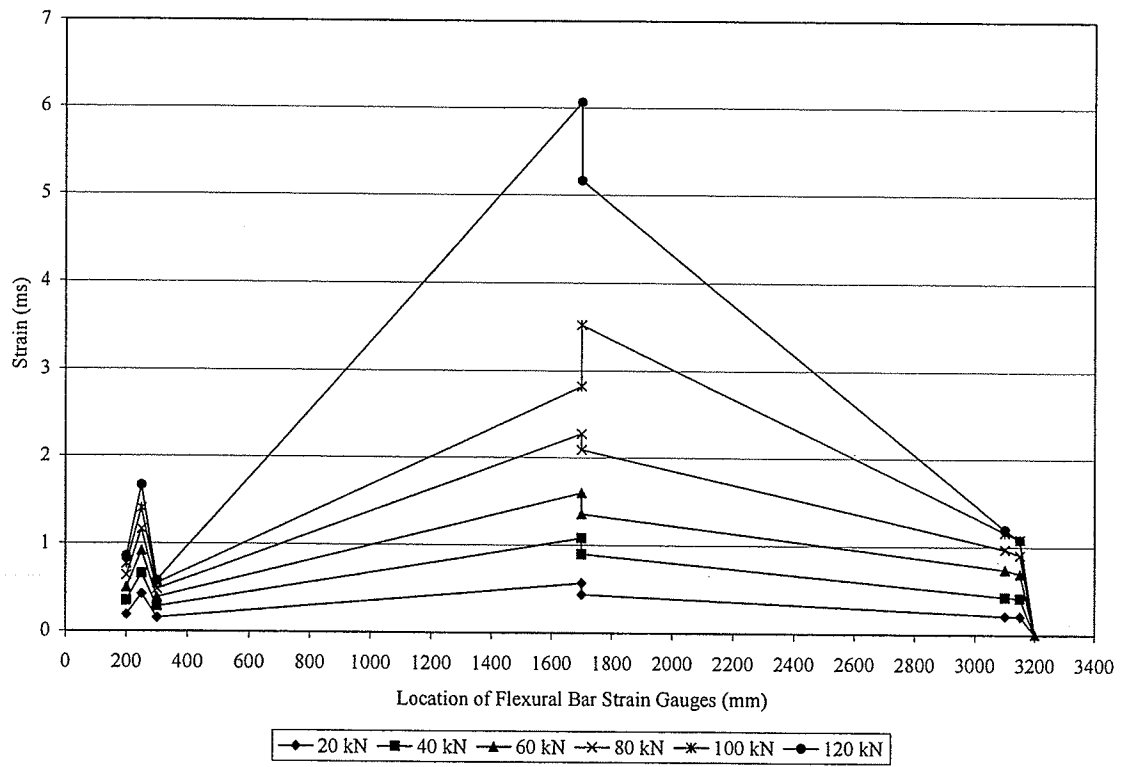


Figure B40 – Strain Profile for the Flexural Bars FD6

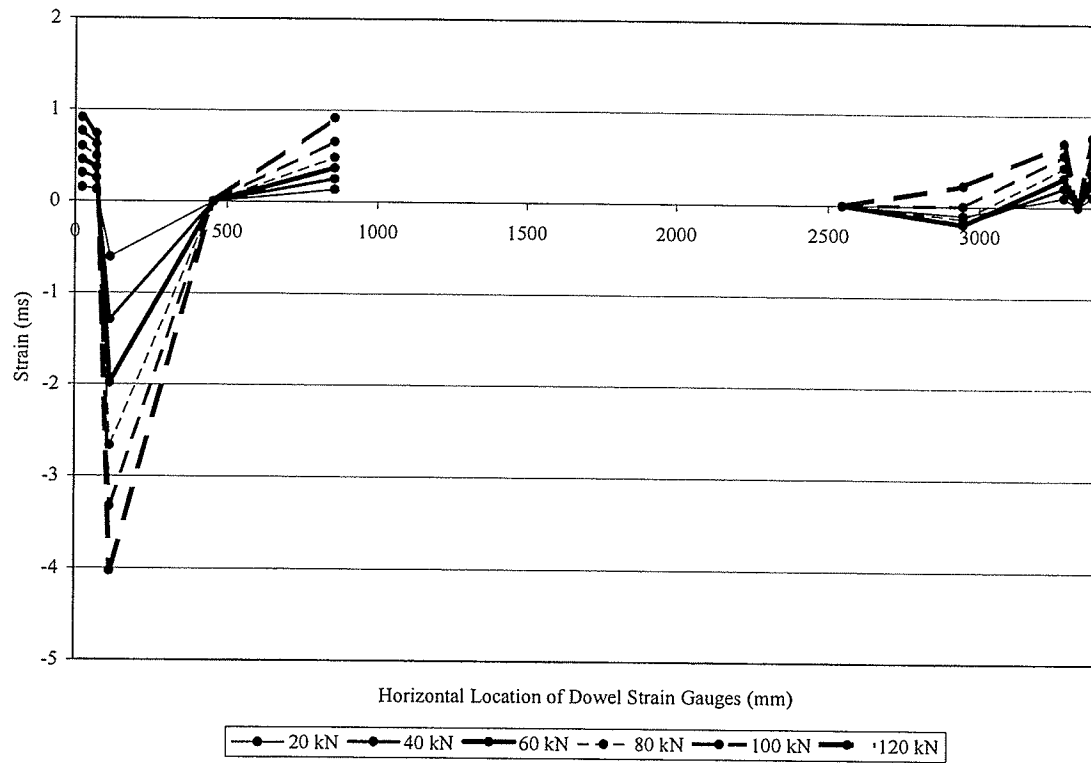


Figure B41 – Dowel Bar Strain Profile FD1

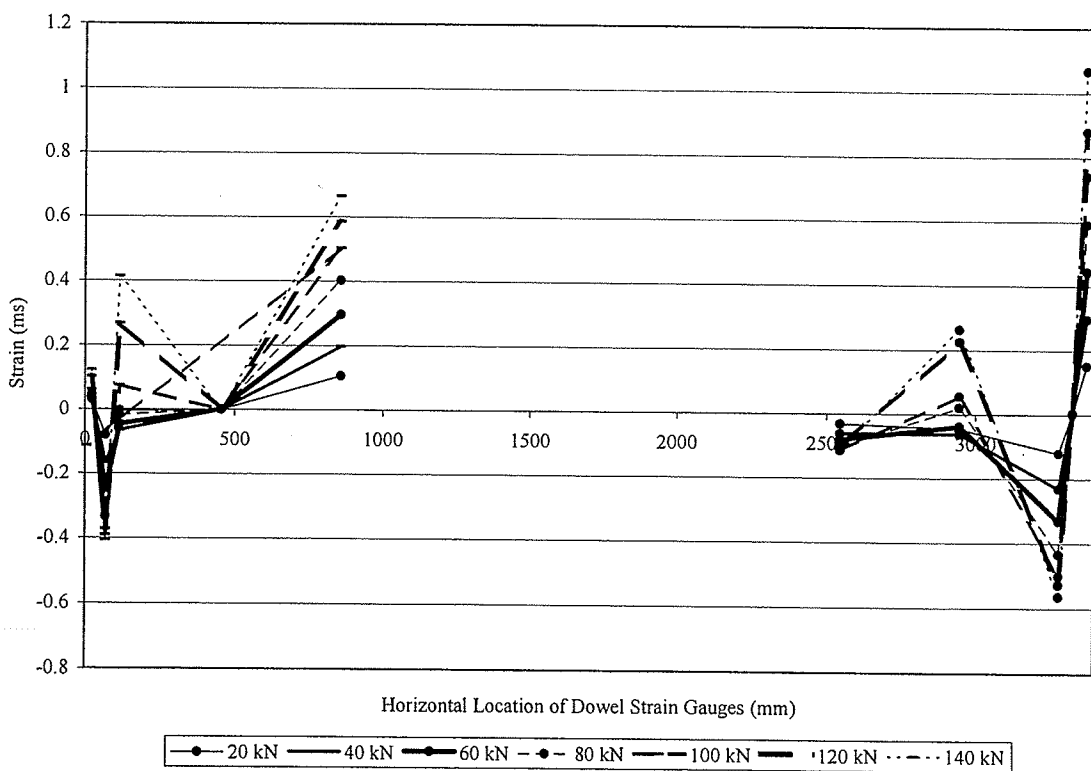


Figure B42 – Dowel Bar Strain Profile FD2

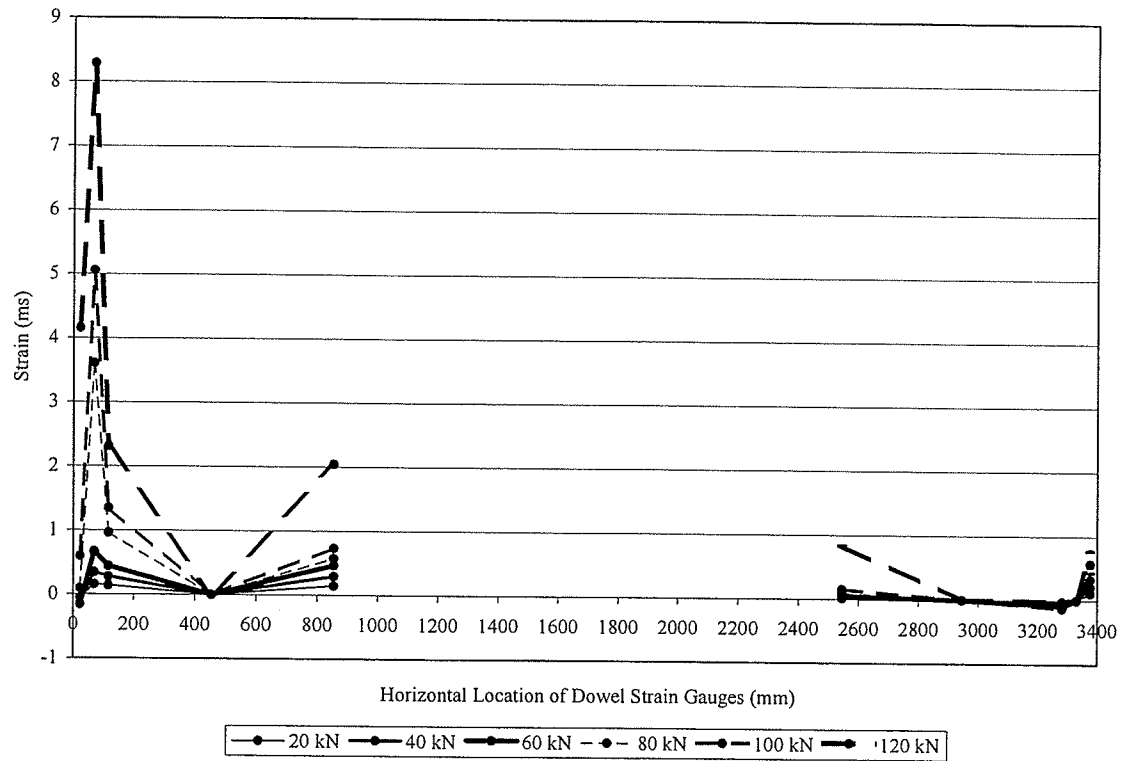


Figure B43 - Dowel Bar Strain Profile FD3

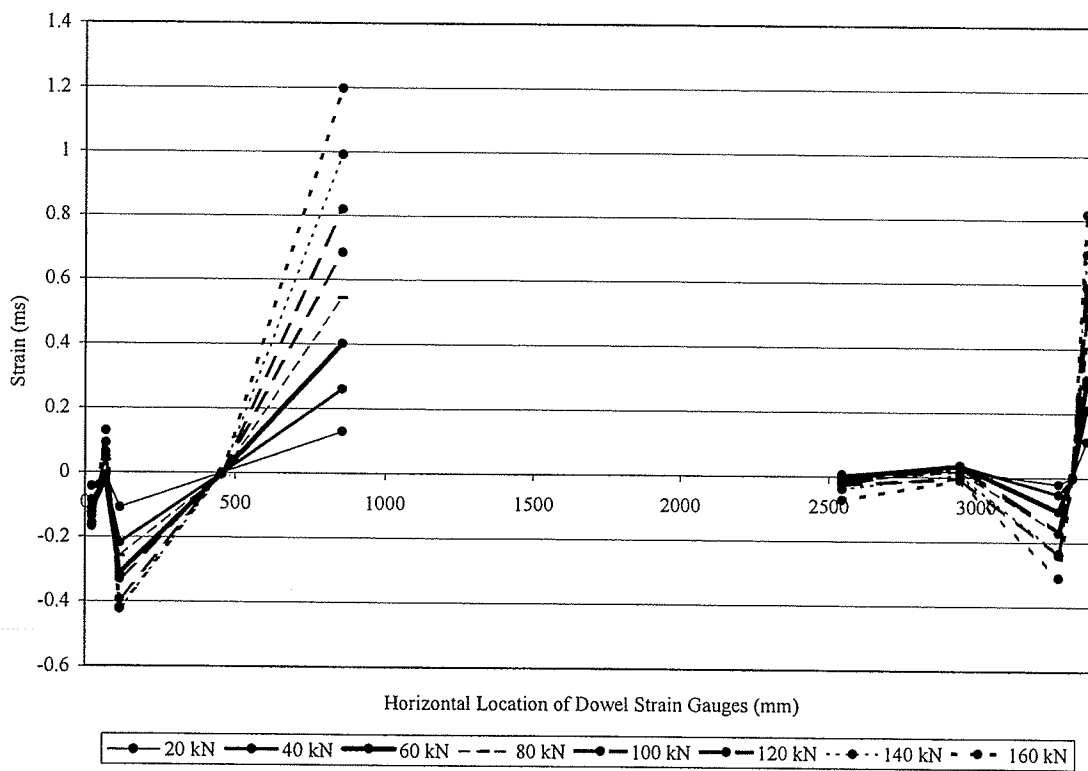


Figure B44 - Dowel Bar Strain Profile FD4

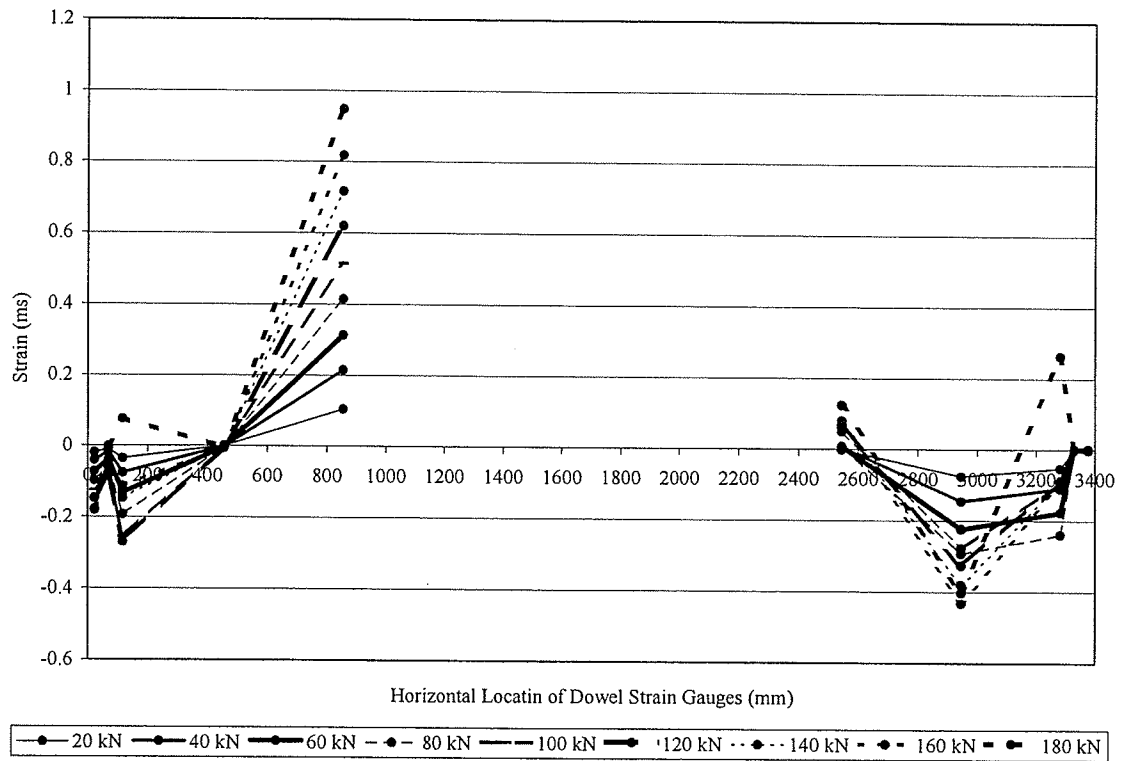


Figure B45 – Dowel Bar Strain Profile FD5

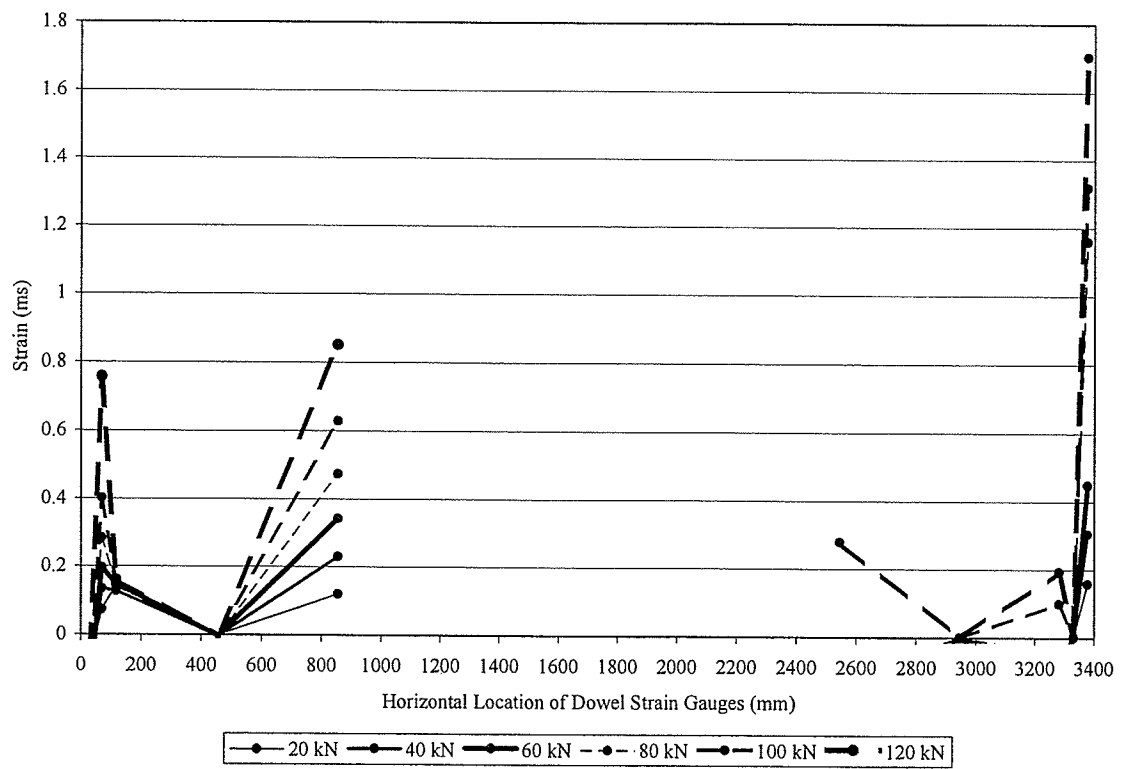


Figure B46 – Dowel Bar Strain Profile FD6

APPENDIX C

1	2	3	4	5	6	7	8	9	10	11	12	13
EI (kNmm ²) x10 ¹²	n _a	y _{bar} (mm)	A(y-y _{bar}) ² (mm ⁴)	I+4 (mm ⁴) x10 ⁶	2x4 (mm ⁴) x10 ⁶	I _{tr} 5+6 (mm ⁴) x10 ⁶	E _{GFRP} (MPa)	n _b $\frac{\delta x 7}{I}$	S _b (mm ³) x10 ⁶	E _w $\frac{\delta}{9}$ (MPa)	Ultimate Load (kN)	Tensile Stress (MPa)
3.93	2.00	199.9	400	533.3	8.182	541.5	47400	6.48	2.708	7257.4	94.33	29.6
3.93	6.48	199.8	400	533.3	26.478	559.8	47400	6.69	2.801	7020.2	94.33	28.6
3.93	6.69	199.8	400	533.3	27.334	560.6	47400	6.71	2.805	7009.5	94.33	28.6
3.93	6.71	199.8	400	533.3	27.416	560.7	47400	6.71	2.806	7008.5	94.33	28.6

a - estimated

b - calculated

A - area of stringer = 40,000 mm²

I – moment of inertia of nominal section = 0.53 x10⁹ mm⁴

y – centroid of nominal section = 200 mm

L- length of the stringer = 3400 mm

For column 13 see equation 5.1